Procedència i evolució dels sistemes sedimentaris de la conca de Jaca (conca d'avantpaís Sudpirinenca):

Interacció entre diverses àrees font en un context tectònic actiu

Marta Roigé Taribó

Tesi Doctoral
2018

Universitat Autònoma de Barcelona

Facultat de Ciències
Departament de Geologia

Capítol 7

New insights into the chronology of the South Pyrenean basin from U-Pb provenance data: the record of Miocene volcanic zircon in the San Juan de la Peña fan

El capítol 7 correspon a un article enviat a la revista científica *Terra Nova*.

M. Roigé ha mostrejat tota la secció i ha realitzat la separació de minerals pesants durant una estada de de recerca de tres mesos a la la *Università di Bologna* (Itàlia). També va realitzar tots els anàlisis d'U-Pb en zircons detrítics al laboratori *UTChron* de la *Univeristy of Texas at Austin*. Ha redactat gran part del text i ha realitzat totes les figures, menys la Figura 4.

New insights into the chronology of the South Pyrenean basin from U-Pb provenance data: the record of Miocene volcanic zircon in the San Juan de la Peña fan

Roigé, M.[1]*, Gómez-Gras, D.[1], Daniel F. Stockli[2], Antonio Teixell[1], Salvador Boya[1], Eduard Remacha[1]

[1]Department de Geologia, Universitat Autònoma de Barcelona, 08193 Bellaterra, Spain

[2]The University of Texas at Austin, Department of Geological Sciences, Austin, TX 78712, USA

(*) Corresponding author

Keywords: Provenance, geochronology, zircon, Pyrenees, volcanism

ABSTRACT

In the Jaca Basin, the western portion of the South Pyrenean foreland, massive conglomeratic deposits characterize the last stage of basin fill. We conducted detrital zircon U-Pb geochronology in a 3000m-thick Cenozoic section that contains the transition from deltaic to alluvial environments with the aim of reconstructing provenance changes. The last basin deposits belong to the San Juan de la Peña alluvial fan, which has previously been assigned an early Oligocene age. Our results reveal the presence of earliest Miocene detrital zircons at the base of the fan. Zircon double dating reveals identical U-Pb and (U-Th)/He ages indicative of a volcanic origin for these zircons. Therefore, we conclude that this fan was deposited essentially during early Miocene times. The new data establishes a new chronologic framework for deformation and sedimentation in the South Pyrenean foreland, with strong implications for the dynamics and paleogeography governing the last episodes of basin fill.

1. Introduction

Foreland basins record the erosional history of their source areas providing invaluable information about the chronology of deformation and unroofing of the active orogenic wedges (e.g. Dickinson and Suczek, 1979). In order to relate source-to-sink processes and to decipher the tectonic, exhumational, and depositional evolution from the source areas to the sedimentary basin sink, precise timing of the syntectonic foreland basin deposits is essential (e.g. DeCelles and Giles, 1996).

The Jaca Basin, in the western portion of the South Pyrenean foreland basin (Fig. 1A), provides an excellent opportunity to investigate the relationship between tectonics and sedimentation in light of a well-established chronostratigraphic framework, in particular for the Eocene deep-water stage of foredeep development (e.g. Canudo and Molina, 1988; Labaume *et al.*, 1985; Oms *et al.*, 2003).

However, there are only sparse and contradictory age constraints on the transition to conglomeratic molasse deposition in the basin (Puigdefàbregas, 1975; Hogan and Burbank, 1996; Oliva-Urcia *et al.*, 2015). These deposits consist of fluvial to alluvial strata that represent the overfilling basin stage and record the late erosional and exhumational history of the Pyrenees (Puigdefàbregas, 1975).

This study presents new detrital zircon (DZ) U-Pb data from a 3000 m-thick succession of these last alluvial deposits, elucidating their provenance evolution. In addition, selected DZ U-Pb and (U-Th)/He double dating was performed to provide important new constraints on the chronostratigraphy of these strata. These results imply a younger age for these molasses deposits and require a revision of both the chronostratigraphic record as well as the late-stage fill history of the Jaca Basin.

2. Geological setting

The Pyrenees formed during late Cretaceous to early Miocene times as a result of the collision between the Eurasian and Iberian plates (Roure *et al.*, 1989; Muñoz, 1992; Teixell, 1998; Vergés *et al.*, 2002). The southern side of the Pyrenean belt consists on a south-vergent, basement-involved thrust stack that in the west-central Pyrenees is composed by four main thrust sheets. These are from north to south: the Lakora-Eaux-Chaudes, Gavarnie, Broto and Guarga thrusts (Teixell, 1996; Labaume *et al.*, 2016) (Fig. 1B). These thrust sheets involve Paleozoic basement and a sedimentary cover consisting of pre-orogenic Mesozoic rocks and Late Cretaceous-early Miocene foreland basin strata -the so-called Jaca thrust-top Basin.

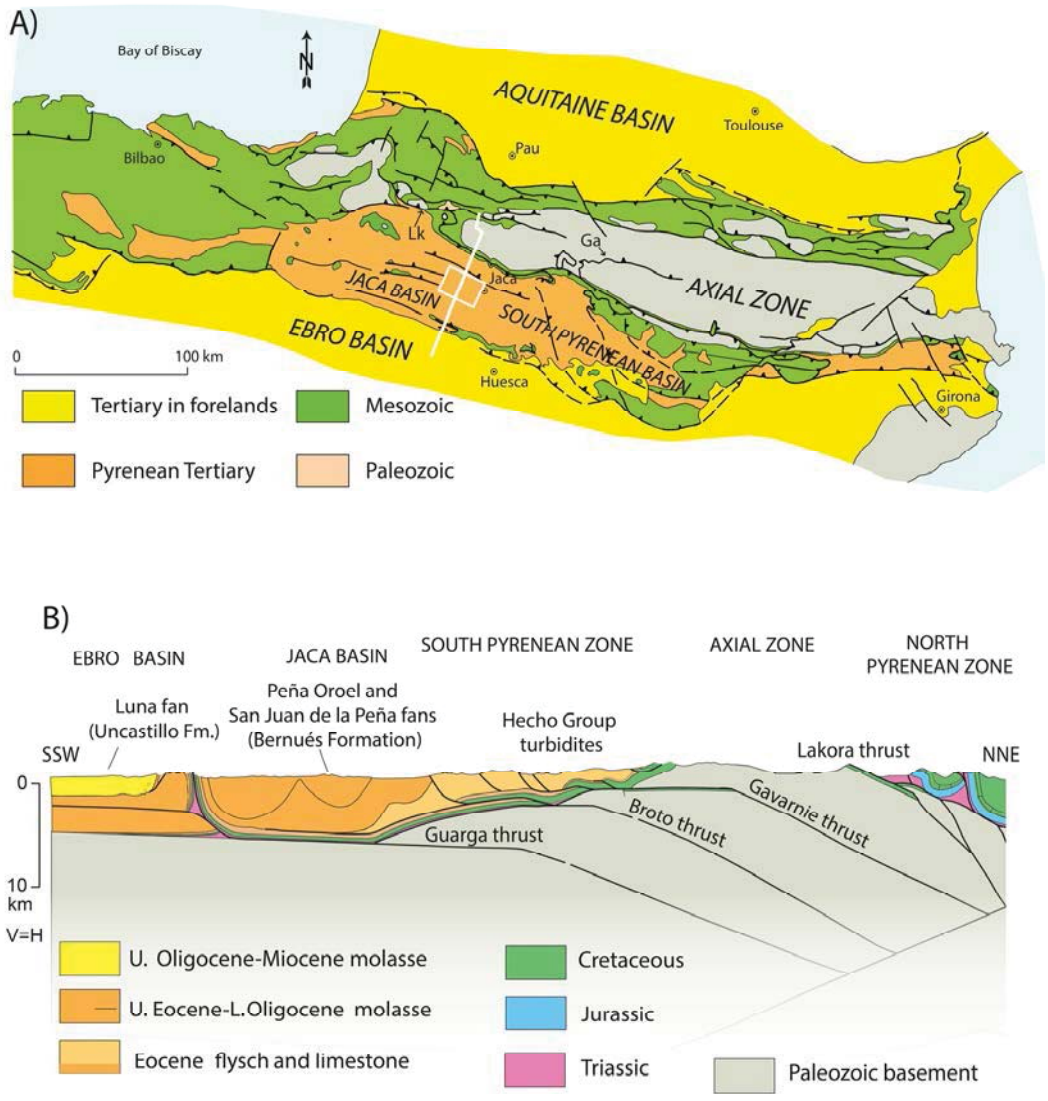

Figure 1. (A) Simplified geological map of the Pyrenees (redrawn from Teixell, 1996), showing the location of the study area (white frame). White line indicates cross-section in Figure 1B. Lk: Lakora thrust; Ga: Gavarnie thrust. (B) Crustal cross-section of the west-central Pyrenees (simplified from Teixell et al., 2016), showing the Jaca thrust-top Basin of the Southern Pyrenees.

The Paleozoic basement constitutes the core of the belt -the Axial Zone- and is mainly composed of Variscan low-grade metamorphic rocks and granitoids, that are unconformably overlain by Permo-Triassic red beds or directly by Cretaceous limestones. South of the Axial Zone, synorogenic rocks of Santonian to Miocene age constitute the South Pyrenean foreland basin, including the Jaca, Ainsa, and Tremp-Graus Basins, which thrust southwards over the Ebro basin.

The Jaca Basin (Fig. 2) is characterized by deep-water turbidite sedimentation during early-mid Eocene times (Hecho Group turbidites), that evolved to the coastal and fluvial/alluvial molasses in the upper Eocene-Oligocene (Campodarbe and Bernués Formations) (Puigdefàbregas, 1975). Stratigraphically above the Eocene-Oligocene Campodarbe Formation, the Bernués Formation consists on massive conglomeratic deposits, mainly represented by the San Juan de la Peña and Peña Oroel alluvial fans (Fig. 2) (Puigdefàbregas, 1975). The cessation of sedimentation in the Jaca Basin is usually attributed to activity on the Guarga thrust (Oligocene-early Miocene), ultimately resulting in the uplift and erosion of the basin as recorded in the alluvial sedimentation of the Uncastillo Formation, in the Ebro basin (Teixell, 1996; Labaume *et al.*, 2016).

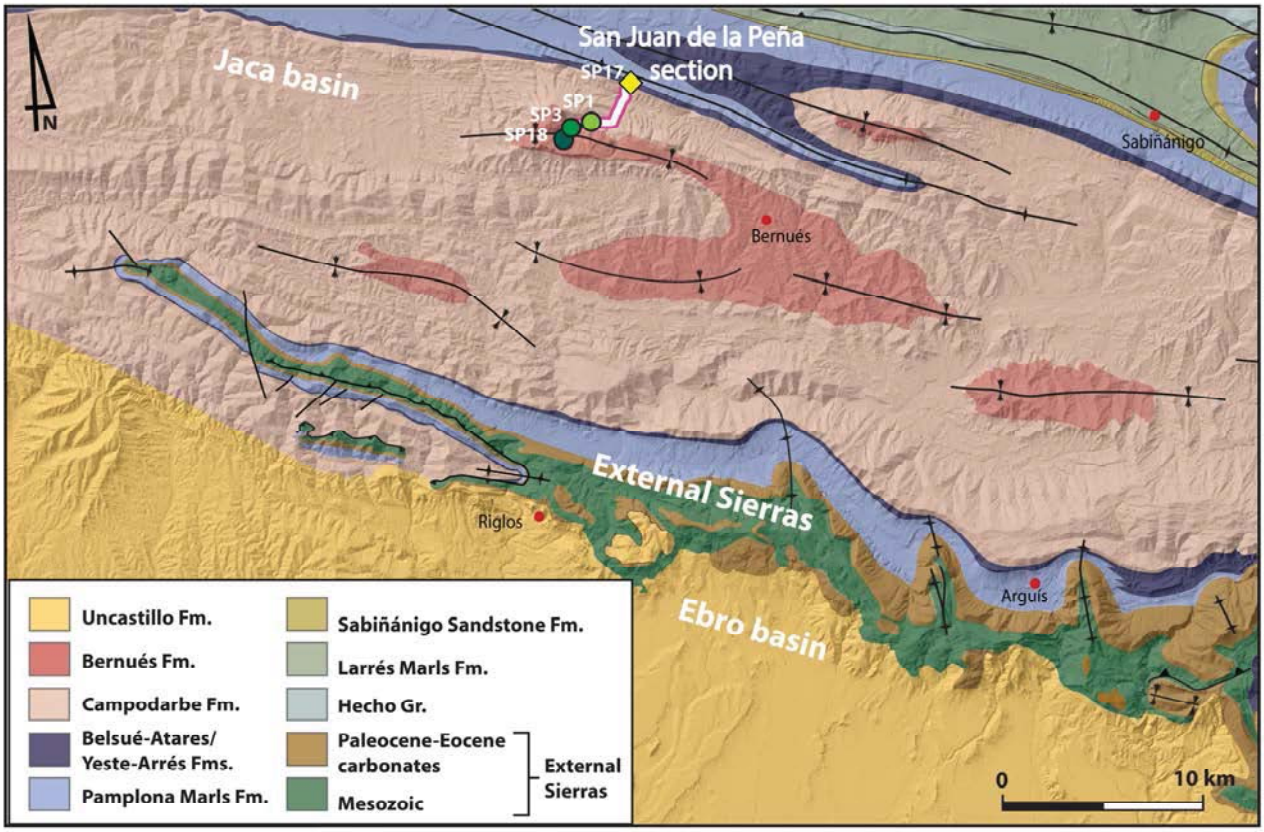

Figure 2. Geological map of the central part of the souhern Jaca Basin and northern margin of the Ebro Basin (modified from Puigdefàbregas, 1975). White-purple line shows the location of the San Juan de la Peña stratigraphic section analyzed in this work. Circles and triangle show the position of the analysed samples. Map coordinates for bottom right are (30T) 721339E/4676503N, and top left are (30T) 666069E/4715901N.

3. Stratigraphic framework

The Campodarbe Formation reaches a maximum thickness of more than 3000m in the central part of the Jaca Basin, where two main sediment routing systems merge: an axial east-derived fluvial system and a transverse north-derived system (Puigdefàbregas, 1975; Montes and Colombo, 1996). Above the Campodarbe Formation, the Bernués Formation conglomerates represent the youngest preserved sedimentation derived from the persistent erosion of the Pyrenees and the emerging fold-and-thrust belt to the north of the basin.

The age of Campodarbe Formation was originally proposed to be late Eocene-Oligocene (Soler and Puigdefàbregas, 1970), while the age of the overlying Bernués Formation was suggested to be Chattian at the base and potentially Aquitanian to the top, by correlation with the Uncastillo Formation (Arenas, 1993) in the Ebro basin (Fig. 2). In contrast, more recently Hogan and Burbank (1996), Montes (2002) and Oliva-Urcia *et al.* (2015) proposed significantly older ages for the top of the Campodarbe Formation and the Bernués Formation, setting a Priabonian to Rupelian age for them based on magnetostratigraphy and stratigraphic correlations. According to their data, the Chattian-Burdigalian Uncastillo Formation of the Ebro Basin could not be contemporaneous with the Bernués Formation of the Jaca Basin.

4. Methodology

The fluvial-alluvial deposits of San Juan de la Peña section (Fig. 2) were measured and sampled for DZ U-Pb and (U-Th)/He geo- and thermochronologic analysis. Four medium-grained sandstone samples (2-5 kg) were collected along the section (Fig. 3). The lowermost sample (SP17) was obtained from the lower Campodarbe Formation fluvial deposits, while samples SP1, SP3 and SP18 were obtained from the conglomeratic beds of the San Juan de la Peña fan (Bernués Formation, according to Puigdefàbregas, 1975). Following standard heavy mineral separation procedures, samples were crushed and sieved to obtain the 63-250µm fraction. Zircon grains were isolated using the Gemini water table separation, Frantz isodynamic magnetic separation, and heavy liquid separation (sodium metatungstate; ρ=2.87 g/cm^3). Mineral separation was performed in the heavy mineral laboratory of the University of Bologna according to procedures described by Mange and Maurer (1992). All DZ U-Pb and (U-Th)/He analyses were conducted at the UTChron geo- and thermochronology laboratory at the University of Texas at Austin following procedures described in Hart *et al.* (2016) for LA-ICP-MS U-Pb dating and Wolfe and Stockli (2010) for ZHe dating.

5. Results and discusion

All DZ U-Pb zircon results are shown in Figure 3 as pie charts, kernel density estimation plots (Vermeesch, 2012), and histograms (see Supplementary Files S1 and S2 for complete data). For the pie diagrams, DZ U-Pb ages are binned into groups (Fig. 3) that represent the most important magmatic/tectonic phases of the Pyrenean evolution, similar to those established in Thomson *et al.* (2017) for the nearby Ainsa basin.

The basal sample (SP17), which belongs to the fluvial Campodarbe Formation, shows three main age components at 310-380 Ma, 500-780 Ma and 900-1120 Ma. It lacks any late Variscan signal (280-310 Ma), but exhibits marked age peaks at 325 Ma and 375 Ma. The overlying San Juan de la Peña conglomeratic strata (samples SP1, SP3, SP18) show also minor to absent late Variscan ages, but a significant up-section increase in Cadomian zircons (520-700 Ma) (Fig. 3).

Compared to the Campodarbe fluvial sandstone, the Bernués alluvial conglomerates either lack or show low abundances of 360-400 Ma zircons and are characterized by an increased age component at ~700-900 Ma. These changes are likely attributable to provenance shifts resulting from the replacement of an east-derived fluvial system (sample SP17) by a north-derived alluvial system (samples SP1, SP3, SP18), as previously proposed by Puigdefàbregas (1975). The presence of early Variscan age components in the east-derived fluvial system suggests erosion and recycling of Carboniferous strata of the east-central Axial Zone (Roigé *et al.*, 2017), which have been shown to contain early Variscan DZ ages (Martínez *et al.*, 2015).

In contrast, the conglomeratic beds show a pronounced decrease in the 360-440 Ma zircon signal, that could be due to a lack of significant contributions from the Paleozoic basement and a dramatic increase of recycling of the Hecho Group turbidites, forming the tectonically inverting hinterland north of the basin at that time (Puigdefàbregas, 1975).

The DZ spectrum of ~120 zircons for sample SP3 yielded a single zircon with a U-Pb age of 22.1±0.6 Ma, representing the youngest zircon age found in the South Pyrenean domain and with strong implications for the chronostratigraphy of the Jaca basin. Consequently, additional U-Pb DZ analyses were performed, targeting only euhedral grains of variable sizes to verify the presence of young Cenozoic zircons (Fig. 3).

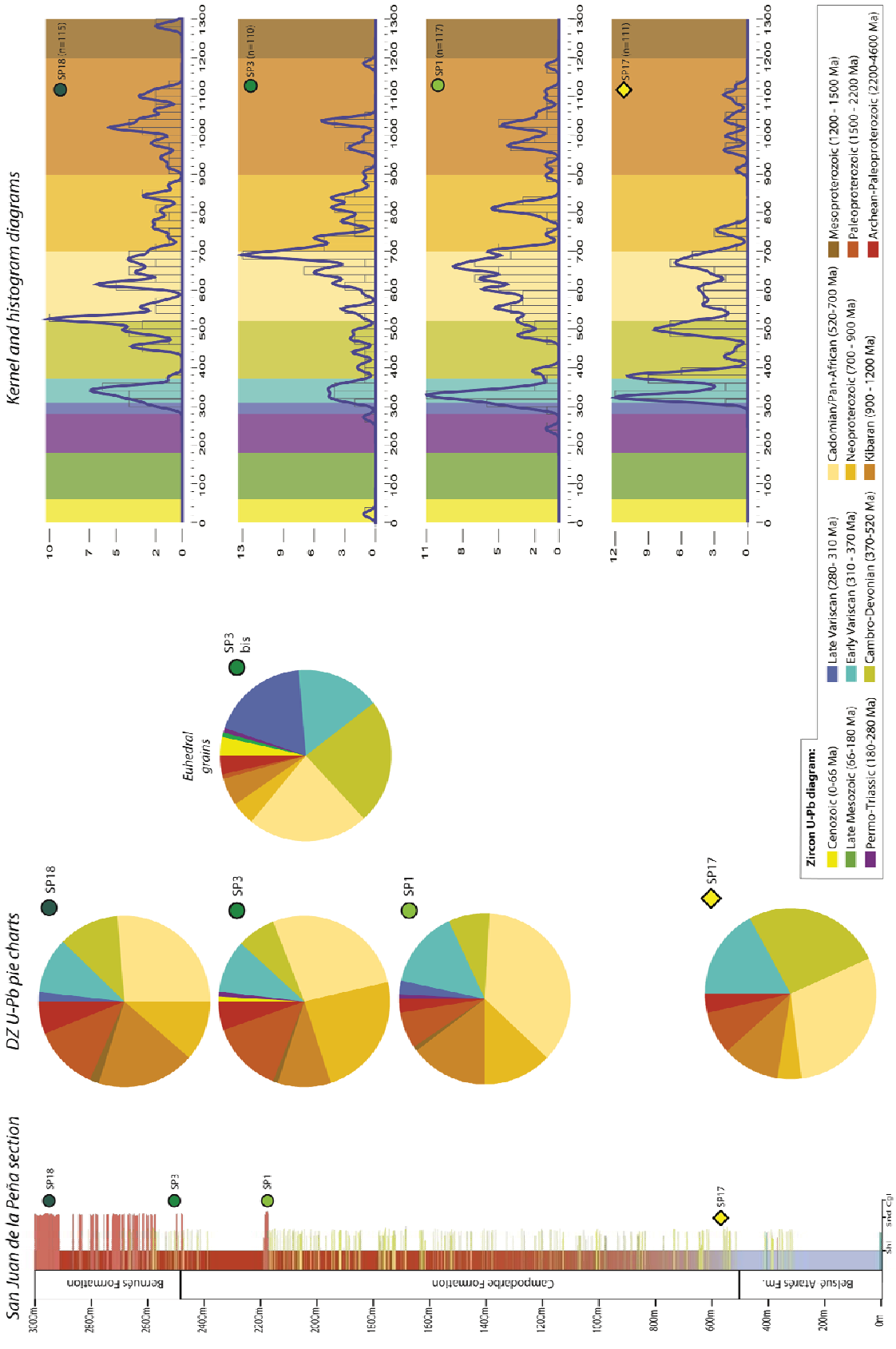

Figure 3. Detrital zircon U-Pb results for the San Juan de la Peña section (see location in Figure 2), with the stratigraphic log and position of the analyzed samples. Color legend used for Pie diagrams is also represented in the Kernel (KDE) and histogram diagrams for a better visualization of data. Note that SP3 bis is labeled as "euhedral grains", as it represents the population of euhedral grains of sample SP3.

These additional analyses of sample SP3 (labeled SP3bis) yielded four more young ages (23.8±0.9 Ma; 26.6±1.1 Ma; 24.9±1.1 Ma and 22.9±0.8 Ma), corroborating the presence of Oligo-Miocene zircons and improving statistics of the determination of the maximum depositional age for the strata (Fig. 4) (Dickinson and Gehrels, 2009). Furthermore, in order to resolve a volcanic origin of these Oligo-Miocene grains, (U-Th)/(He-Pb) double dating was applied.

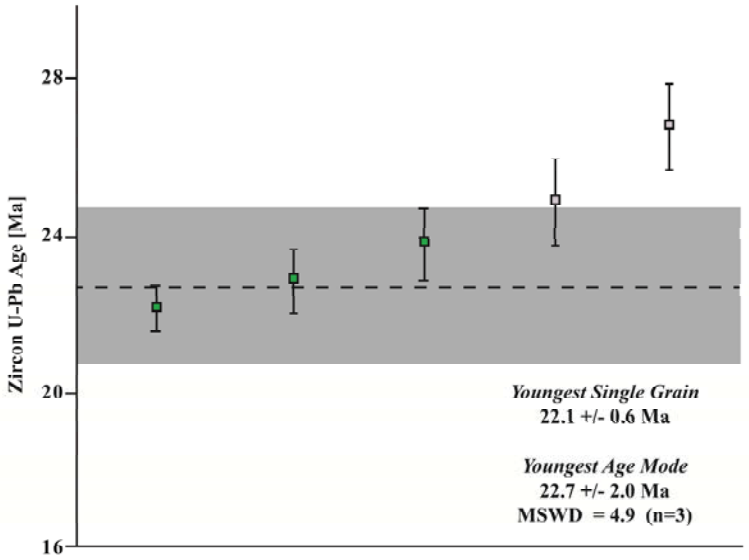

Figure 4. Zircon U-Pb ages of the Cenozoic grains. Weighted mean ages are calculated with Isoplot program following the procedure described in Dickinson and Gehrels (2009). Black boxes are the error bars (2σ error). Horizontal grey band shows the probable age of the zircon population.

All young zircons show identical U-Pb and (U-Th)/He ages corroborating a volcanic origin and lending additional support for them to constrain the actual (maximum) depositional age (Fig. 5).

As there is no documented felsic Cenozoic volcanism in the Pyrenees that could source these grains, the most plausible origin for them is Oligo-Miocene calc-alkaline magmatism reported from the Mediterranean basin (Fig. 6) related to the opening of the Valencia through (Marti *et al.*, 1992; Sabat *et al.*, 1995).

This hypothesis would assume airborne transport of the volcanic zircons and disposition as airfall either directly to the Jaca Basin or into the hinterland source area. This explanation is also supported by the presence of an ash layer that has been reported in several localities in the Ebro Basin (Fig. 6), which yielded a radiometric sanidine $^{40}Ar/^{39}Ar$ age of 19 Ma (Odin *et al.*, 1997).

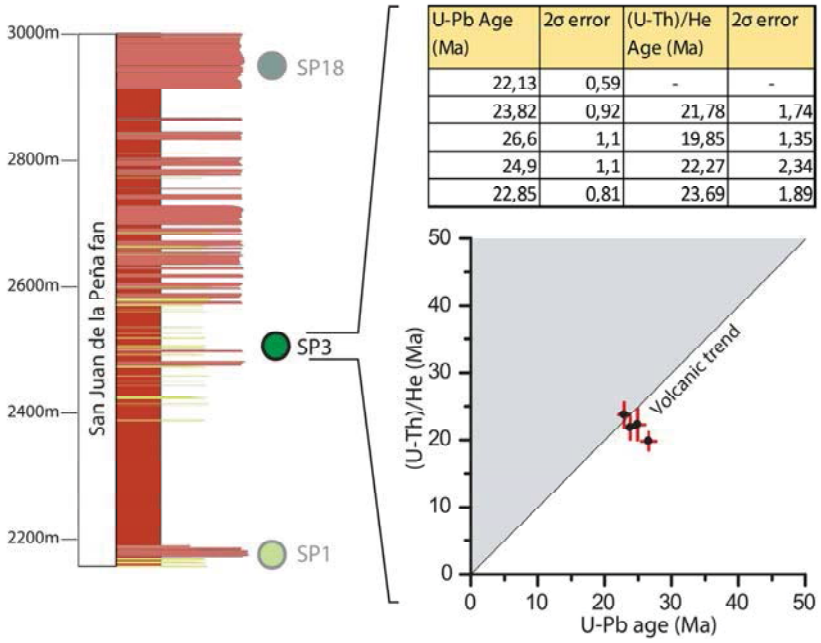

Figure 5. (U-Th)/(He) age versus U-Pb age for double dated Cenozoic grains (red error bars represents 2σ error) of sample SP3 from the basal Bernués Formation.

The occurrence of earliest Miocene volcanic zircons at the base of the alluvial fan and the >400 m-thick sequence of conglomerate above, strongly suggests an early Miocene age for these deposits. This new isotopic maximum depositional age constraints validate the early work of Puigdefàbregas (1975) and Arenas (1993) who pointed to the possibility of an Oligo-Miocene age for this fan (Bernués Formation) on the basis of facies correlation to the Uncastillo Formation in the adjacent Ebro Basin (Fig. 7) (Puigdefàbregas, 1975; Millán-Garrido *et al.*, 1995; Nichols and Hirst, 1998). However subsequent works by Hogan (1993), Montes (2002) and Oliva-Urcia *et al.* (2015) suggested a lower Oligocene age for the Bernués Formation (Fig. 7), implying no temporal correlation between it and the Uncastillo Formation.

These new DZ U-Pb geochronology results clearly reveal a time equivalence of the Bernués and Uncastillo Formations (Fig. 7). This substantiated correlation entails a new Oligo-Miocene paleogeography characterized by alluvial sedimentation within the Jaca Basin (Bernués Formation) at the same time that the southern portions of the basin were uplifted and subjected to erosion and shed into the basin through large alluvial fans in the Ebro foreland basin (Uncastillo Formation).

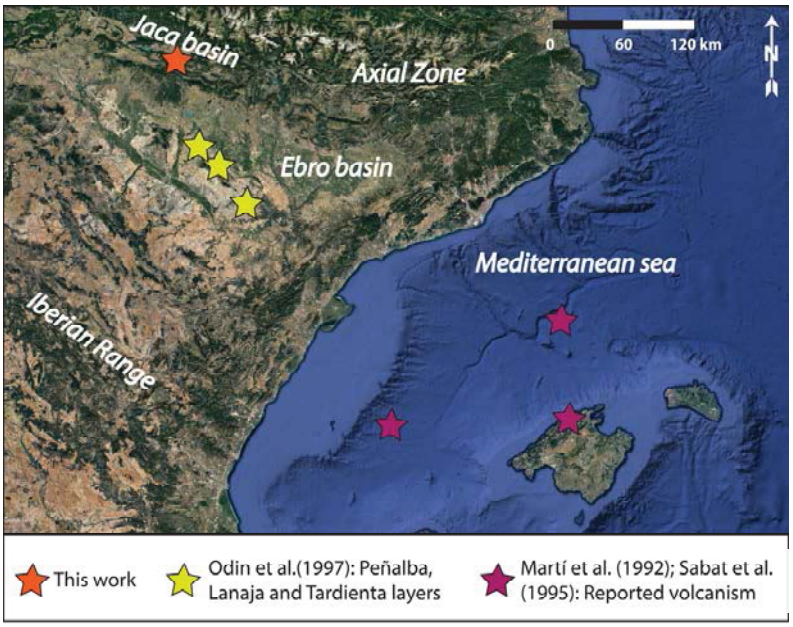

Figure 6. Satellite view of northeastern Iberia, showing the location of the study area (Jaca Basin), the reported outcrops of a Miocene volcanic ash layer in the Ebro Basin (Lanaja, Tardienta and Peñalba) and the position of Oligo-Miocene volcanic domes in the Mediterranean basin.

Likewise, the new proposed age has also implications on the sedimentation rate calculated for the Jaca basin. While Costa *et al.* (2010) proposed an increase of the sediment rates from 25 cm/kyr to 63 cm/kyr (Fig. 8) during the transition from marine to terrestrial environments in the southern part of the basin, our results imply a much lower sedimentation rate and closer those defined for the eastern Ebro Basin.

Considering that in the San Juan de la Peña section, the 2460m of stratigraphic thickness encompasses the last marine deposits (~36 Ma, Costa *et al.* 2010) and the layer containing the volcanic grains (~23 Ma), we can broadly calculate an approximate average sedimentation rate of 16 cm/kyr (Fig. 8). Although this value is only a rough approximation assuming a continuous sedimentation rate, it would be consistent with the response of the sedimentary systems to the basin closure, in which a base level rise in a stage of aggradation and backfilling is expected, as observed in other localities of the Pyrenees (Coney *et al.*, 1996).

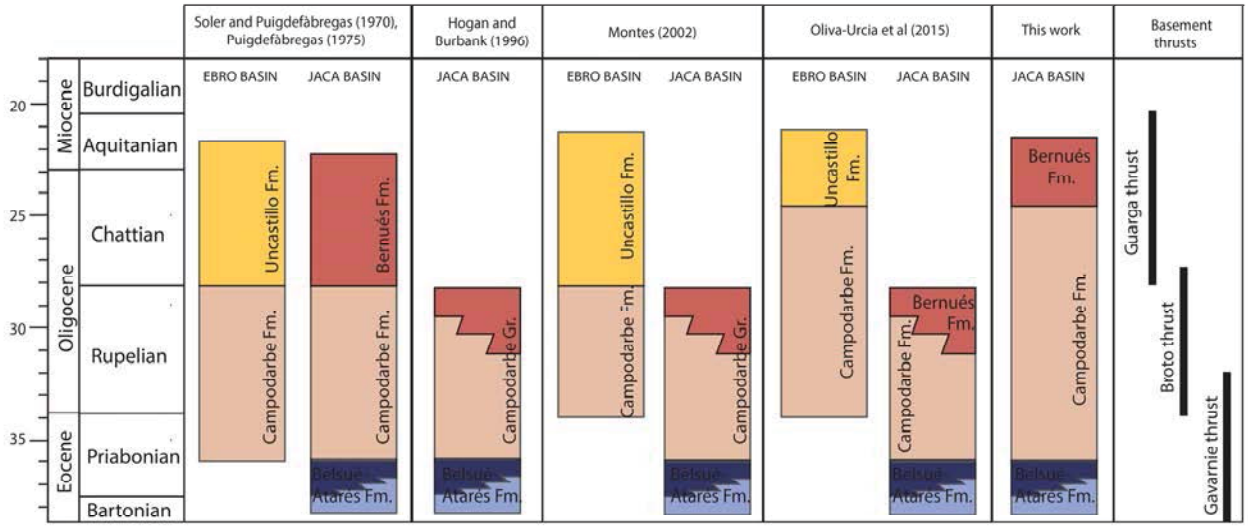

Figure 7. Stratigraphic chart showing the datings and time equivalences between fluvial-alluvial sedimentary formations of the Jaca and Ebro basins proposed by different authors, and the results obtained by this work. Also shown is the timing of the thrusts defined for the Jaca Basin (after Labaume et al., 2016).

This change in age of the synorogenic deposits also requires a reconsideration of the chronology of thrust activity with respect to the basin stratigraphy. The alluvial sedimentation in the Jaca Basin was linked to the Gavarnie thrust (Teixell, 1998; Roigé *et al.*, 2016; Roigé *et al.*, 2017; Labaume *et al.*, 2016), while the Guarga thrust was assumed to set up the uplift and the interruption of sedimentation in the Jaca Basin, which then shifted to the Ebro Basin.

However, the new proposed Miocene age for the San Juan de la Peña strata implies that the accumulation of the conglomerates and clastics were linked to activity along the Guarga thrust and that the tectonic uplift did not impede the sedimentation within the thrust-top basin. The episode of coeval sedimentation in the Jaca and Ebro Basins can be correlated with the strong period of exhumation in the western Axial Zone during Miocene times as recorded by thermochronology (Bosch *et al.*, 2016; Labaume *et al.*, 2016).

Although our results are restricted to the northern part of the Jaca Basin, they emphasize the need for better timing constraints for the syntectonic conglomerates of the southern Pyrenees, which constitute the clues to decipher the last stages of the Pyrenean belt tectono-sedimentary evolution.

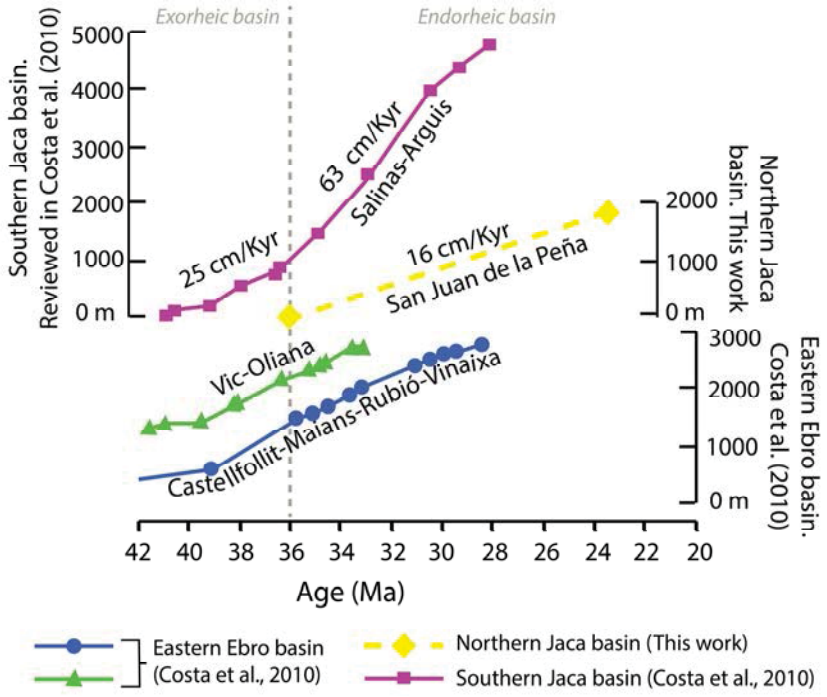

Figure 8. Sedimentation rates for the Jaca Basin and eastern Ebro Basin modified from Costa et al., (2010). The yellow dashed line represents the inferred sedimentation trend from the zircon ages presented in this work.

6. Conclusions

New U-Pb detrital zircon results in the Jaca thrust-top basin of the Southern Pyrenees allow to characterize the provenance changes that occur in the upper fluvial-alluvial deposits of the basin. A sample from the fluvial sediments of the late Eocene to Oligocene Campodarbe Formation is characterized by the dominance of early Variscan zircons (325 and 375 Ma) that are consistent with the erosion of the Carboniferous strata of the Axial Zone or the east-central Pyrenees. However, the overlying alluvial conglomerates of the San Juan de la Peña fan show a progressive decrease on the Variscan signals, that could be associated to the replacement of the eastern Paleozoic source area by a northern source area that produced the recycling of the Eocene Hecho Group turbidites from a less exhumed hinterland.

DZ U-Pb analysis yielded four Cenozoic aged zircons at the base of the San Juan de la Peña fan. According to (U-Th)/(He-Pb) double dating results, these grains have a volcanic origin, likely interpreted as linked with the distant Oligo-Miocene Mediterranean volcanism. This finding allows to propose a Miocene age for the San Juan de la Peña fan, an age much younger than considered before. Therefore, we can infer a new Oligo-Miocene paleogeography for the South Pyrenean foreland characterized by alluvial sedimentation within the Jaca Basin, at the same time that it was uplifted and submitted to erosion by the Guarga thrust, being recycled into the large alluvial fans of the Ebro foreland Basin.

7. Acknowledgements

This work is a contribution to project CGL2014-54180-P, financed by the MINECO of Spain. The authors are grateful for support from the UTChron laboratory of the Jackson School of Geosciences (UT). We thank Lisa Gilley Stockli, Kelly Thomson and Margo Odlum for assistance during the DZ U-Pb analysis and for fruitful discussions.

8. References

Arenas, C., 1993. Sedimentologia y paleogeografia del Terciario del margen pirenaico y sector central de la Cuenca del Ebro (zona aragonesa occidental): Universidad de Zaragoza, 858 p.

Bosch, G. V., Teixell, A., Jolivet, M., Labaume, P., Stockli, D., Domènech, M. and Monié, P., 2016. Timing of Eocene-Miocene thrust activity in the Western Axial Zone and Chaînons Béarnais (west-central Pyrenees) revealed by multi-method thermochronology: *Comptes Rendus - Geoscience*, **348**, p. 246–256, doi: 10.1016/j.crte.2016.01.001.

Canudo, J.I. and Molina, E., 1988. Biocronología de foraminíferos planctónicos de la secuencia deposicional de Jaca (Pirineo Aragonés): Eoceno medio y superior. In: *II Cong. Geol. Esp.* SGE, Granada, p. 273–276.

Coney, P.J., Munoz, J. a., McCLAY, K.R. and Evenchick, C. a., 1996. Syntectonic burial and post-tectonic exhumation of the southern Pyrenees foreland fold-thrust belt: *Journal of the Geological Society*, **153**, p. 9–16, doi: 10.1144/gsjgs.153.1.0009.

Costa, E., Garcés, M., López-Blanco, M., Beamud, E., Gómez-Paccard, M. and Larrasoaña, J.C., 2010. Closing and continentalization of the South Pyrenean foreland basin (NE Spain): Magnetochronological constraints: *Basin Research*, **22**, p. 904–917, doi: 10.1111/j.1365-2117.2009.00452.x.

DeCelles, P.G. and Giles, K.A., 1996. Foreland basin systems - Reply: *Basin Research*, **9**, p. 172–176.

Dickinson, W.R. and Gehrels, G.E., 2009. Use of U-Pb ages of detrital zircons to infer maximum depositional ages of strata: A test against a Colorado Plateau Mesozoic database: *Earth and Planetary Science Letters*, **288**, p. 115–125.

Dickinson, W.R. and Suczek, C.A., 1979. Plate tectonics and sandstone compositions: *AAPG Bulletin*, **63**, p. 2164–2182.

Hart, N.R., Stockli, D.F. and Hayman, N.W., 2016. Provenance evolution during progressive rifting and

hyperextension using bedrock and detrital zircon U-Pb geochronology, Mauléon Basin, western Pyrenees: *Geosphere*, **12**, p. 1166–1186, doi: 10.1130/GES01273.1.

Hogan, P.J., 1993. Geochronologic, Tectonic and Stratigraphic Evolution of the Southwest Pyrenean Foreland Basin, Northern Spain.: University of Southern California, 208 p.

Hogan, P.J. and Burbank, D.W., 1996. Evolution of the Jaca piggyback basin and emergence of the External Sierra, southern Pyrenees: *Tertiary basins of Spain the stratigraphic record of crustal kinematics*, **1**, p. 153–160, doi: 10.1017/CBO9781107415324.004.

Labaume, P., Meresse, F., Jolivet, M., Teixell, A. and Lahfid, A., 2016. Tectono-thermal history of an exhumed trhust-sheet-top basin: an example from the south Pyrenean thrust belt: *Tectonics*,.

Labaume, P., Séguret, M. and Seyve, C., 1985. Evolution of a turbiditic foreland basin and analogy with an accretionary prism: Example of the Eocene South-Pyrenean Basin: *Tectonics*, **4**, p. 661–685, doi: 10.1029/TC004i007p00661.

Mange, M. and Maurer, H.F.W., 1992. *Heavy Minerals in Colour*: Chapman & Hall, London.

Marti, J., Mitjavila, J., Roca, E. and Aparicio, A., 1992. Cenozoic magmatism of the Valencia trough (western Mediterranean): relationships between structural evolution and volcanism (E. Banda and P. Santanach, Eds.): *Tectonophysics*, **203**, p. 145–165.

Martínez, F.J., Dietsch, C., Aleinikoff, J., Cirés, J., Arboleya, M.L. and Reche, J., 2015. Provenance , age , and tectonic evolution of Variscan flysch , southeastern France and northeastern Spain , based on zircon geochronology: *Geological Society of America Bulletin*,, p. 1–18, doi: 10.1130/B31316.1.

Millán-Garrido, H., Pocoví, A. and Casas, A.M., 1995. El frente cabalgamiento surpirenaico en el extremo occidental de las Sierras Exteriores: *Revista de la Sociedad Geologica de España*, **8**, p. 73–90.

Montes, M., 2002. Estratigrafia del Eoceno-Oligoceno de la Cuenca de Jaca (Sinclinorio del Guarga): Universitat de Barcelona, 365 p.

Montes, M. and Colombo, F., 1996. Análisis secuencial y correlación de los abanicos aluviales de Peña Oroel y la Sierra de Candas.(Eoceno superior. Cuenca Surpirenaica Central): *Geogaceta*, **20**, p. 76–79.

Muñoz, J.A., 1992. Evolution of a continental collision belt: ECORS-Pyrenees crustal balanced cross-section. In: *Thrust Tectonics* (McClay, K.R., ed.) Chapman & Hall, London, U.K., p. 235–246.

Nichols, G.J. and Hirst, J.P., 1998. Alluvial fans and fluvial distributary systems, Oligo-Miocene, northern Spain; contrasting processes and products: *Journal of Sedimentary Research*, **68**, p. 879–889, doi: 10.2110/jsr.68.879.

Odin, G.S., Cuenca, G., Canudo, J.I., Cosca, M. and Lago, M., 1997. Biostratigraphy and geochronology of a Miocene continental volcaniclastic layer from the Ebro basin, Spain. In: *Miocene Stratigraphy: an integrated approach* (Montanary, A.,, Odin, G.S., and Coccioni, R., eds.) Elsevier Science, p. 297–310.

Oliva-Urcia, B., Beamud, E., Garces, M., Arenas, C., Soto, R., Pueyo, E.L. and Pardo, G., 2015. New magnetostratigraphic dating of the Palaeogene syntectonic sediments of the west-central Pyrenees: tectonostratigraphic implications: *Palaeomagnetism in Fold and Thrust Belts: New Perspectives. Geological Society, London, Special Publications*, **425**, p. 107–128, doi: 10.1144/SP425.5.

Oms, O., Dinarès-Turell, J. and Remacha, E., 2003. Magnetic stratigraphy from deep clastic turbidites: An example from the Eocene Hecho group (Southern Pyrenees): *Studia Geophysica et Geodaetica*, **47**, p. 275–288, doi: 10.1023/A:1023719607521.

Puigdefàbregas, C., 1975. La sedimentación molásica en la cuenca de Jaca: *Pirineos*, **104**, p. 1–188.

Roigé, M., Gómez-Gras, D., Remacha, E., Boya, S., Viaplana-Muzas, M. and Teixell, A., 2017. Recycling an uplifted early foreland basin fill: An example from the Jaca basin (Southern Pyrenees, Spain): *Sedimentary Geology*, **360**, p. 1–21, doi: 10.1016/j.sedgeo.2017.08.007.

Roigé, M., Gómez-Gras, D., Remacha, E., Daza, R. and Boya, S., 2016. Tectonic control on sediment sources in the Jaca basin (Middle and Upper Eocene of the South-Central Pyrenees): *Comptes Rendus - Geoscience*, **348**, p. 236–245, doi: 10.1016/j.crte.2015.10.005.

Roure, F., Choukroune, P., Berastegui, X., Muñoz, J.A., Villien, A. and Matheron, P., 1989. ECORS deep seismic data and balanced cross sections: Geometric constrains on the evolution of the Pyrenees: *Tectonics*, **8**, p. 41–50.

Sabat, F., Roca, E., Muñoz, J.A., Verges, J., Santanach, P., Masana, E., Sans, M., Estevez, A. and Santiesteban, C., 1995. Role of extension and compression in the evolution of the eastern margin of Iberia: the ESCI-Valencia through seismic profile: *Revista de la Sociedad Geológica de España*, **8**, p. 431–448.

Soler-Sampere, M. and Puigdefàbregas, C., 1970. Líneas generales de la geología del Alto Aragón Occidental: *Pirineos*,, p. 5–20.

Teixell, A., 1998. Crustal structure and orogenic material budget in the west central Pyrenees: *Tectonics*, **17**,

p. 395–406.

Teixell, A., 1996. The Anso transect of the southern Pyrenees: basement and cover thrust geometries: *Journal of the Geological Society*, **153**, p. 301–310, doi: 10.1144/gsjgs.153.2.0301.

Thomson, K.D., Stockli, D.F., Clark, J.D., Puigdefàbregas, C. and Fildani, A., 2017. Detrital zircon (U-Th)/(He-Pb) double-dating constraints on provenance and foreland basin evolution of the Ainsa Basin, south-central Pyrenees, Spain: *Tectonics*, **36**, p. 1352–1375, doi: 10.1002/2017TC004504.

Vergés, J., Fernàndez, M. and Martínez, A., 2002. The Pyrenean orogen: pre-, syn-, and post-collisional evolution: *Journal of the Virtual Explorer*, **8**, p. 57–76, doi: 10.3809/jvirtex.2002.00058.

Vermeesch, P., 2012. On the visualisation of detrital age distributions: *Chemical Geology*, **312**, p. 190–194.

Wolfe, M.R. and Stockli, D.F., 2010. Zircon (U–Th)/He thermochronometry in the KTB drill hole, Germany, and its implications for bulk He diffusion kinetics in zircon: *Earth and Planetary Science Letters*, **295**, p. 69–82.

Supplementary information. Table 1 Reduced detrital zircon U-Pb dataset for all analysis.

Sample Name	[U]	U/Th	207/235	2σ error	206/238	2σ error	RHO	207/235 Age	2σ error	206/238 Age	2σ error	207/206 Age	2σ error	Best age	2σ error	Discordance	Rim /
_Grain	ppm							(Ma)	(Ma)	(Ma)	(Ma)	(Ma)	(Ma)	(Ma)	(Ma)	%	Core
SP17_1_	358	0.795	0.436	0.011	0.059	0.0014	0.67788	366.8	7.7	369.3	8.7	359	46	369.3	8.7	0.682	
SP17_2_	80.2	3.881	0.784	0.03	0.0945	0.0024	0.33354	589	16	582	14	544	84	582	14	1.188	
SP17_3_	78.9	2.692	1.66	0.034	0.1688	0.003	0.4044	992	13	1005	17	961	43	961	43	4.579	
SP17_4_	333.4	8.56	6.7	0.16	0.388	0.011	0.53001	2069	21	2117	55	1996	45	1996	45	6.062	
SP17_5_	207	1.161	0.946	0.024	0.1111	0.0025	0.63483	676	12	679	15	653	43	679	15	0.444	
SP17_6_	89	83.4	1.019	0.028	0.1164	0.0027	0.51686	711	14	710	16	699	56	710	16	0.141	
SP17_7_	277	1.165	0.446	0.0069	0.06211	0.0008	0.17889	374.8	4.9	388.4	4.8	281	45	388.4	4.8	3.629	
SP17_8_	39.8	0.983	12.78	0.16	0.5066	0.0089	0.43741	2665	12	2646	37	2665	29	2665	29	0.713	
SP17_9_	336	1.472	1.817	0.034	0.1773	0.0043	0.68805	1051	12	1052	23	1041	40	1041	40	1.057	
SP17_10_	51	2.284	0.851	0.029	0.0994	0.0023	0.3493	628	17	611	13	699	75	611	13	2.707	
SP17_11_	273.3	10.74	0.639	0.024	0.0834	0.0029	0.50258	503	15	516	17	462	84	516	17	2.584	
SP17_12_	217	1.679	0.3639	0.0076	0.0512	0.00098	0.29816	314.8	5.6	321.8	6	279	53	321.8	6	2.224	
SP17_13_	378	2.61	0.3827	0.0078	0.0523	0.0011	0.40833	328.7	5.7	328.5	6.6	344	54	328.5	6.6	0.061	
SP17_14_	54.4	2.373	6.72	0.15	0.3771	0.0097	0.60081	2074	20	2062	45	2101	46	2101	46	1.856	
SP17_15_	31.8	1.013	0.988	0.044	0.1138	0.003	0.29536	697	22	694	17	778	90	694	17	0.430	
SP17_16_	200.9	0.678	0.9	0.028	0.1056	0.0032	0.61434	650	15	647	19	659	64	647	19	0.462	
SP17_17_	578	1.24	0.4338	0.0074	0.0598	0.001	0.33424	365.6	5.3	374.6	6.2	318	44	374.6	6.2	2.462	
SP17_18_	752	3.38	0.3624	0.0097	0.05125	0.00096	0.19434	313.8	7.2	322.2	5.9	250	64	322.2	5.9	2.677	
SP17_19_	155	1.56	0.902	0.02	0.1105	0.002	0.45198	653	11	675	12	574	46	675	12	3.369	
SP17_20_	141	1.54	1.706	0.03	0.1698	0.0027	0.5631	1014	11	1011	15	1034	28	1034	28	2.224	
SP17_21_	60.6	1.417	0.767	0.043	0.0913	0.003	0.02098	575	24	563	18	620	110	563	18	2.087	
SP17_22_	61.9	8.28	0.978	0.026	0.1119	0.0026	0.15047	695	14	684	15	729	65	684	15	1.583	
SP17_23_	518	2.712	0.8	0.012	0.0962	0.0013	0.62509	597.6	6.7	593.5	8	591	31	593.5	8	0.686	
SP17_24_	644	11.6	0.527	0.012	0.0685	0.0016	0.65906	429.5	7.9	426.9	9.4	435	41	426.9	9.4	0.605	
SP17_25_	359	2.52	2.046	0.045	0.1862	0.0048	0.76499	1129	15	1100	26	1128	37	1128	37	2.482	
SP17_26_	76.3	1.133	0.844	0.026	0.0984	0.002	0.21285	622	14	605	11	655	72	605	11	2.733	
SP17_27_	403	1.245	1.141	0.018	0.1262	0.0023	0.71379	772.1	8.5	767	13	756	25	767	13	0.661	
SP17_29_	138.6	0.827	1.663	0.03	0.1688	0.0027	0.46125	996	11	1005	15	962	36	962	36	4.470	
SP17_30_	288	2.853	0.3788	0.0097	0.05157	0.00077	0.23384	325.7	7.1	324.1	4.7	301	54	324.1	4.7	0.491	
SP17_31_	162	2.352	0.652	0.014	0.0813	0.0014	0.27975	510.2	8.6	503.5	8.5	525	51	503.5	8.5	1.313	
SP17_32_	66	0.925	0.943	0.026	0.1094	0.0021	0.29733	674	14	669	12	695	61	669	12	0.742	
SP17_33_	240	10.92	0.567	0.019	0.0724	0.002	0.54599	455	12	450	12	443	69	450	12	1.099	
SP17_34_	298	2.554	0.3695	0.0074	0.051	0.00093	0.39052	319	5.5	320.6	5.7	320	54	320.6	5.7	0.502	
SP17_35_	1056	1.458	0.4197	0.0068	0.05508	0.0008	0.54494	355.7	4.9	345.6	4.9	428	32	345.6	4.9	2.839	
SP17_36_	1071	3.37	0.526	0.014	0.0692	0.0018	0.4999	428.5	9.2	431	11	443	62	431	11	0.583	
SP17_37_	122.6	2.138	0.72	0.019	0.085	0.0014	0.09319	550	11	525.8	8.2	646	64	525.8	8.2	4.400	
SP17_38_	1202	11.97	0.462	0.019	0.0604	0.002	0.15682	385	13	378	12	450	120	378	12	1.818	
SP17_39_	124.4	1.95	0.682	0.022	0.0803	0.0017	0.12597	527	13	498	10	657	85	498	10	5.503	
SP17_40_	442	62	0.45	0.031	0.0601	0.0029	0.44085	386	27	376	18	410	190	376	18	2.591	Rim
SP17_40_	144.2	1.491	0.992	0.024	0.1146	0.0024	0.48663	701	12	699	14	725	48	699	14	0.285	Core
SP17_41_	267	7.79	2.023	0.037	0.1923	0.0042	0.51276	1123	12	1133	23	1086	39	1086	39	4.328	
SP17_42_	439	18	0.663	0.011	0.0839	0.0011	0.44715	516.2	6.4	519.3	6.8	506	34	519.3	6.8	0.601	
SP17_44_	309	2.81	1.093	0.026	0.1246	0.0023	0.70255	748	12	757	13	739	36	757	13	1.203	
SP17_45_	73.8	1.354	3.61	0.18	0.247	0.011	0.86635	1564	44	1421	55	1767	56	1767	56	19.581	
SP17_46_	125.7	0.564	0.748	0.016	0.0916	0.0018	0.3413	566.2	9.3	565	11	583	52	565	11	0.212	
SP17_48_	401	1.562	0.4541	0.0072	0.05924	0.0008	0.19405	380.6	5.2	371	4.9	400	45	371	4.9	2.522	

Sample Name	[U]	U/Th	207/235	2σ error	206/238	2σ error	RHO	207/235 Age	2σ error	206/238 Age	2σ error	207/206 Age	2σ error	Best age	2σ error	Discordance	Rim /
_Grain	ppm							(Ma)	(Ma)	(Ma)	(Ma)	(Ma)	(Ma)	(Ma)	(Ma)	%	Core
SP17_49_	547	18.3	0.4706	0.0086	0.06221	0.00091	0.63789	392	5.8	389	5.5	400	33	389	5.5	0.765	
SP17_50_	290	4.03	0.988	0.026	0.1082	0.0024	0.41536	700	14	662	14	813	65	662	14	5.429	
SP17_51_	114	1.279	11.84	0.19	0.4938	0.0074	0.54847	2591	15	2591	33	2581	24	2581	24	0.387	
SP17_52_	399	2.047	0.3907	0.0082	0.0532	0.001	0.40848	334.5	6	334.4	6.3	335	55	334.4	6.3	0.030	
SP17_54_	125	1.425	0.433	0.011	0.058	0.0011	0.04777	364.8	7.9	363.1	6.7	366	73	363.1	6.7	0.466	
SP17_55_	101.5	2.058	7.78	0.24	0.401	0.012	0.72319	2207	29	2171	56	2230	43	2230	43	2.646	
SP17_47_	171	2.8	1.104	0.024	0.1241	0.0026	0.52393	754	11	754	15	770	52	754	15	0.000	
SP17_56_	112.7	1.166	1.724	0.036	0.1716	0.0045	0.54062	1016	13	1020	25	1002	44	1002	44	1.796	
SP17_57_	310	2.089	5.38	0.11	0.337	0.0063	0.6479	1882	19	1871	31	1897	30	1897	30	1.371	
SP17_58_	337	4.36	0.6336	0.0093	0.0808	0.0011	0.58647	498.1	5.8	500.6	6.8	504	31	500.6	6.8	0.502	
SP17_59_	175	4.64	0.597	0.016	0.0779	0.0019	0.38848	474.7	9.9	483	11	453	60	483	11	1.748	
SP17_60_	116	1.525	5.71	0.11	0.3535	0.0068	0.70176	1933	17	1954	32	1915	26	1915	26	2.037	
SP17_62_	183.2	2.512	7.29	0.11	0.3955	0.0052	0.72848	2147	13	2147	24	2149	18	2149	18	0.093	
SP17_63_	280.7	1.42	0.4609	0.0098	0.0616	0.0011	0.46099	385.2	6.9	385.6	6.7	380	44	385.6	6.7	0.104	
SP17_64_	259.2	2.616	0.3659	0.0091	0.04952	0.00092	0.22311	316.2	6.7	312.3	5.5	354	59	312.3	5.5	1.233	
SP17_65_	134	1.922	0.643	0.014	0.0821	0.0012	0.12393	503.3	8.9	508.4	7.4	496	62	508.4	7.4	1.013	
SP17_66_	201	1.986	0.427	0.013	0.05122	0.00098	0.26824	360.4	9.3	321.9	6	682	75	DISC	DISC	10.683	
SP17_67_	469	3.02	0.612	0.013	0.0792	0.0017	0.58528	485.9	8.4	491	10	491	44	491	10	1.050	
SP17_68_	544	1.414	0.3849	0.0064	0.05332	0.00084	0.41014	330.5	4.7	334.8	5.2	333	39	334.8	5.2	1.301	
SP17_69_	773	4.85	0.893	0.021	0.1079	0.0024	0.74615	647	11	662	15	574	33	662	15	2.318	
SP17_70_	881	2.218	0.3612	0.0058	0.05	0.00069	0.16305	312.9	4.3	314.5	4.2	309	39	314.5	4.2	0.511	
SP17_71_	158	15.3	1.013	0.07	0.1136	0.0057	0.67622	708	35	693	33	710	100	693	33	2.119	Rim
SP17_71_	208	1.066	4.327	0.098	0.2853	0.0057	0.49799	1698	19	1618	28	1786	48	1786	48	9.406	Core
SP17_73_	170	5.63	0.61	0.015	0.0779	0.0017	0.46241	482.9	9.5	483.6	9.9	460	56	483.6	9.9	0.145	
SP17_74_	103	1.065	17.21	0.32	0.575	0.012	0.66094	2946	17	2926	48	2973	26	2973	26	1.581	
SP17_75_	438	1.053	0.46	0.013	0.0609	0.0016	0.60085	383.8	9.3	381.2	9.5	402	57	381.2	9.5	0.677	
SP17_76_	823	64	0.435	0.01	0.05831	0.00095	0.44297	366.5	7.3	365.3	5.8	385	53	365.3	5.8	0.327	Rim
SP17_76_	36.8	1.06	0.893	0.068	0.1105	0.0059	0.18775	644	37	683	36	590	190	683	36	6.056	Core
SP17_77_	144.7	2.17	0.615	0.014	0.0784	0.0016	0.46231	486.8	8.5	486.5	9.7	481	50	486.5	9.7	0.062	
SP17_78_	241	2.91	0.655	0.034	0.0645	0.0013	0.39814	514	21	403	7.8	1027	89	DISC	DISC	21.595	
SP17_79_	153.9	2.05	0.879	0.017	0.1037	0.0019	0.27034	639.3	9.2	636	11	630	47	636	11	0.516	
SP17_80_	511	1.852	0.952	0.015	0.1102	0.0024	0.70994	678.5	7.9	673	14	656	33	673	14	0.811	
SP17_81_	569	3.57	0.3811	0.0075	0.05155	0.00089	0.5562	327.6	5.5	324	5.4	317	40	324	5.4	1.099	
SP17_83_	273	1.858	0.3695	0.0098	0.05118	0.00093	0.33428	319.8	7.4	321.7	5.7	275	57	321.7	5.7	0.594	
SP17_84_	262	2.712	0.649	0.017	0.0804	0.0021	0.40222	507	11	498	13	575	59	498	13	1.775	
SP17_85_	331	177	0.378	0.02	0.0516	0.0022	0.20803	325	14	325	13	290	120	325	13	0.000	Rim
SP17_85_	192	0.724	0.87	0.02	0.1047	0.0024	0.41317	636	11	642	14	637	55	642	14	0.943	Core
SP17_87_	42.1	0.795	7.21	0.14	0.3947	0.0079	0.59117	2137	17	2148	38	2108	27	2108	27	1.898	
SP17_88_	61.3	0.838	1.411	0.069	0.1478	0.0049	0.49223	902	29	888	27	911	88	911	88	2.525	
SP17_89_	456	3.96	0.3849	0.0091	0.0523	0.0012	0.4567	330.3	6.7	328.6	7.1	356	52	328.6	7.1	0.515	
SP17_90_	146.9	32.9	0.908	0.022	0.1088	0.0024	0.61833	658	11	666	14	631	43	666	14	1.216	
SP17_91_	1077	19.9	0.4685	0.0088	0.0627	0.0011	0.5969	390.8	6.2	391.7	6.8	379	36	391.7	6.8	0.230	
SP17_92_	740	174	0.439	0.012	0.0604	0.0023	0.19599	369.5	8.6	378	14	350	120	378	14	2.300	Rim
SP17_92_	260	1.48	0.834	0.016	0.1004	0.0015	0.23467	615.3	8.8	616.7	8.9	610	51	616.7	8.9	0.228	Core
SP17_93_	638	10.39	0.641	0.019	0.0807	0.0022	0.55332	502	12	500	13	527	64	500	13	0.398	
SP17_94_	89	1.849	0.734	0.027	0.0893	0.0026	0.52707	559	16	553	16	607	72	553	16	1.073	

Sample Name	[U]	U/Th	207/235	2σ error	206/238	2σ error	RHO	207/235 Ag	2σ error	206/238 Ag	2σ error	207/206 Ag	2σ error	Best age	2σ error	Discordance	Rim /
_Grain	ppm							(Ma)	(Ma)	(Ma)	(Ma)	(Ma)	(Ma)	(Ma)	(Ma)	%	Core
SP17_95_	152.6	1.794	0.801	0.017	0.0984	0.0018	0.25074	599.5	9.8	605	10	574	56	605	10	0.917	
SP17_96_	62.8	0.734	0.77	0.032	0.0911	0.0027	0.38974	580	19	562	16	644	87	562	16	3.103	
SP17_97_	276	2.12	0.364	0.022	0.0432	0.0031	0.61353	315	16	272	19	670	110	DISC	DISC	13.651	
SP17_98_	383	0.966	0.711	0.012	0.0875	0.0016	0.49076	544.9	7	540.7	9.3	548	40	540.7	9.3	0.771	
SP17_99_	1046	2.608	0.809	0.016	0.0934	0.002	0.60169	601.4	9.1	576	12	673	42	576	12	4.223	
SP17_100_	333	2.48	0.442	0.018	0.0511	0.001	0.35201	370	12	320.9	6.4	636	80	DISC	DISC	13.270	
SP17_101_	152.7	3.27	0.639	0.017	0.0826	0.002	0.15837	501	10	513	12	447	63	513	12	2.395	
SP17_102_	1050	1.271	0.4216	0.0086	0.0558	0.0011	0.51505	356.8	6.1	350.1	6.9	415	44	350.1	6.9	1.878	
SP17_103_	205	1.398	1.668	0.046	0.1584	0.005	0.16083	995	17	947	28	1104	66	1104	66	14.221	
SP17_104_	429.4	1.005	1.84	0.025	0.1786	0.0023	0.5114	1060.5	8.9	1061	13	1056	27	1056	27	0.473	
SP17_105_	104.9	1.584	1.934	0.051	0.1805	0.0057	0.57832	1091	18	1069	31	1107	50	1107	50	3.433	
SP17_106_	364	2.74	0.3812	0.0072	0.05107	0.0009	0.18975	327.7	5.3	321.7	5.6	369	51	321.7	5.6	1.831	
SP17_108_	179	2.97	0.915	0.022	0.1069	0.002	0.32606	661	12	655	12	678	51	655	12	0.908	
SP17_109_	310	1.97	0.46	0.011	0.0608	0.0014	0.50631	383.7	7.5	380.7	8.8	380	50	380.7	8.8	0.782	
SP17_110_	256	2.41	1.062	0.023	0.1217	0.0028	0.53659	735	11	743	17	663	48	743	17	1.088	
SP17_111_	879	2.02	0.454	0.011	0.0603	0.0011	0.37541	380	7.4	377.5	6.8	331	61	377.5	6.8	0.658	
SP17_113_	400	2.93	0.803	0.015	0.0969	0.0019	0.59152	599.7	8.7	596	11	597	38	596	11	0.617	
SP17_114_	139.9	4.441	0.641	0.014	0.0802	0.0015	0.52953	502.1	8.4	498.3	8.6	474	42	498.3	8.6	0.757	
SP17_115_	134.8	0.801	2.015	0.064	0.1956	0.0055	0.63899	1117	22	1151	30	996	47	996	47	15.562	
SP17_116_	70.7	1.443	6.37	0.14	0.3699	0.0085	0.7007	2028	19	2027	40	2013	35	2013	35	0.695	
SP17_118_	333	2.71	0.663	0.011	0.0844	0.0012	0.5096	516.3	6.7	522.3	6.9	455	33	522.3	6.9	1.162	
SP17_119_	83	2.8	0.785	0.025	0.095	0.0032	0.52199	587	14	585	19	655	68	585	19	0.341	
SP17_120_	200	1.132	0.842	0.014	0.1012	0.0021	0.45559	620	7.8	621	13	606	48	621	13	0.161	
SP1_1_	130.5	1.112	0.775	0.02	0.0908	0.0018	0.69014	583	11	560	11	646	45	560	11	3.945	
SP1_2_	306	2.65	0.758	0.037	0.09	0.0047	0.65116	571	22	555	28	824	79	555	28	2.802	Rim
SP1_2_	283.1	2.67	0.667	0.085	0.1316	0.0035	0.26973	511	49	797	20	1160	120	DISC	DISC	55.969	Core
SP1_3_	201.1	0.2818	0.861	0.018	0.1019	0.0019	0.4021	630	9.6	625	11	628	40	625	11	0.794	
SP1_4_	151	0.688	0.96	0.036	0.1149	0.0024	0.00032	682	18	701	14	866	79	701	14	2.786	
SP1_5_	61.4	2.29	0.599	0.02	0.078	0.0022	0.31194	477	13	486	13	431	84	486	13	1.887	
SP1_6_	481	8.43	0.888	0.012	0.1065	0.0016	0.69806	644.7	6.5	652.5	9.4	617	22	652.5	9.4	1.210	
SP1_8_	372	2.863	1.809	0.031	0.1772	0.003	0.52343	1049	11	1051	17	1025	29	1025	29	2.537	
SP1_9_	602	1.821	1.312	0.023	0.1449	0.0021	0.6807	851.6	9.7	872	12	803	28	803	12	2.395	
SP1_10_	220.5	1.78	0.797	0.018	0.097	0.0016	0.56121	596	10	597	9.6	587	44	597	9.6	0.168	
SP1_11_	352	1.73	0.986	0.02	0.1148	0.0022	0.6231	696	10	700	13	658	41	700	13	0.575	
SP1_12_	305	1.439	0.487	0.011	0.0632	0.0014	0.46118	403.2	7.6	394.9	8.3	455	55	394.9	8.3	2.059	
SP1_13_	58.7	1.831	0.717	0.036	0.0851	0.0026	0.45595	558	23	526	15	660	100	526	15	5.735	
SP1_14_	599	1.945	1.1	0.017	0.1298	0.0025	0.58877	753	8	786	14	691	30	786	14	4.382	
SP1_15_	100.9	1.475	0.968	0.025	0.1151	0.0022	0.35504	688	13	702	13	628	59	702	13	2.035	
SP1_16_	99.6	0.35	14.45	0.63	0.2145	0.0071	0.78038	2781	44	1251	38	4227	35	DISC	DISC	70.405	
SP1_17_	81.2	1.528	5.76	0.1	0.3638	0.007	0.61813	1938	16	2003	34	1911	33	1911	33	4.814	
SP1_18_	388	10.91	0.781	0.011	0.098	0.0016	0.53293	585.7	6.2	602.6	9.6	543	31	602.6	9.6	2.885	
SP1_19_	63.8	0.881	1.726	0.039	0.1741	0.0035	0.49969	1018	15	1034	19	1017	38	1017	38	1.672	
SP1_20_	167.5	3.86	0.949	0.024	0.1117	0.0024	0.58404	676	13	683	14	659	48	683	14	1.036	
SP1_21_	196.7	0.756	5.605	0.059	0.3558	0.0043	0.78484	1916.1	9.2	1965	21	1877	16	1877	16	4.688	
SP1_22_	355	1.52	0.377	0.0098	0.0501	0.0015	0.60462	324.5	7.2	315.3	9	402	47	315.3	9	2.835	

Sample Name	[U]	U/Th	207/235	2σ error	206/238	2σ error	RHO	207/235 Age	2σ error	206/238 Age	2σ error	207/206 Age	2σ error	Best age	2σ error	Discordance	Rim /
_Grain	ppm							(Ma)	(Ma)	(Ma)	(Ma)	(Ma)	(Ma)	(Ma)	(Ma)	%	Core
SP1_23_	189.8	9.9	0.865	0.042	0.1033	0.0029	0.25979	632	23	634	17	650	110	634	17	0.316	Rim
SP1_23_	128.1	0.75	1.891	0.078	0.1817	0.0059	0.68483	1076	27	1076	32	1115	51	1115	51	3.498	Core
SP1_24_	289	2.77	0.863	0.021	0.1039	0.0027	0.64756	631	11	637	16	632	46	637	16	0.951	
SP1_25_	880	2.18	0.3897	0.0063	0.05401	0.00073	0.38484	333.9	4.6	339	4.5	331	37	339	4.5	1.527	
SP1_26_	149.6	2.23	0.868	0.041	0.1083	0.0022	0.4588	633	22	663	13	580	100	663	13	4.739	
SP1_27_	363	3.13	0.297	0.011	0.0384	0.0014	0.34094	264.1	8.7	242.6	8.4	493	82	242.6	8.4	8.141	
SP1_28_	230.2	0.593	1.581	0.051	0.1515	0.004	0.66981	961	20	909	23	1095	46	1095	46	16.986	
SP1_29_	98.6	0.616	1.983	0.045	0.1968	0.0045	0.6105	1110	15	1158	24	1022	42	1022	42	13.307	
SP1_30_	74.3	0.588	1.932	0.044	0.1953	0.0035	0.51845	1097	15	1150	19	1034	44	1034	44	11.219	
SP1_32_	566	2.329	0.4625	0.0075	0.0626	0.0011	0.36808	385.7	5.2	391.6	6.5	349	45	391.6	6.5	1.530	
SP1_33_	1018	11.47	0.952	0.021	0.1136	0.0037	0.48018	680	12	697	21	636	60	697	21	2.500	Rim
SP1_33_	431	3.81	2.4	0.13	0.19	0.014	0.80588	1240	39	1122	74	1486	70	1486	70	24.495	Core
SP1_34_	732	1.451	0.3567	0.0064	0.04809	0.0007	0.43898	309.6	4.8	302.8	4.3	356	41	302.8	4.3	2.196	
SP1_35_	271.8	1.497	0.951	0.078	0.098	0.0031	0.38154	671	38	602	18	890	140	DISC	DISC	10.283	
SP1_36_	169	2.162	0.731	0.021	0.0942	0.0025	0.35968	556	12	580	15	465	79	580	15	4.317	
SP1_37_	408	2.97	0.3744	0.0076	0.0517	0.001	0.46921	323.2	5.7	325	6.2	326	42	325	6.2	0.557	
SP1_38_	188.8	4.32	1.404	0.095	0.0898	0.003	0.29399	886	42	554	18	1860	110	DISC	DISC	37.472	
SP1_39_	160.2	0.664	1.202	0.034	0.1344	0.0035	0.40904	801	15	813	20	758	66	813	20	1.498	
SP1_40_	535	1.673	12.93	0.18	0.536	0.0081	0.85989	2674	13	2765	34	2593	13	2593	13	6.633	
SP1_41_	1580	3.18	0.857	0.024	0.0979	0.0029	0.82699	628	13	605	16	733	35	605	16	3.662	
SP1_42_	185.3	1.261	1.343	0.019	0.1479	0.0025	0.46232	863.9	8.3	889	14	804	36	804	14	2.905	
SP1_43_	345.5	3.84	1.187	0.023	0.134	0.0032	0.68305	793	11	810	18	743	34	810	18	2.144	
SP1_44_	67.4	0.769	2.203	0.067	0.201	0.0045	0.47685	1183	21	1180	24	1180	57	1180	57	0.000	
SP1_45_	362	9.83	0.654	0.013	0.0828	0.0015	0.50901	511	8.1	513	8.8	505	40	513	8.8	0.391	
SP1_46_	396	23.1	0.67	0.012	0.0849	0.0016	0.49449	520.3	7.6	525.2	9.6	471	43	525.2	9.6	0.942	
SP1_47_	128	1.37	1.059	0.024	0.1224	0.0025	0.38247	734	11	744	15	679	44	744	15	1.362	
SP1_48_	235.1	1.557	0.415	0.012	0.0525	0.0013	0.43669	353.2	8.4	330.1	8.1	480	70	330.1	8.1	6.540	
SP1_49_	744	3.35	0.381	0.011	0.0507	0.0019	0.60709	327.6	7.8	319	12	390	62	319	12	2.625	
SP1_50_	243	1.521	1.26	0.034	0.1341	0.0035	0.68378	826	15	811	20	871	44	811	20	1.816	
SP1_52_	506	2.354	0.93	0.017	0.109	0.002	0.4991	668	8.6	667	11	647	35	667	11	0.150	
SP1_53_	753	3.12	1.296	0.03	0.1374	0.0047	0.74364	844	13	830	26	922	36	830	26	1.659	
SP1_54_	135.7	1.162	1.218	0.028	0.1366	0.0037	0.60303	810	13	825	21	767	44	825	21	1.852	
SP1_55_	412	8.49	1.583	0.033	0.1639	0.0031	0.51512	963	13	978	17	923	41	923	41	5.959	
SP1_56_	140.7	0.619	2.008	0.037	0.1989	0.0042	0.50601	1117	13	1169	22	1038	45	1038	45	12.620	
SP1_57_	286	0.858	1.706	0.039	0.1683	0.0042	0.75579	1009	15	1002	23	1026	34	1026	34	2.339	
SP1_58_	423	0.4249	0.888	0.017	0.1067	0.002	0.72443	645.8	9	653	11	637	31	653	11	1.115	
SP1_59_	234	2.79	0.694	0.014	0.0899	0.002	0.48042	534.4	8.6	555	12	413	50	555	12	3.855	
SP1_60_	1510	0.776	0.4421	0.0057	0.05961	0.00086	0.69717	371.5	4	373.2	5.2	371	23	373.2	5.2	0.458	
SP1_61_	418	1.18	0.892	0.022	0.1017	0.0024	0.5512	646	12	624	14	728	48	624	14	3.406	
SP1_62_	371	3.01	0.3406	0.0082	0.04728	0.00091	0.4578	298.7	6.2	297.8	5.6	293	52	297.8	5.6	0.301	
SP1_63_	68.5	0.677	6.27	0.11	0.3632	0.0071	0.59879	2012	15	2000	34	2043	28	2043	28	2.105	
SP1_64_	140.2	0.825	0.723	0.023	0.089	0.0023	0.14056	552	14	549	14	559	87	549	14	0.543	
SP1_65_	192	8	0.644	0.037	0.0801	0.0053	0.49933	509	23	496	32	550	130	496	32	2.554	
SP1_66_	360	2.059	0.789	0.015	0.0979	0.002	0.52785	590.2	8.4	602	12	552	43	602	12	1.999	
SP1_67_	492	3.28	0.3786	0.0072	0.0534	0.0011	0.48106	325.8	5.3	335.3	6.6	296	47	335.3	6.6	2.916	
SP1_68_	406	2.163	0.3817	0.0078	0.05177	0.00094	0.31997	328	5.7	325.3	5.8	376	45	325.3	5.8	0.823	

Sample Name	[U]	U/Th	207/235	2σ error	206/238	2σ error	RHO	207/235 Age	2σ error	206/238 Age	2σ error	207/206 Age	2σ error	Best age	2σ error	Discordance	Rim /
_Grain	ppm							(Ma)	(Ma)	(Ma)	(Ma)	(Ma)	(Ma)	(Ma)	(Ma)	%	Core
SP1_69_	329	3.9	0.39	0.013	0.0534	0.0018	0.38534	334	9.4	337	10	373	79	337	10	0.898	
SP1_70_	297.6	2.497	0.702	0.017	0.0885	0.0019	0.62884	539	10	547	11	547	44	547	11	1.484	
SP1_71_	795	1.385	0.431	0.012	0.0507	0.0019	0.51832	365.6	7.9	319	12	693	69	DISC	DISC	12.746	
SP1_72_	175.2	1.064	1.481	0.03	0.1508	0.0034	0.60122	924	12	905	19	966	37	966	37	6.315	
SP1_73_	868	15.4	6.53	0.14	0.3887	0.0071	0.82992	2049	19	2116	33	2000	20	2000	20	5.800	Rim
SP1_73_	72.2	1.42	13.34	0.28	0.531	0.011	0.54739	2703	20	2743	47	2648	33	2648	33	3.588	Core
SP1_74_	598	1.382	0.4055	0.0072	0.0562	0.001	0.63071	345.4	5.2	352.1	6.2	298	33	352.1	6.2	1.940	
SP1_75_	158.8	3.06	0.674	0.018	0.0864	0.002	0.5118	522	11	534	12	481	52	534	12	2.299	
SP1_76_	155.9	1.122	4.14	0.11	0.307	0.0078	0.67779	1662	21	1725	39	1574	34	1574	34	9.593	
SP1_77_	430	9.23	0.661	0.01	0.0826	0.0013	0.50549	515.6	6.2	512.7	7.3	506	33	512.7	7.3	0.562	
SP1_78_	368	30.5	0.89	0.036	0.1024	0.0042	0.77073	645	20	628	25	671	67	628	25	2.636	
SP1_79_	616	2.52	0.3763	0.0074	0.05249	0.00099	0.42236	324.1	5.4	329.8	6.1	284	48	329.8	6.1	1.759	
SP1_80_	438	5.67	0.622	0.013	0.0772	0.0014	0.45378	490.5	8.3	479.3	8.5	558	48	479.3	8.5	2.283	
SP1_81_	491	1.86	0.391	0.0081	0.0528	0.0012	0.66882	334.7	5.9	331.4	7.4	346	36	331.4	7.4	0.986	
SP1_82_	141.4	0.705	0.855	0.015	0.102	0.0017	0.36952	626.5	8.4	626	10	640	43	626	10	0.080	
SP1_83_	946	20.2	0.3782	0.0056	0.05175	0.00079	0.62846	325.5	4.1	325.2	4.9	328	27	325.2	4.9	0.092	
SP1_84_	101	1.908	0.982	0.038	0.0885	0.0019	0.29474	691	19	548	12	1179	76	DISC	DISC	20.695	
SP1_85_	841	1.143	1.495	0.03	0.155	0.0026	0.79174	927	12	929	15	896	25	896	25	3.683	
SP1_86_	162.5	2.041	1.038	0.024	0.1149	0.0027	0.52813	724	12	703	16	785	44	703	16	2.901	
SP1_87_	482	5.04	0.787	0.011	0.0953	0.0013	0.55084	590.2	6.1	586.5	7.9	609	32	586.5	7.9	0.627	
SP1_88_	501	1.184	0.912	0.013	0.107	0.0016	0.52578	657.5	6.8	654.9	9.1	647	30	654.9	9.1	0.395	
SP1_89_	476	2.33	0.3844	0.0072	0.05023	0.00081	0.28617	330	5.3	315.9	5	406	44	315.9	5	4.273	
SP1_90_	80.4	1.421	1.795	0.036	0.1714	0.0041	0.52654	1042	13	1019	22	1063	48	1063	48	4.139	
SP1_91_	188.9	6.05	0.929	0.025	0.1104	0.0039	0.63743	666	13	674	23	643	52	674	23	1.201	
SP1_92_	453	1.675	5.67	0.1	0.3581	0.0076	0.68482	1927	16	1971	36	1866	27	1866	27	5.627	
SP1_93_	63.7	0.881	2.023	0.058	0.196	0.0047	0.65615	1120	20	1157	26	1053	44	1053	44	9.877	
SP1_94_	106.5	1.31	0.363	0.012	0.0496	0.0012	0.19848	315.5	8.7	311.9	7.2	307	75	311.9	7.2	1.141	
SP1_95_	185	2.023	0.401	0.011	0.054	0.0012	0.08919	342.2	8.1	339.1	7.2	367	68	339.1	7.2	0.906	
SP1_96_	204.1	1.93	0.619	0.013	0.0777	0.0012	0.58719	488.6	8.3	482.6	7.4	485	40	482.6	7.4	1.228	
SP1_97_	200	1.097	3.244	0.098	0.2354	0.0076	0.94821	1468	23	1367	39	1612	22	1612	22	15.199	
SP1_98_	188	0.94	1.796	0.032	0.1811	0.003	0.63945	1043	11	1073	17	987	29	987	29	8.713	
SP1_99_	209	0.789	0.866	0.015	0.1034	0.0016	0.49989	632.5	8.2	634.4	9.5	647	35	634.4	9.5	0.300	
SP1_100_	158	1.619	7.55	0.13	0.4251	0.0087	0.74734	2179	15	2281	39	2090	23	2090	23	9.139	
SP1_101_	500	12.23	0.927	0.015	0.1073	0.0019	0.71496	665.3	8.1	657	11	688	29	657	11	1.248	
SP1_102_	368	2.42	0.962	0.024	0.1093	0.0024	0.54585	685	13	668	14	756	50	668	14	2.482	
SP1_103_	125	0.93	0.816	0.024	0.0983	0.0032	0.4493	606	13	604	19	603	83	604	19	0.330	
SP1_104_	508	1.4	0.3391	0.0064	0.04788	0.00085	0.37157	297.6	4.6	301.5	5.3	275	45	301.5	5.3	1.310	
SP1_105_	234.4	2.31	0.811	0.014	0.0987	0.0016	0.51105	604.5	7.5	607.8	9.1	611	38	607.8	9.1	0.546	
SP1_106_	741	186	0.879	0.024	0.1063	0.0032	0.71684	642	13	651	19	614	52	651	19	1.402	Rim
SP1_106_	194.2	1.717	1.626	0.049	0.1698	0.0063	0.79902	980	19	1011	35	972	47	972	47	4.012	Core
SP1_107_	284	1.615	0.439	0.014	0.0555	0.0013	0.38497	369.2	9.7	348	7.8	537	63	348	7.8	5.742	
SP1_108_	155.2	1.166	1.816	0.024	0.1861	0.0024	0.474	1052.7	8.2	1101	13	976	26	976	26	12.807	
SP1_109_	1143	3.107	0.922	0.019	0.109	0.0026	0.75669	663	10	667	15	677	32	667	15	0.603	
SP1_110_	174	2.48	0.725	0.018	0.0915	0.0023	0.54794	552	11	564	13	537	56	564	13	2.174	
SP1_111_	226	5.69	0.3804	0.0087	0.05269	0.00087	0.36842	328.5	6.2	331	5.4	304	49	331	5.4	0.761	
SP1_112_	198.6	3.96	0.771	0.036	0.0931	0.0051	0.61369	581	20	573	30	600	100	573	30	1.377	

Sample Name	[U]	U/Th	207/235	2σ error	206/238	2σ error	RHO	207/235 Age	2σ error	206/238 Age	2σ error	207/206 Age	2σ error	Best age	2σ error	Discordance
_Grain	ppm							(Ma)	(Ma)	(Ma)	(Ma)	(Ma)	(Ma)	(Ma)	(Ma)	%
SP1_113_	316.3	1.231	0.902	0.017	0.1079	0.0015	0.40722	653.2	9.1	660.6	8.8	643	37	660.6	8.8	1.133
SP1_114_	439	2.413	0.942	0.016	0.1114	0.0019	0.58642	673.1	8.3	680	11	647	33	680	11	1.025
SP1_115_	538	39.7	0.92	0.034	0.1107	0.0045	0.62997	661	18	677	26	623	82	677	26	2.421
SP1_115_	92.8	1.1	1.646	0.046	0.1642	0.0058	0.35476	991	17	980	32	995	74	995	74	1.508
SP1_116_	90.8	1.759	0.964	0.03	0.1169	0.0033	0.24139	685	16	713	19	570	83	713	19	4.088
SP1_117_	103.5	1.478	0.956	0.023	0.1118	0.0025	0.55575	680	12	683	14	665	52	683	14	0.441
SP1_118_	40.2	0.976	13.02	0.24	0.525	0.012	0.64183	2678	17	2717	50	2634	29	2634	29	3.151
SP1_119_	316.6	0.895	1.746	0.026	0.1753	0.0031	0.68633	1025	9.7	1043	17	974	30	974	30	7.084
SP1_120_	141.7	2.01	1.373	0.075	0.1357	0.0025	0.45471	863	25	820	14	962	69	820	14	4.983
SP3_1_	180.2	0.855	0.913	0.037	0.1056	0.0031	0.42603	658	19	647	18	714	79	647	18	1.672
SP3_2_	385	3.3	0.992	0.015	0.1166	0.0024	0.54538	699.4	7.7	711	14	640	36	711	14	1.659
SP3_3_	939	24.2	0.4217	0.0081	0.0581	0.0014	0.58756	357.9	6	364	8.6	306	44	364	8.6	1.704
SP3_5_	78.8	1.033	1.719	0.035	0.1751	0.0029	0.44141	1019	12	1040	16	968	38	968	38	7.438
SP3_6_	190	3.01	0.837	0.016	0.1005	0.0019	0.34525	616.7	8.9	617	11	618	47	617	11	0.049
SP3_7_	329.5	1.26	1.335	0.036	0.1345	0.0045	0.55335	861	16	813	25	945	54	813	25	5.575
SP3_9_	48.7	2.322	1.492	0.049	0.154	0.0046	0.53086	927	19	923	26	904	69	904	69	2.102
SP3_10_	213	2.27	7.38	0.45	0.319	0.018	0.8867	2159	54	1790	85	2551	51	2551	51	29.831
SP3_11_	271.5	1.126	0.879	0.015	0.1059	0.0018	0.59836	639.9	8.3	649	10	622	35	649	10	1.422
SP3_12_	277	5.89	0.919	0.026	0.1113	0.0029	0.48329	661	14	680	17	576	60	680	17	2.874
SP3_13_	95	1.002	7.33	0.13	0.4256	0.0091	0.73872	2151	16	2284	41	2017	33	2017	33	13.237
SP3_14_	158.5	3.37	0.712	0.015	0.0898	0.0018	0.34218	546.3	8.7	554	10	522	52	554	10	1.409
SP3_15_	162.3	0.2542	13.16	0.15	0.5395	0.0064	0.66477	2691	11	2780	27	2616	16	2616	16	6.269
SP3_16_	219	1.101	1.001	0.023	0.1187	0.0027	0.61085	705	12	723	16	644	46	723	16	2.553
SP3_17_	101.1	1.382	0.828	0.026	0.0964	0.0028	0.48366	611	14	593	16	709	78	593	16	2.946
SP3_18_	526	1.698	1.511	0.037	0.1384	0.0034	0.88517	937	15	835	19	1177	23	DISC	DISC	10.886
SP3_20_	175	1.74	0.402	0.0087	0.05414	0.00094	0.27909	342.7	6.3	339.9	5.8	380	52	339.9	5.8	0.817
SP3_21_	164	2.663	1.796	0.034	0.1848	0.0038	0.66399	1046	12	1095	20	978	31	978	31	11.963
SP3_22_	399	1.54	0.974	0.021	0.1122	0.002	0.43176	692	11	685	12	719	47	685	12	1.012
SP3_23_	274	1.123	0.93	0.016	0.1073	0.0018	0.43918	666.9	8.2	657	11	708	36	657	11	1.484
SP3_24_	145	0.797	5.725	0.08	0.3619	0.0061	0.64428	1937	13	1990	29	1873	22	1873	22	6.247
SP3_25_	115.8	1.063	4.092	0.066	0.3037	0.0044	0.63633	1651	13	1709	22	1574	26	1574	26	8.577
SP3_27_	346.2	1.612	1.251	0.012	0.1402	0.0015	0.4504	823.7	5.6	845.8	8.7	770	24	845.8	8.7	2.683
SP3_28_	48.2	2.208	1.346	0.047	0.1431	0.0036	0.41082	863	21	862	20	857	78	857	78	0.583
SP3_29_	240.9	0.783	0.945	0.018	0.114	0.0019	0.72709	674.7	9.2	696	11	585	36	696	11	3.157
SP3_30_	674	0.927	0.928	0.015	0.1113	0.0015	0.43915	667.9	7.3	680.2	8.6	636	35	680.2	8.6	1.842
SP3_31_	231.1	9.2	0.645	0.017	0.0763	0.0021	0.53067	505	10	474	13	592	60	474	13	6.139
SP3_32_	452	1.82	2.024	0.055	0.1986	0.0051	0.81265	1122	18	1167	27	1041	30	1041	30	12.104
SP3_33_	171.5	0.615	0.859	0.022	0.1016	0.002	0.60223	632	12	624	11	694	42	624	11	1.266
SP3_34_	144.8	2.08	5.78	0.082	0.3695	0.0059	0.58887	1943	12	2030	27	1860	26	1860	26	9.140
SP3_35_	234	1.383	1.211	0.018	0.1387	0.0019	0.49153	805.9	7.9	837	11	731	32	837	11	3.859
SP3_36_	281	0.3601	1.013	0.027	0.1216	0.0019	0.33709	710	13	740	11	629	47	740	11	4.225
SP3_37_	98	1.152	1.402	0.026	0.1504	0.0029	0.4106	888	11	903	16	839	38	839	16	1.689
SP3_38_	143.3	1.2	0.965	0.023	0.1133	0.0025	0.49754	686	12	691	15	695	49	691	15	0.729
SP3_39_	286	0.871	13.54	0.42	0.542	0.018	0.94153	2717	30	2785	75	2656	18	2656	18	4.857
SP3_40_	1430	7.13	0.3831	0.0072	0.0518	0.001	0.82851	329.8	5.4	325.5	6.2	353	27	325.5	6.2	1.304

Sample Name	[U]	U/Th	207/235	2σ error	206/238	2σ error	RHO	207/235 Age	2σ error	206/238 Age	2σ error	207/206 Age	2σ error	Best age	2σ error	Discordance	Rim /
_Grain	ppm							(Ma)	(Ma)	(Ma)	(Ma)	(Ma)	(Ma)	(Ma)	(Ma)	%	Core
SP3_41_	292	1.954	1.785	0.038	0.181	0.0043	0.76192	1039	14	1072	24	963	34	963	34	11.319	
SP3_42_	92.4	0.815	6.38	0.11	0.3795	0.0068	0.81075	2029	15	2072	32	1980	22	1980	22	4.646	
SP3_43_	990	1.657	0.4016	0.0072	0.05542	0.00069	0.38933	342.6	5.2	347.7	4.2	317	33	347.7	4.2	1.489	
SP3_44_	39.3	2.6	4.11	0.13	0.242	0.01	0.81145	1658	28	1405	55	2057	44	DISC	DISC	31.697	
SP3_45_	68.3	1.86	1.383	0.03	0.1497	0.0019	0.2558	882	13	899	11	809	43	809	11	1.927	
SP3_46_	675	3.54	0.681	0.016	0.075	0.0028	0.68795	526.8	9.6	466	17	779	58	DISC	DISC	11.541	
SP3_47_	206	1.165	1.078	0.026	0.1209	0.0033	0.55954	741	13	735	19	769	48	735	19	0.810	
SP3_48_	27.8	0.445	4.49	0.35	0.265	0.018	0.5076	1726	66	1510	90	2020	130	2020	130	25.248	
SP3_49_	249	6.46	0.566	0.018	0.0703	0.0023	0.65169	457	11	438	14	512	63	438	14	4.158	
SP3_50_	198	1.366	5.272	0.098	0.3251	0.0071	0.57777	1865	16	1818	33	1936	30	1936	30	6.095	
SP3_51_	351	37.3	6.97	0.19	0.411	0.012	0.83916	2113	24	2215	56	1998	24	1998	24	10.861	
SP3_52_	783	3.34	0.968	0.013	0.1153	0.0015	0.59033	687.9	7.1	703.3	8.7	630	27	703.3	8.7	2.239	
SP3_53_	98.7	1.032	1.009	0.022	0.1131	0.002	0.28268	707	11	690	12	786	51	690	12	2.405	
SP3_55_	121	4.02	3.67	0.14	0.279	0.0089	0.86608	1563	31	1585	45	1598	46	1598	46	0.814	
SP3_56_	363	2.419	1.123	0.015	0.1286	0.0014	0.39219	764	7.3	780.9	8.4	713	31	780.9	8.4	2.212	
SP3_57_	140.4	0.4222	0.385	0.015	0.0493	0.0014	0.27437	330	11	310.2	8.4	474	94	310.2	8.4	6.000	
SP3_58_	208	53.3	0.465	0.022	0.0632	0.0024	0.49073	387	15	395	14	427	97	395	14	2.067	Rim
SP3_58_	108.1	8.51	1.604	0.069	0.1231	0.0036	0.46148	970	27	753	22	1488	83	DISC	DISC	22.371	Core
SP3_59_	273.4	1.957	1.002	0.014	0.1204	0.0014	0.44424	704.5	6.9	733	8.2	632	29	733	8.2	4.045	
SP3_60_	140.4	1.985	0.963	0.037	0.1118	0.0041	0.44548	684	19	683	24	711	83	683	24	0.146	Rim
SP3_60_	155.1	2.034	12.65	0.29	0.511	0.016	0.88106	2653	22	2677	64	2674	30	2674	30	0.112	Core
SP3_61_	157.5	0.588	6.435	0.086	0.3896	0.0052	0.7262	2036	12	2120	24	1970	17	1970	17	7.614	
SP3_62_	377	2.991	0.482	0.016	0.0533	0.0013	0.72028	398	11	334.4	7.9	793	50	DISC	DISC	15.980	
SP3_63_	667	1.267	8.65	0.12	0.4348	0.0077	0.86408	2301	13	2327	35	2274	14	2274	14	2.331	
SP3_64_	243	2.21	3.09	0.23	0.243	0.019	0.98433	1417	62	1390	100	1481	23	1481	23	6.144	
SP3_65_	339	3.438	18.9	0.38	0.612	0.017	0.72396	3036	20	3075	68	3035	35	3035	35	1.318	
SP3_66_	42.8	0.744	2.462	0.052	0.2271	0.0042	0.3444	1265	15	1319	22	1185	48	1185	48	11.308	
SP3_67_	222.4	1.848	1.513	0.036	0.1661	0.004	0.56758	937	15	990	22	815	44	815	22	5.656	
SP3_68_	1233	5.13	0.938	0.011	0.1167	0.0014	0.69042	671.5	5.7	711.6	8.2	546	22	711.6	8.2	5.972	
SP3_69_	542	5.516	0.91	0.014	0.113	0.0018	0.74313	657.3	7.3	690	10	557	23	690	10	4.975	
SP3_70_	2630	2.497	0.527	0.018	0.0479	0.0017	0.88932	429	12	301	10	1203	32	DISC	DISC	29.837	
SP3_71_	348	1.35	0.873	0.015	0.1042	0.0019	0.54315	637.7	8.4	640	11	627	37	640	11	0.361	
SP3_72_	592	1.969	0.3131	0.0065	0.04315	0.00095	0.51436	276.4	5	272.3	5.9	316	45	272.3	5.9	1.483	
SP3_73_	608	0.894	0.0223	0.0012	0.003439	0.000093	0.2255	22.4	1.2	22.13	0.59	60	110	22.13	0.59	1.205	
SP3_74_	281	1.349	0.824	0.02	0.1008	0.003	0.65026	611	11	618	17	578	52	618	17	1.146	
SP3_75_	39.7	1.631	12.64	0.72	0.358	0.02	0.91389	2635	52	1964	95	3246	39	DISC	DISC	39.495	
SP3_76_	397	5.77	0.3941	0.0068	0.05427	0.00061	0.21982	337.1	4.9	340.7	3.7	309	40	340.7	3.7	1.068	
SP3_77_	626	10.38	0.95	0.02	0.1139	0.0021	0.58049	678	10	695	12	604	39	695	12	2.507	
SP3_78_	335	1.34	1.844	0.042	0.1769	0.0049	0.69247	1060	15	1050	27	1030	46	1030	46	1.942	
SP3_79_	366	2.72	0.407	0.011	0.0569	0.0013	0.33593	346.3	7.7	357.7	8.4	277	67	357.7	8.4	3.292	
SP3_80_	300	2.682	0.869	0.013	0.1046	0.0016	0.50472	634.8	7.2	641.3	9.6	608	33	641.3	9.6	1.024	
SP3_81_	1360	6.14	0.627	0.015	0.0804	0.002	0.87287	493.6	9.6	498	12	462	27	498	12	0.891	
SP3_82_	88.5	1.338	1.76	0.05	0.1738	0.0047	0.71907	1030	19	1032	26	1038	43	1038	43	0.578	
SP3_83_	252.3	1.039	7.34	0.15	0.429	0.011	0.67337	2151	19	2305	48	2032	35	2032	35	13.435	
SP3_84_	100.2	0.3359	0.973	0.022	0.1135	0.002	0.27107	690	11	693	12	692	48	693	12	0.435	
SP3_85_	521	1.422	0.876	0.013	0.1074	0.0018	0.5155	638.4	6.9	657	10	550	34	657	10	2.914	

Sample Name	[U]	U/Th	207/235	2σ error	206/238	2σ error	RHO	207/235 Age	2σ error	206/238 Age	2σ error	207/206 Age	2σ error	Best age	2σ error	Discordance	Rim /
_Grain	ppm							(Ma)	(Ma)	(Ma)	(Ma)	(Ma)	(Ma)	(Ma)	(Ma)	%	Core
SP3_86_	201	0.823	0.929	0.018	0.1126	0.0022	0.37493	667.5	9.5	687	13	613	36	687	13	2.921	
SP3_87_	122.2	2.475	1.388	0.034	0.1473	0.0031	0.40646	884	15	886	17	882	50	882	50	0.454	
SP3_88_	620	7.96	0.589	0.017	0.0764	0.002	0.75065	470	11	475	12	444	48	475	12	1.064	
SP3_89_	197	2.453	1.092	0.021	0.1285	0.0029	0.45066	750	10	779	16	672	45	779	16	3.867	
SP3_90_	109.9	0.57	0.388	0.013	0.0526	0.0012	0.21595	333	9.4	330.6	7.2	345	81	330.6	7.2	0.721	
SP3_91_	213	1.996	0.3998	0.0082	0.05135	0.00083	0.21755	341.2	6	322.8	5.1	485	50	322.8	5.1	5.393	
SP3_92_	372	7.46	0.6173	0.0085	0.0793	0.0014	0.47236	488.6	5.5	491.6	8.1	454	38	491.6	8.1	0.614	
SP3_93_	515	2.72	0.947	0.019	0.1139	0.0022	0.61779	675	10	695	13	618	38	695	13	2.963	
SP3_94_	834	3.19	0.3677	0.0068	0.0505	0.001	0.69757	317.7	5	317.3	6.4	324	35	317.3	6.4	0.126	
SP3_95_	599	0.89	0.969	0.018	0.1138	0.0022	0.65724	689.4	9.1	694	13	639	33	694	13	0.667	
SP3_96_	70.4	0.603	0.865	0.026	0.0996	0.0025	0.1739	634	15	612	15	642	83	612	15	3.470	
SP3_97_	222	1.653	0.761	0.022	0.0895	0.0025	0.5283	575	13	553	15	620	66	553	15	3.826	
SP3_98_	253	2.15	1.216	0.039	0.1311	0.0052	0.48506	807	18	793	29	872	73	793	29	1.735	
SP3_99_	188	3.01	0.697	0.018	0.0856	0.0022	0.31626	536	11	531	13	542	69	531	13	0.933	
SP3_100_	217.9	2.58	0.566	0.014	0.0709	0.0012	0.40514	455.8	9.1	441.8	7.2	485	54	441.8	7.2	3.072	
SP3_101_	91	2.191	1.038	0.03	0.1213	0.003	0.44546	721	15	738	17	661	64	738	17	2.358	
SP3_102_	522	5.01	0.879	0.03	0.1044	0.0031	0.83137	640	16	640	18	635	44	640	18	0.000	Rim
SP3_102_	174	0.706	2.138	0.066	0.206	0.0054	0.72392	1159	21	1207	29	1038	43	1038	43	16.281	Core
SP3_103_	357	2.38	0.4104	0.0085	0.05597	0.00085	0.42084	348.8	6.1	351	5.2	310	48	351	5.2	0.631	
SP3_104_	517	2.48	1.277	0.02	0.1355	0.0021	0.70248	836.8	9.1	819	12	877	26	819	12	2.127	
SP3_105_	598	1.475	4.68	0.16	0.293	0.011	0.86542	1756	28	1650	56	1904	33	1904	33	13.340	
SP3_107_	236.2	1.301	0.92	0.014	0.1084	0.0011	0.29412	664.4	7.4	663.3	6.1	653	33	663.3	6.1	0.166	
SP3_108_	442	28.8	0.977	0.015	0.1159	0.0019	0.52198	692.3	7.6	707	11	641	31	707	11	2.123	
SP3_109_	405	1.759	1.333	0.028	0.1485	0.0029	0.70502	859	12	892	16	772	27	772	16	3.842	
SP3_110_	156	1.357	1.718	0.038	0.1703	0.0034	0.55023	1016	14	1013	19	998	36	998	36	1.503	
SP3_111_	810	8.38	1.03	0.011	0.1191	0.0012	0.56623	718.8	5.5	725.1	7	695	22	725.1	7	0.876	
SP3_112_	1247	16.66	0.4866	0.0067	0.0652	0.001	0.6736	402.4	4.5	407	6.2	344	27	407	6.2	1.143	
SP3_113_	952	74	2.007	0.041	0.1964	0.0044	0.85369	1116	14	1155	24	1036	22	1036	22	11.486	
SP3_114_	158.5	1.357	1.255	0.022	0.1385	0.0022	0.09778	826.6	9.6	836	13	797	48	836	13	1.137	
SP3_115_	68.3	1.365	8.13	0.13	0.4369	0.0061	0.4976	2246	15	2336	27	2192	28	2192	28	6.569	
SP3_116_	182	8.29	0.69	0.017	0.0887	0.0021	0.44125	532	10	548	12	449	57	548	12	3.008	
SP3_117_	384	2.163	5.315	0.07	0.3325	0.0051	0.77183	1873	12	1850	25	1896	19	1896	19	2.426	
SP3_118_	73.1	1.296	1.004	0.034	0.1158	0.0022	0.3565	704	17	706	13	691	64	706	13	0.284	
SP3_119_	96.4	0.902	5.96	0.3	0.379	0.025	0.71323	1968	44	2060	110	1832	79	1832	79	12.445	
SP3_120_	633	71.7	1.043	0.018	0.1222	0.0024	0.59168	724.9	9.1	743	14	654	38	743	14	2.497	
SP3(bis)_1	363	3.73	0.583	0.011	0.0748	0.0016	0.33974	466.2	7.1	466.4	9.9	495	54	466.4	9.9	0.043	
SP3(bis)_2	488	1.56	0.767	0.038	0.0794	0.0046	0.66102	584	23	492	27	1043	91	DISC	DISC	15.753	
SP3(bis)_3	189	5.11	1.569	0.046	0.1595	0.0056	0.64843	961	18	953	31	997	56	997	56	4.413	
SP3(bis)_4	401	1.414	0.0249	0.0018	0.0037	0.00014	0.15705	24.9	1.8	23.82	0.92	140	150	23.82	0.92	4.337	
SP3(bis)_5	331	2.7	0.3793	0.0092	0.0527	0.0012	0.27047	327.3	6.4	330.9	7.3	312	58	330.9	7.3	1.100	
SP3(bis)_6	41.9	0.764	0.116	0.013	0.01586	0.00084	0.09611	110	11	101.4	5.3	260	220	101.4	5.3	7.818	
SP3(bis)_7	312	2.017	0.388	0.013	0.05	0.0019	0.61657	332.6	9.9	316	11	495	81	316	11	4.991	
SP3(bis)_8	64	1.67	0.974	0.035	0.1136	0.0046	0.42461	688	18	692	26	766	80	692	26	0.581	
SP3(bis)_9	306.3	4.14	0.634	0.017	0.0777	0.0016	0.23413	498	10	482.3	9.6	619	64	482.3	9.6	3.153	
SP3(bis)_10	146.1	1.688	1.224	0.022	0.1358	0.0028	0.41975	812	10	821	16	802	45	821	16	1.108	

Sample Name	[U]	U/Th	207/235	2σ error	206/238	2σ error	RHO	207/235 Age	2σ error	206/238 Age	2σ error	207/206 Age	2σ error	Best age	2σ error	Discordance	Rim /
_Grain	ppm							(Ma)	(Ma)	(Ma)	(Ma)	(Ma)	(Ma)	(Ma)	(Ma)	%	Core
SP3(bis)_11	118.6	2.267	0.842	0.028	0.0969	0.0039	0.57389	622	16	600	22	746	81	600	22	3.537	
SP3(bis)_12	601	1.279	0.028	0.0022	0.00413	0.00017	0.01418	28	2.2	26.6	1.1	240	190	26.6	1.1	5.000	
SP3(bis)_13	473	2.234	0.3441	0.0095	0.0469	0.001	0.37572	299.8	7.2	295.2	6.2	330	60	295.2	6.2	1.534	
SP3(bis)_14	276.7	2.39	0.363	0.01	0.0496	0.0012	0.40757	313.7	7.6	311.7	7.5	354	65	311.7	7.5	0.638	
SP3(bis)_15	190.1	1.31	0.834	0.022	0.102	0.0029	0.57225	616	12	626	17	595	55	626	17	1.623	
SP3(bis)_16	504	4.43	0.579	0.014	0.0761	0.0021	0.57137	465	8.4	473	13	429	49	473	13	1.720	
SP3(bis)_17	134.9	1.042	0.684	0.029	0.0781	0.002	0.51517	528	17	484	12	737	85	484	12	8.333	
SP3(bis)_18	549	3.01	0.3513	0.0079	0.0478	0.0013	0.52293	305.5	5.9	301.1	8.1	391	58	301.1	8.1	1.440	
SP3(bis)_19	690	3.28	0.748	0.02	0.0896	0.0033	0.47258	566	12	553	20	672	70	553	20	2.297	
SP3(bis)_20	409	1.713	0.848	0.026	0.1006	0.0031	0.36816	623	14	618	18	655	74	618	18	0.803	
SP3(bis)_21	686	9.9	0.573	0.032	0.0731	0.0035	0.38119	459	21	455	21	560	130	455	21	0.871	
SP3(bis)_22	310	1.85	0.3444	0.0083	0.0477	0.0011	0.49153	301.8	6	300.5	6.5	309	52	300.5	6.5	0.431	
SP3(bis)_23	417	38.1	0.595	0.029	0.0731	0.0038	0.67572	473	18	461	25	550	100	461	25	2.537	Rim
SP3(bis)_23	400	1.258	1.587	0.052	0.1631	0.0058	0.72609	964	20	973	32	972	50	972	50	0.103	Core
SP3(bis)_24	168	0.72	0.751	0.017	0.0912	0.0023	0.31283	568.1	9.6	563	14	645	62	563	14	0.898	
SP3(bis)_25	84.8	1.98	1.122	0.037	0.1243	0.0038	0.49051	765	17	755	21	822	64	755	21	1.307	
SP3(bis)_26	324	2.504	0.3759	0.0088	0.0503	0.001	0.2701	324.6	6.7	316.6	6.2	400	59	316.6	6.2	2.465	
SP3(bis)_27	439	1.635	0.3411	0.0085	0.0478	0.0011	0.54141	299.3	6.4	301	6.7	260	53	301	6.7	0.568	
SP3(bis)_28	466	1.457	0.3547	0.0087	0.04702	0.00084	0.6029	307.9	6.5	296.2	5.2	375	48	296.2	5.2	3.800	
SP3(bis)_29	280	1.168	0.652	0.016	0.0792	0.0017	0.50995	508.9	9.5	491	10	594	48	491	10	3.517	
SP3(bis)_30	305	2.122	0.841	0.038	0.1054	0.0028	0.64705	619	21	646	16	574	74	646	16	4.362	
SP3(bis)_31	572	1.44	9.19	0.23	0.4224	0.0082	0.74263	2358	22	2270	37	2453	30	2453	30	7.460	
SP3(bis)_32	196.4	2.275	0.757	0.016	0.0922	0.0021	0.53458	572.9	9.8	569	12	612	48	569	12	0.681	
SP3(bis)_33	357	1.942	9.25	0.22	0.374	0.0082	0.86346	2360	22	2047	38	2637	20	2637	20	22.374	
SP3(bis)_34	275	0.959	1.73	0.026	0.1692	0.0029	0.60423	1023.4	9.8	1007	16	1068	32	1068	32	5.712	
SP3(bis)_35	274	5.21	0.58	0.013	0.0749	0.0019	0.64939	465.9	7.9	465	11	456	45	465	11	0.193	
SP3(bis)_36	469	2.68	0.688	0.013	0.0859	0.0015	0.5575	534.1	8.1	531.4	8.9	531	39	531.4	8.9	0.506	
SP3(bis)_37	121	1.094	0.717	0.018	0.0832	0.0019	0.51352	551	11	515	11	695	55	515	11	6.534	
SP3(bis)_38	1380	2.04	0.321	0.01	0.0428	0.0012	0.73019	281.9	7.9	269.9	7.2	401	46	269.9	7.2	4.257	
SP3(bis)_39	380	2.25	0.813	0.016	0.0938	0.0017	0.69041	603.3	8.9	578	10	675	34	578	10	4.194	
SP3(bis)_40	181.7	6.64	0.537	0.016	0.0705	0.002	0.31957	438	10	439	12	433	76	439	12	0.228	
SP3(bis)_41	127.7	0.955	1.552	0.044	0.1559	0.0038	0.4458	950	18	934	21	998	55	998	55	6.413	
SP3(bis)_42	301	2.144	0.356	0.011	0.0477	0.001	0.62087	309.6	8.1	300.3	6.4	350	58	300.3	6.4	3.004	
SP3(bis)_43	125	2.78	0.921	0.036	0.1121	0.004	0.59311	662	19	685	23	623	65	685	23	3.474	
SP3(bis)_44	219	1.74	0.598	0.014	0.0751	0.0015	0.41495	476.3	8.9	466.7	8.7	487	45	466.7	8.7	2.016	
SP3(bis)_45	446	1.61	0.91	0.018	0.105	0.0019	0.59864	657.4	9.3	643	11	653	36	643	11	2.190	
SP3(bis)_46	190	2.61	0.39	0.01	0.0501	0.0013	0.39297	334	7.6	315.1	8	419	69	315.1	8	5.659	
SP3(bis)_47	228	1.969	0.747	0.023	0.088	0.0023	0.50608	566	13	544	13	643	56	544	13	3.887	
SP3(bis)_48	287	1.74	0.344	0.0097	0.045	0.0019	0.51728	300	7.4	284	12	412	79	284	12	5.333	
SP3(bis)_49	137	0.974	0.748	0.022	0.0912	0.0018	0.41567	567	13	563	11	563	63	563	11	0.705	
SP3(bis)_50	202	4.21	0.328	0.012	0.0444	0.0013	0.54455	288.6	8.9	280.9	7.8	333	68	280.9	7.8	2.668	
SP3(bis)_51	265	1.37	6.56	0.23	0.375	0.014	0.84687	2059	27	2066	63	2076	35	2076	35	0.482	
SP3(bis)_52	265	3.19	0.909	0.028	0.1093	0.0036	0.49479	655	15	669	21	602	71	669	21	2.137	
SP3(bis)_53	300	2.158	0.3399	0.0085	0.0488	0.001	0.38505	296.7	6.5	307.3	6.1	217	61	307.3	6.1	3.573	
SP3(bis)_54	79.5	0.935	2.335	0.077	0.1581	0.0056	0.61326	1220	24	945	31	1783	63	DISC	DISC	46.999	
SP3(bis)_55	387	1.715	0.3482	0.0075	0.04807	0.00099	0.61535	303.1	5.7	303.3	6.2	296	44	303.3	6.2	0.066	

Sample Name	[U]	U/Th	207/235	2σ error	206/238	2σ error	RHO	207/235 Ag	2σ error	206/238 Ag	2σ error	207/206 Ag	2σ error	Best age	2σ error	Discordance	Rim /
_Grain	ppm							(Ma)	(Ma)	(Ma)	(Ma)	(Ma)	(Ma)	(Ma)	(Ma)	%	Core
SP3(bis)_56	238	2.299	0.3574	0.0083	0.04783	0.00097	0.16554	309.9	6.2	301.2	5.9	337	67	301.2	5.9	2.807	
SP3(bis)_57	135.2	1.409	0.513	0.016	0.0695	0.0016	0.29832	420	10	432.8	9.8	357	71	432.8	9.8	3.048	
SP3(bis)_58	112.4	1.496	0.61	0.032	0.0739	0.0039	0.67754	482	20	459	24	601	94	459	24	4.772	
SP3(bis)_59	256	7.17	0.643	0.016	0.0814	0.002	0.56552	506	10	504	12	478	52	504	12	0.395	
SP3(bis)_60	307	1.586	0.3623	0.0096	0.04862	0.00086	0.49563	314.2	7.2	306	5.3	329	51	306	5.3	2.610	
SP3(bis)_61	282	1.637	0.438	0.015	0.0565	0.0014	0.31851	368	11	354.4	8.7	444	81	354.4	8.7	3.696	
SP3(bis)_62	227	1.131	0.778	0.034	0.082	0.0042	0.73308	583	20	508	25	865	64	DISC	DISC	12.864	
SP3(bis)_63	303	8.33	0.534	0.014	0.0656	0.0014	0.63777	434.9	9.6	409.8	8.5	527	39	409.8	8.5	5.771	
SP3(bis)_64	507	2.57	0.622	0.016	0.0779	0.0026	0.48648	490.3	9.9	484	16	530	58	484	16	1.285	
SP3(bis)_65	355	1.761	0.777	0.015	0.0933	0.0019	0.46053	583	8.9	575	11	595	43	575	11	1.372	
SP3(bis)_66	863	2.95	0.38	0.013	0.0513	0.0016	0.81379	325.8	9.3	322	10	339	42	322	10	1.166	
SP3(bis)_67	405	2.88	0.4071	0.0085	0.0553	0.0011	0.47261	346.4	6.1	347.5	6.6	330	43	347.5	6.6	0.318	
SP3(bis)_68	433	1.337	0.0274	0.0033	0.00386	0.00017	0.13747	27.4	3.3	24.9	1.1	260	250	24.9	1.1	9.124	
SP3(bis)_69	270	1.37	0.806	0.021	0.0973	0.002	0.78159	599	12	598	12	620	37	598	12	0.167	
SP3(bis)_70	499	1.45	0.37	0.012	0.0497	0.0016	0.68637	319.8	8.8	312.5	9.9	374	54	312.5	9.9	2.283	
SP3(bis)_71	417	3	1.007	0.021	0.1165	0.003	0.66386	706	10	710	18	690	41	710	18	0.567	
SP3(bis)_72	950	5.94	0.2687	0.0082	0.0332	0.0012	0.63487	241.4	6.5	210.4	7.4	557	61	DISC	DISC	12.842	
SP3(bis)_73	301	2.149	0.608	0.015	0.0762	0.0017	0.47666	481.7	9.6	473	10	552	57	473	10	1.806	
SP3(bis)_74	493	1.541	0.3678	0.0097	0.0494	0.0012	0.58912	317.7	7.2	310.9	7.4	372	55	310.9	7.4	2.140	
SP3(bis)_75	210.2	1.32	1.059	0.025	0.1187	0.0021	0.48277	735	12	723	12	746	45	723	12	1.633	
SP3(bis)_76	536	2.96	0.387	0.011	0.0504	0.0014	0.28015	331.7	8	318.1	8.9	463	76	318.1	8.9	4.100	
SP3(bis)_77	1030	21.1	0.593	0.019	0.0743	0.0028	0.81456	472	12	462	16	487	69	462	16	2.119	Rim
SP3(bis)_77	152	1.656	14.49	0.74	0.467	0.029	0.92123	2771	52	2460	130	3003	47	3003	47	18.082	Core
SP3(bis)_78	111.7	2.42	0.792	0.021	0.0959	0.0023	0.47706	593	12	592	14	614	62	592	14	0.169	
SP3(bis)_79	204	2.49	0.561	0.015	0.0709	0.0022	0.34114	452.4	9.5	441	13	485	77	441	13	2.520	
SP3(bis)_80	212	8.97	0.518	0.015	0.0648	0.0018	0.36389	424.6	9.6	404	11	519	68	404	11	4.852	
SP3(bis)_81	65.9	1.827	1.027	0.037	0.1152	0.0033	0.26186	719	18	703	19	799	68	703	19	2.225	
SP3(bis)_82	187	0.994	0.765	0.025	0.0918	0.0031	0.64616	578	14	566	18	625	63	566	18	2.076	
SP3(bis)_83	208	2.82	0.72	0.014	0.085	0.0016	0.58182	549.9	8.2	525.5	9.4	600	39	525.5	9.4	4.437	
SP3(bis)_84	216	4.64	0.566	0.017	0.0692	0.0015	0.3591	454	11	431	9.1	586	66	431	9.1	5.066	
SP3(bis)_85	451	2.64	0.364	0.013	0.0468	0.0014	0.43458	316	10	294.9	8.6	440	76	294.9	8.6	6.677	
SP3(bis)_86	217.1	2.67	0.368	0.0087	0.0504	0.0012	0.39092	318.5	6.6	317.1	7.6	298	58	317.1	7.6	0.440	
SP3(bis)_87	226	1.72	0.358	0.011	0.049	0.0013	0.40856	309.9	8.1	308	7.8	305	63	308	7.8	0.613	
SP3(bis)_88	234	0.768	0.805	0.017	0.0976	0.0021	0.48782	598.9	9.5	600	12	606	46	600	12	0.184	
SP3(bis)_89	369	3.72	0.3505	0.0072	0.04837	0.00099	0.52194	305.6	5.5	304.5	6.1	292	46	304.5	6.1	0.360	
SP3(bis)_90	394	1.828	0.3566	0.0079	0.04812	0.00095	0.59367	309.4	5.9	302.9	5.9	382	45	302.9	5.9	2.101	
SP3(bis)_91	218	4.19	0.576	0.013	0.0753	0.0019	0.60578	461.4	8.4	469	11	443	52	469	11	1.647	
SP3(bis)_92	294	2.85	0.595	0.018	0.0739	0.0022	0.48456	473	12	459	13	548	68	459	13	2.960	
SP3(bis)_93	59	1.978	1.441	0.042	0.1434	0.0035	0.42492	904	18	864	20	997	65	997	65	13.340	
SP3(bis)_94	805	0.862	0.0235	0.0016	0.00355	0.00013	0.03984	23.5	1.5	22.85	0.81	110	140	22.85	0.81	2.766	
SP3(bis)_95	274	2.82	0.3674	0.0086	0.0497	0.001	0.397	317.3	6.3	313.6	6.1	327	51	313.6	6.1	1.166	
SP3(bis)_96	267	7.91	0.38	0.014	0.0535	0.0018	0.48243	327	10	336	11	315	86	336	11	2.752	
SP3(bis)_97	156	2.097	0.959	0.032	0.1065	0.0027	0.43694	684	16	652	16	797	59	652	16	4.678	
SP3(bis)_98	170	0.778	0.345	0.018	0.0474	0.0018	0.63688	300	14	299	11	285	83	299	11	0.333	
SP3(bis)_99	432	2.288	0.407	0.014	0.0545	0.0016	0.11482	346.1	9.8	342	9.5	396	93	342	9.5	1.185	
SP3(bis)_100	386	1.84	0.908	0.024	0.1074	0.0028	0.59185	657	12	657	17	666	53	657	17	0.000	

Sample Name _Grain	[U] ppm	U/Th	207/235	2σ error	206/238	2σ error	RHO	207/235 Age (Ma)	2σ error (Ma)	206/238 Age (Ma)	2σ error (Ma)	207/206 Age (Ma)	2σ error (Ma)	Best age (Ma)	2σ error (Ma)	Discordance %	Rim / Core
SP3(bis)_101	169	2.121	0.3325	0.0094	0.0475	0.001	0.45167	292	7.3	298.9	6.4	270	57	298.9	6.4	2.363	
SP3(bis)_102	237	3.33	0.577	0.014	0.074	0.0017	0.52043	463.1	9.1	460	10	507	50	460	10	0.669	
SP3(bis)_103	462	1.594	0.375	0.014	0.0518	0.0019	0.7126	322	10	326	12	263	66	326	12	1.242	
SP3(bis)_104	315	4.66	0.592	0.013	0.0752	0.0016	0.32938	472.8	7.9	467.5	9.4	437	56	467.5	9.4	1.121	
SP3(bis)_105	160	2.71	2.328	0.055	0.2168	0.0058	0.64447	1222	17	1264	31	1156	45	1156	45	9.343	
SP3(bis)_106	89.3	0.809	8.75	0.28	0.392	0.014	0.80986	2313	30	2128	67	2458	32	2458	32	13.426	
SP3(bis)_107	287	1.463	0.516	0.021	0.0372	0.0018	0.1653	420	14	235	11	1544	97	DISC	DISC	44.048	
SP3(bis)_108	143	2.17	0.64	0.024	0.0811	0.0019	0.23807	501	15	503	12	500	78	503	12	0.399	
SP3(bis)_110	257	2.627	0.382	0.013	0.0501	0.0012	0.45938	329.4	9.1	315.3	7.6	367	74	315.3	7.6	4.281	
SP3(bis)_111	130.3	9.21	0.907	0.029	0.1083	0.0041	0.22422	654	15	662	24	620	100	662	24	1.223	
SP3(bis)_112	628	2.534	0.3502	0.0083	0.04661	0.00097	0.48518	305.3	6.2	293.6	6	336	46	293.6	6	3.832	
SP3(bis)_113	245	8.86	0.711	0.019	0.0901	0.0024	0.57889	546	11	556	14	481	51	556	14	1.832	
SP3(bis)_114	566	1.899	0.268	0.0086	0.0277	0.0011	0.44515	241.9	7.1	176.3	6.9	929	73	DISC	DISC	27.119	
SP3(bis)_115	377	1.636	0.3684	0.0079	0.0497	0.0011	0.41325	318.2	5.9	312.9	6.7	347	54	312.9	6.7	1.666	
SP3(bis)_116	528	2.504	0.632	0.017	0.0787	0.0023	0.57131	497	10	490	14	521	59	490	14	1.408	
SP3(bis)_117	613	2.53	0.3668	0.0083	0.049	0.0011	0.51001	316.9	6.2	308.3	7	340	51	308.3	7	2.714	
SP3(bis)_118	238	1.816	0.354	0.015	0.048	0.0019	0.41304	307	11	302	12	217	79	302	12	1.629	
SP3(bis)_119	226	1.21	0.339	0.01	0.04468	0.00091	0.35476	297.7	7.7	281.8	5.6	383	72	281.8	5.6	5.341	
SP3(bis)_120	273	3.03	0.505	0.021	0.0564	0.0016	0.58995	414	14	353.5	9.7	772	65	DISC	DISC	14.614	
SP3(bis)_121	523	1.424	0.748	0.025	0.0866	0.0031	0.62936	569	14	535	18	665	62	535	18	5.975	
SP18_1_	859	56.2	7.76	0.2	0.3452	0.0086	0.86127	2205	24	1910	41	2481	25	2481	25	23.015	
SP18_2_	644	16.7	6.35	0.19	0.3101	0.0093	0.66599	2022	27	1740	46	2320	46	2320	46	25.000	
SP18_3_	91.3	0.913	0.719	0.016	0.0898	0.0018	0.6297	552	9.4	554	11	531	42	554	11	0.362	
SP18_4_	130	1.521	2.077	0.084	0.18	0.0083	0.70401	1137	28	1065	45	1285	68	1285	68	17.121	
SP18_5_	298	1.721	6.7	0.19	0.37	0.013	0.81819	2068	24	2023	59	2120	33	2120	33	4.575	
SP18_6_	57	3.12	0.604	0.026	0.0727	0.0025	0.2827	481	17	452	15	623	98	452	15	6.029	
SP18_7_	187	1.136	0.953	0.026	0.0952	0.0027	0.53854	680	14	586	16	1001	53	DISC	DISC	13.824	
SP18_8_	91.5	2.054	1.87	0.027	0.1834	0.0029	0.55006	1069.8	9.7	1085	16	1026	31	1026	31	5.750	
SP18_9_	69.7	2.94	6.86	0.13	0.3802	0.0081	0.69308	2094	16	2081	39	2118	26	2118	26	1.747	
SP18_10_	177.4	6.14	0.623	0.021	0.0782	0.0023	0.43069	491	13	485	14	497	79	485	14	1.222	
SP18_11_	62	2.86	1.655	0.081	0.1675	0.0082	0.68165	989	31	998	45	938	77	938	77	6.397	
SP18_12_	558	3.146	0.4023	0.0069	0.05451	0.00099	0.50911	343.1	4.9	342.1	6	351	39	342.1	6	0.291	
SP18_13_	233	9.17	0.729	0.014	0.091	0.0019	0.46705	556.5	8.1	561	11	526	40	561	11	0.809	
SP18_14_	936	1.71	0.4005	0.0056	0.05452	0.00086	0.65722	341.8	4.1	342.2	5.3	351	28	342.2	5.3	0.117	
SP18_15_	246	5.06	1.472	0.042	0.1528	0.0048	0.74334	920	17	920	26	919	42	919	42	0.109	
SP18_16_	515	11.1	1.131	0.04	0.1166	0.0065	0.62088	767	19	710	38	921	93	710	38	7.432	
SP18_17_	40.1	0.53	4.804	0.077	0.3241	0.0067	0.4369	1785	13	1809	33	1756	32	1756	32	3.018	
SP18_18_	66.6	0.49	0.895	0.022	0.1053	0.002	0.3672	652	12	645	12	687	55	645	12	1.074	
SP18_19_	322	35.5	1.044	0.026	0.1213	0.0034	0.73028	724	13	738	19	718	43	738	19	1.934	
SP18_20_	96.6	3.39	1.436	0.036	0.1475	0.0047	0.72484	902	15	886	26	949	41	949	41	6.639	
SP18_21_	556	2.29	0.855	0.018	0.1011	0.002	0.63776	629.4	9.2	621	12	656	34	621	12	1.335	
SP18_22_	100	2.251	1.655	0.035	0.1569	0.004	0.61157	990	13	942	22	1120	43	1120	43	15.893	
SP18_23_	192.3	2.348	7.237	0.09	0.3909	0.0052	0.52641	2140	11	2126	24	2165	22	2165	22	1.801	
SP18_24_	68.7	1.35	0.658	0.015	0.0844	0.0017	0.20212	513.5	9.1	522	10	497	59	522	10	1.655	
SP18_25_	222	2.81	1.161	0.026	0.129	0.0024	0.67007	783	12	782	14	814	32	782	14	0.128	

Sample Name	[U]	U/Th	207/235	2σ error	206/238	2σ error	RHO	207/235 Age	2σ error	206/238 Age	2σ error	207/206 Age	2σ error	Best age	2σ error	Discordance	Rim /
_Grain	ppm							(Ma)	(Ma)	(Ma)	(Ma)	(Ma)	(Ma)	(Ma)	(Ma)	%	Core
SP18_26_	528	4.24	4.09	0.17	0.238	0.011	0.94228	1650	34	1374	56	2019	23	DISC	DISC	31.947	
SP18_27_	990	23.1	0.4437	0.0089	0.0599	0.0013	0.70202	372.4	6.3	375.1	7.9	341	41	375.1	7.9	0.725	
SP18_28_	410	8.67	0.935	0.021	0.1102	0.0028	0.71854	669	10	673	16	703	42	673	16	0.598	
SP18_29_	77.1	1.262	1.893	0.03	0.182	0.0028	0.44372	1078	10	1080	14	1114	30	1114	30	3.052	
SP18_30_	217	7.1	4.531	0.08	0.305	0.007	0.81233	1737	14	1714	35	1793	24	1793	24	4.406	
SP18_31_	163.9	2.528	0.831	0.023	0.1005	0.0028	0.67213	614	12	617	16	596	44	617	16	0.489	
SP18_32_	107	6.48	0.692	0.025	0.0839	0.0027	0.55325	535	15	519	16	602	72	519	16	2.991	
SP18_33_	141.8	1.287	0.831	0.02	0.0993	0.002	0.49687	614	11	610	11	672	55	610	11	0.651	
SP18_34_	174	2.28	0.672	0.014	0.0851	0.0017	0.59099	521.4	8.2	526.2	9.9	500	39	526.2	9.9	0.921	Rim
SP18_34_	170.5	2.22	0.671	0.014	0.0853	0.0017	0.6356	520.7	8.2	528	10	507	40	528	10	1.402	Core
SP18_35_	241	6.02	0.845	0.018	0.1056	0.0022	0.47293	621	10	647	13	564	48	647	13	4.187	
SP18_36_	89	2.91	3.21	0.24	0.215	0.017	0.81426	1455	62	1249	89	1813	82	DISC	DISC	31.109	
SP18_37_	109.8	1.374	1.583	0.032	0.1539	0.0031	0.57898	964	12	923	17	1045	43	1045	43	11.675	
SP18_38_	315	0.977	4.088	0.09	0.2924	0.0072	0.70685	1651	18	1653	36	1648	32	1648	32	0.303	
SP18_39_	25.9	1.129	1.133	0.044	0.1079	0.0041	0.20944	767	21	660	24	1100	90	DISC	DISC	13.950	
SP18_40_	191.4	1.348	1.339	0.023	0.1404	0.0031	0.47544	864	10	847	17	900	43	847	17	1.968	
SP18_41_	98.8	0.829	5.62	0.1	0.3503	0.0078	0.65019	1917	15	1934	37	1890	28	1890	28	2.328	
SP18_42_	159.5	1.355	11.53	0.21	0.47	0.011	0.68026	2565	17	2483	47	2626	28	2626	28	5.446	
SP18_43_	205.8	12.04	0.618	0.011	0.0802	0.0012	0.55307	488.5	6.8	497.5	7.3	450	38	497.5	7.3	1.842	
SP18_44_	331.2	2.898	0.878	0.021	0.1015	0.003	0.7183	641	11	623	17	649	50	623	17	2.808	
SP18_45_	257	1.882	2.051	0.028	0.1913	0.0032	0.5834	1132.8	9.5	1128	18	1096	30	1096	30	2.920	
SP18_46_	165	2.23	6.84	0.35	0.368	0.033	0.75502	2086	45	2050	140	2140	110	2140	110	4.206	Rim
SP18_46_	125	1.077	13.42	0.47	0.518	0.019	0.82471	2704	33	2702	85	2689	40	2689	40	0.483	Core
SP18_47_	132	7.02	1.678	0.059	0.1544	0.0058	0.6491	998	23	925	32	1099	60	1099	60	15.833	
SP18_48_	182	4.03	2.348	0.092	0.2061	0.0098	0.6873	1223	29	1206	52	1280	63	1280	63	5.781	
SP18_49_	300	2.07	0.361	0.01	0.0478	0.0019	0.57192	313.4	7.9	301	12	368	76	301	12	3.957	
SP18_50_	487	1.606	0.688	0.014	0.0856	0.0018	0.60059	530.9	8.5	529	10	546	42	529	10	0.358	
SP18_51_	115.6	1.41	5.242	0.08	0.3325	0.0055	0.68119	1858	13	1850	26	1886	23	1886	23	1.909	
SP18_52_	898	1.99	0.4168	0.0077	0.0559	0.0012	0.68182	353.5	5.5	350.5	7.3	404	38	350.5	7.3	0.849	
SP18_53_	38.9	1.945	0.663	0.029	0.08	0.0032	0.48337	517	18	496	19	632	93	496	19	4.062	
SP18_54_	336	6.02	16.85	0.27	0.575	0.014	0.75328	2928	16	2926	59	2914	22	2914	22	0.412	
SP18_55_	342	11.51	0.466	0.017	0.0538	0.003	0.18376	387	12	338	18	700	130	DISC	DISC	12.661	
SP18_56_	140.6	0.996	0.681	0.023	0.0836	0.002	0.41623	526	14	520	13	586	77	520	13	1.141	
SP18_57_	162.1	0.957	0.916	0.018	0.1075	0.0023	0.58573	659.4	9.7	658	13	678	39	658	13	0.212	
SP18_58_	93.2	1.859	1.6	0.044	0.1645	0.0045	0.52341	972	17	981	25	974	56	974	56	0.719	
SP18_59_	268.9	1.378	1.63	0.033	0.1623	0.0053	0.60846	981	12	969	29	1064	49	1064	49	8.929	
SP18_60_	793	1.861	0.3781	0.0049	0.05239	0.00071	0.43269	325.5	3.6	329.2	4.3	309	28	329.2	4.3	1.137	
SP18_61_	213	7.1	0.636	0.011	0.0812	0.0017	0.48413	499.5	7.1	502.9	9.9	503	45	502.9	9.9	0.681	
SP18_62_	352	7.11	0.632	0.016	0.0796	0.0023	0.65289	496.1	9.6	494	14	543	51	494	14	0.423	
SP18_63_	162.9	4.23	1.268	0.049	0.1203	0.0052	0.78211	832	21	731	30	1131	67	DISC	DISC	12.139	
SP18_64_	72.6	13.4	6.09	0.11	0.3586	0.0081	0.79069	1988	16	1974	38	2017	24	2017	24	2.132	
SP18_65_	399	1.697	0.3691	0.006	0.0507	0.0009	0.46855	319.3	4.4	318.7	5.5	329	41	318.7	5.5	0.188	
SP18_66_	166	2.558	0.908	0.017	0.1089	0.0022	0.55532	656.3	9	666	13	627	40	666	13	1.478	
SP18_67_	246.6	4.37	1.367	0.022	0.1478	0.0024	0.56723	875.6	9.2	888	14	871	30	871	30	1.952	
SP18_68_	597	21.2	1.06	0.08	0.1154	0.0072	0.79813	732	40	704	41	835	95	704	41	3.825	Rim
SP18_68_	85.5	1.121	5.27	0.11	0.3297	0.008	0.62877	1866	17	1836	39	1920	35	1920	35	4.375	Core

Sample Name	[U]	U/Th	207/235	2σ error	206/238	2σ error	RHO	207/235 Age	2σ error	206/238 Age	2σ error	207/206 Age	2σ error	Best age	2σ error	Discordance	Rim /
_Grain	ppm							(Ma)	(Ma)	(Ma)	(Ma)	(Ma)	(Ma)	(Ma)	(Ma)	%	Core
SP18_69_	320	7.3	0.666	0.022	0.0862	0.0023	0.70775	518	13	533	13	475	53	533	13	2.896	
SP18_70_	163.2	3.16	1.735	0.029	0.1725	0.0032	0.5522	1021	11	1025	18	1012	35	1012	35	1.285	
SP18_71_	598	3.38	1.93	0.11	0.1467	0.0088	0.67679	1092	37	881	50	1550	91	DISC	DISC	43.161	
SP18_72_	756	2.871	0.456	0.013	0.0522	0.0014	0.4772	382	9.1	327.8	8.4	732	59	DISC	DISC	14.188	
SP18_73_	172	1.017	0.673	0.017	0.0849	0.0019	0.49297	522	10	525	11	521	51	525	11	0.575	
SP18_74_	369.7	2.39	0.709	0.021	0.0899	0.0029	0.7436	545	12	555	17	523	48	555	17	1.835	
SP18_75_	174.2	2.341	0.867	0.024	0.1002	0.0034	0.55173	633	13	615	20	679	62	615	20	2.844	
SP18_76_	70.1	0.73	1.015	0.027	0.1121	0.0025	0.4426	710	14	685	14	811	55	685	14	3.521	
SP18_77_	76.3	1.419	0.946	0.026	0.1117	0.0028	0.46346	678	13	682	16	680	58	682	16	0.590	
SP18_78_	272	3.975	1.28	0.024	0.1414	0.0031	0.43277	836	11	853	18	778	45	778	18	2.033	
SP18_79_	780	1.818	0.413	0.012	0.0501	0.0015	0.45868	352.6	8.9	315.1	9.1	575	68	DISC	DISC	10.635	
SP18_80_	200	1.269	0.3634	0.0098	0.0485	0.0013	0.46317	314.3	7.2	305.5	8.2	391	66	305.5	8.2	2.800	
SP18_81_	357	1.905	0.705	0.016	0.0852	0.0022	0.64748	541.1	9.6	527	13	585	50	527	13	2.606	
SP18_82_	251.3	1.798	1.289	0.024	0.1344	0.004	0.37663	840	11	812	23	908	60	812	23	3.333	
SP18_83_	259	1.8	1.332	0.029	0.1399	0.0038	0.73606	859	13	844	21	876	38	844	21	1.746	
SP18_84_	425	12.92	6.04	0.16	0.348	0.011	0.76473	1981	24	1926	51	2067	39	2067	39	6.821	
SP18_85_	266	2.3	1.097	0.02	0.1257	0.0026	0.53607	751.1	9.5	763	15	704	43	763	15	1.584	
SP18_86_	105	1.09	1.7	0.052	0.1703	0.0052	0.61159	1007	20	1017	29	980	57	980	57	3.776	
SP18_87_	113.5	1.14	1.899	0.063	0.1877	0.0081	0.578	1076	22	1113	46	1042	68	1042	68	6.814	
SP18_88_	663	9	0.625	0.017	0.074	0.0019	0.47298	493	10	460	11	639	48	460	11	6.694	
SP18_89_	64.2	0.959	1.727	0.051	0.1691	0.006	0.58951	1016	19	1006	33	1016	67	1016	67	0.984	
SP18_90_	160.4	0.609	1.569	0.034	0.1547	0.0042	0.54324	957	14	927	24	1039	48	1039	48	10.780	
SP18_91_	156.6	3.27	0.933	0.02	0.1109	0.0026	0.62522	668	10	680	15	628	48	680	15	1.796	
SP18_92_	267	2.71	16.6	0.37	0.551	0.014	0.65306	2912	21	2825	58	2973	30	2973	30	4.978	
SP18_93_	454	5.85	0.68	0.016	0.0861	0.0027	0.55832	525.9	9.4	532	16	498	51	532	16	1.160	
SP18_94_	76.2	1.758	1.607	0.039	0.1626	0.0041	0.36053	971	15	971	23	1019	51	1019	51	4.711	
SP18_95_	96.1	1.4	0.873	0.026	0.0998	0.0033	0.43349	636	14	613	19	778	69	613	19	3.616	
SP18_96_	183	2.14	1.227	0.037	0.1324	0.0051	0.6743	812	17	801	29	889	66	801	29	1.355	
SP18_97_	356	246	0.416	0.023	0.0561	0.0045	0.66232	353	16	352	27	420	130	352	27	0.283	Rim
SP18_97_	166.7	1.201	1.569	0.044	0.1562	0.0048	0.43463	962	16	936	27	1024	68	1024	68	8.594	Core
SP18_98_	189	1.315	4.67	0.15	0.292	0.012	0.59462	1763	28	1653	58	1943	62	1943	62	14.925	
SP18_99_	377	2.4	0.412	0.012	0.054	0.0025	0.4582	351.9	8.2	339	15	454	92	339	15	3.666	
SP18_100_	332	2.29	0.387	0.019	0.0508	0.0029	0.48424	333	13	319	18	430	110	319	18	4.204	
SP18_101_	72.3	1.036	1.631	0.054	0.1633	0.0057	0.52339	983	22	974	31	1020	65	1020	65	4.510	
SP18_102_	297	14.1	1.108	0.05	0.125	0.0063	0.74025	756	24	759	36	825	80	759	36	0.397	Rim
SP18_102_	305	1.163	5.48	0.18	0.342	0.015	0.81467	1902	31	1894	70	1951	45	1951	45	2.922	Core
SP18_103_	321	0.84	0.567	0.012	0.0735	0.0016	0.39691	455.5	8.1	456.8	9.5	453	55	456.8	9.5	0.285	
SP18_104_	554	9.79	0.683	0.019	0.0863	0.0026	0.57431	529	11	533	15	532	56	533	15	0.756	
SP18_105_	131.1	1.603	0.569	0.023	0.0727	0.0041	0.49017	455	15	452	25	490	110	452	25	0.659	
SP18_106_	446	2.25	0.398	0.011	0.0544	0.0016	0.7635	340.5	7.6	341.2	9.6	357	52	341.2	9.6	0.206	
SP18_108_	296	5.79	1.271	0.034	0.1393	0.0046	0.66595	831	15	840	26	810	60	840	26	1.083	
SP18_109_	330	2.126	1.652	0.023	0.1663	0.0026	0.64727	990.8	9	992	14	990	26	990	26	0.202	
SP18_110_	45.9	11.02	0.864	0.031	0.0929	0.0035	0.43917	634	17	572	21	855	78	572	21	9.779	
SP18_111_	296	8.7	0.918	0.04	0.1052	0.005	0.7595	661	21	644	29	729	65	644	29	2.572	Rim
SP18_111_	68.2	1.19	1.641	0.044	0.1577	0.0047	0.63617	985	17	944	26	1102	51	1102	51	14.338	Core
SP18_112_	434	2.46	11.48	0.29	0.466	0.014	0.32254	2561	24	2465	62	2608	61	2608	61	5.483	

Sample Name _Grain	[U] ppm	U/Th	207/235	2σ error	206/238	2σ error	RHO	207/235 Age (Ma)	2σ error (Ma)	206/238 Age (Ma)	2σ error (Ma)	207/206 Age (Ma)	2σ error (Ma)	Best age (Ma)	2σ error (Ma)	Discordance %	Rim / Core
SP18_113_	144	1.54	1.893	0.043	0.1812	0.0047	0.66645	1076	15	1072	26	1067	47	1067	47	0.469	
SP18_114_	299	2.074	0.3969	0.0084	0.0532	0.0012	0.38452	339.8	6	334.2	7.2	323	56	334.2	7.2	1.648	
SP18_115_	413	2.38	0.4344	0.0079	0.0558	0.0013	0.50896	366.7	5.5	350	7.7	400	48	350	7.7	4.554	
SP18_116_	387	2.41	0.4176	0.0089	0.0495	0.00086	0.5128	354	6.3	311.4	5.3	616	49	DISC	DISC	12.034	
SP18_117_	220.8	2.69	0.903	0.015	0.0998	0.0019	0.56746	653.7	7.7	613	11	749	34	613	11	6.226	
SP18_118_	789	7.01	0.4104	0.0093	0.0517	0.0013	0.63014	348.7	6.6	325	7.8	465	43	325	7.8	6.797	
SP18_119_	355	3.69	1.061	0.034	0.114	0.0042	0.80339	734	17	695	24	830	47	695	24	5.313	
SP18_120_	181.3	12.94	0.667	0.015	0.0825	0.0022	0.55749	519.5	9.2	511	13	495	52	511	13	1.636	

Supplementary information. Table 2 Reduced detrital zircon double dating (U-Th)/(He-Pb) data for Cenozoic aged zircons.

Sample	(U-Th)/He Age	2σ error	U	Th	147Sm	[U]e	Th/U	He	mass	Ft	ESR	U-Pb Age	U-Pb 2σ error
	(Ma)	(Ma)	(ppm)	(ppm)	(ppm)			(nmol/g)	(ug)		(um)	(Ma)	(Ma)
zSP3-4	21.78259087	1.742607	359.3121	314.525	5.64325	431.744	0.875353	32.33563	1.22253	0.634472	31.0113	23.82	0.92
zSP3-12	19.84801483	1.347841	342.9796	229.1911	2.981853	395.7543	0.668235	25.6454	0.693653	0.572188	25.5628	26.6	1.1
zSP3-68	22.27447701	2.341958	736.8495	830.1655	3.273286	927.97	1.126642	74.73004	1.26414	0.64248	32.0542	24.9	1.1
zSP3-94	23.68561935	1.89485	323.5695	249.381	1.571383	380.9848	0.770719	29.7909	0.877436	0.609504	28.6073	22.85	0.81

Supplementary information. Table 3 Full detrital zircon U-Pb spectra from 0 Ma to 3500 Ma, displayed as kernel density estimators (KDE) and histograms (Vermeesch, 2012). Nonadaptive KDE bandwidth of 8 Ma, histogram bin width of 20 Ma.

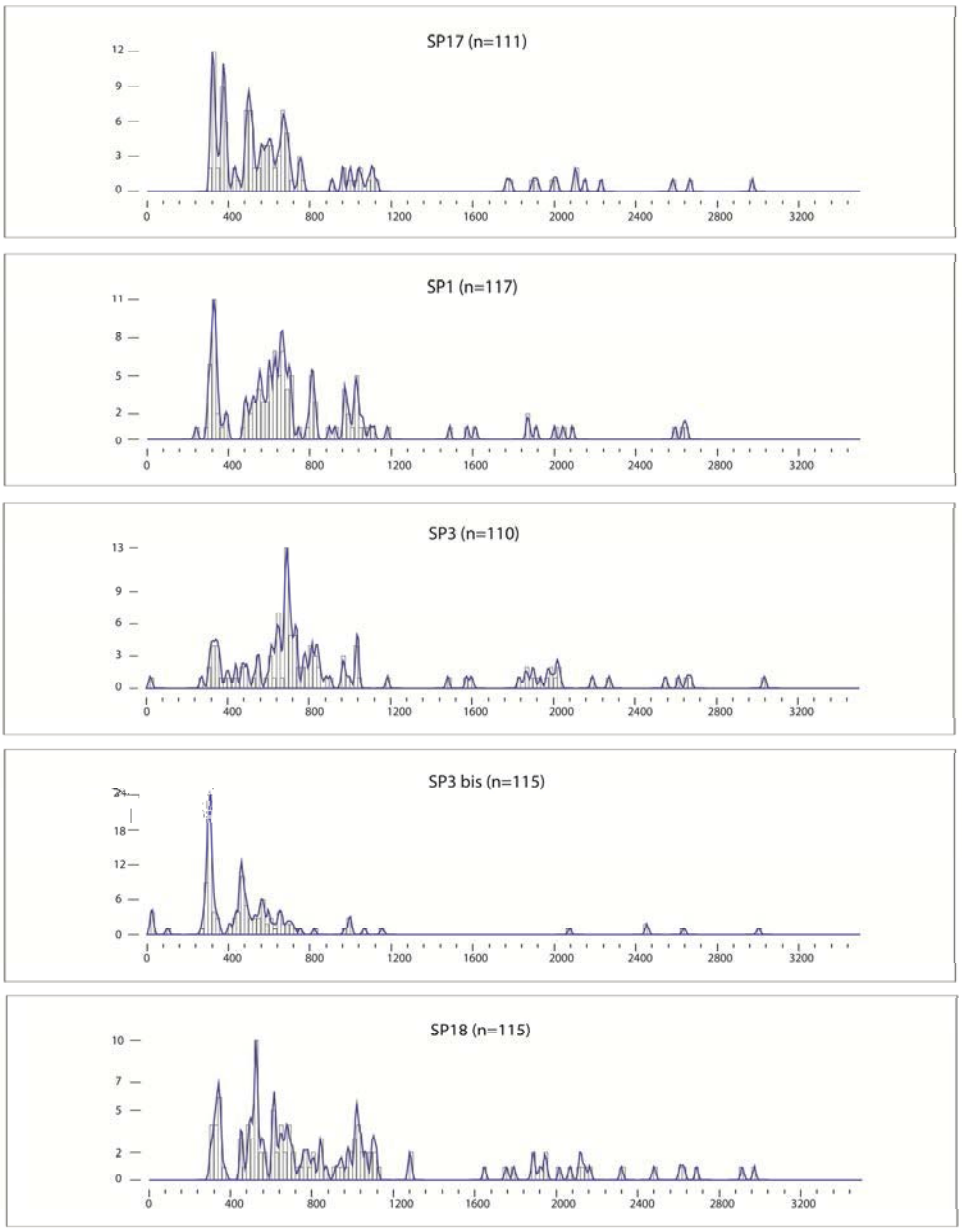

Supplementary information. Table 4. Geographic position of the analysed samples.

Formation	Sample name	Latitude	Longitude
Fluvial Campodarbe	SP17	0° 40' 17.3424" W	42° 32' 5.6148" N
San Juan de la Peña	SP1	0° 40' 45.9012" W	42° 31' 17.5404" N
San Juan de la Peña	SP3	0° 41' 6.3240" W	42° 31' 10.6896" N
San Juan de la Peña	SP18	0° 41' 15.8424" W	42° 30' 25.9164" N

Capítol 8

Interplay of multiple sediment sources in an overfilled foreland basin: axial versus transverse systems in the southern Jaca basin (southern Pyrenees)

El capítol 8 correspon a un article en preparació.

M. Roigé ha mostrejat totes les seccions i ha realitzat tots els comptatges tant dels gresos com dels conglomerats. Ha sintetitzat les dades, les ha projectat en diagrames triangulars i les ha classificat. També ha redactat tot el text i ha realitzat totes les figures.

Interplay of multiple sediment sources in an overfilled foreland basin: axial *versus* transverse systems in the southern Jaca basin (Southern Pyrenees)

Roigé, M.[1*], *et al. in preparation*

[1]Department de Geologia, Universitat Autònoma de Barcelona, 08193 Bellaterra, Spain

[2]The University of Texas at Austin, Department of Geological Sciences, Austin, TX 78712, USA

(*) Corresponding author

Keywords: sandstone petrography, provenance, sediment routing systems, Pyrenees

ABSTRACT

In the southern edge of the Jaca basin two main sediment routing systems merge, providing an excellent example of interaction of different source areas with distinct petrologic signatures, recording different stages of exhumation of the Pyrenean belt. We apply sandstone petrography in the deltaic to alluvial deposits of the southern part of the basin, and also in the time equivalent systems of the nearby Ainsa and Ebro basins, in order to decipher the evolution of source areas from Eocene to Miocene times.

Our sandstone petrography results allow identifying four petrofacies, which evidence the interplay of axially-fed sediments derived from the eastern sources (central Pyrenees) with transversely-fed sediments from the north (west-central Pyrenees), highly controlled by the emergence of tectonic structures. The axially-fed sediments display an important change in the source area that occurred during the Priabonian, and consisted on the shift from carbonate-rich source with plutonic rocks, by a siliciclastic-rich source area with overburden metamorphic lithic grains. The axially fed systems dominated the fluvial deposits of the Campodarbe Formation in the southern edge of the Jaca basin, which were progressively replaced from east to west by transverse-fed systems sourced from northern source areas. In the late stages of basin infill, the Ebro foreland basin and the Jaca thrust-sheet-top basin received north-derived detritus from two distinct source areas. While the Jaca basin continued recording a major recycling of former clastic deposits, the Ebro basin was characterized by additional contributions from Paleozoic sources from the western Pyrenees.

1. Introduction

The South Pyrenean foreland basin accumulates hundreds of meters of deltaic to alluvial sediments that were deposited in thrust-sheet-top basins during middle Eocene to early Miocene times. They record strong stages of exhumation of the Pyrenean chain that delivered detritus derived from a wide range of lithologies from diverse source areas. From late Eocene times, the western sector of the South Pyrenean foreland basin was divided into the Jaca thrust-sheet-top basin to the north and the present-day Ebro Basin to the south due to the growing of the External Sierras thrust system (Fig. 1) (Puigdefàbregas, 1975; Labaume *et al.*, 1985; Pocoví *et al.*, 1990; Teixell and García-Sansegundo, 1995).

In the Jaca basin these deposits are represented by the Belsué-Atarés (deltaic environments), Campodarbe and Bernués (fluvial to alluvial environments) Formations. These formations show the interplay between axial drainage systems fed from eastern sources and transverse drainage systems tapping new uplifted northern sources.

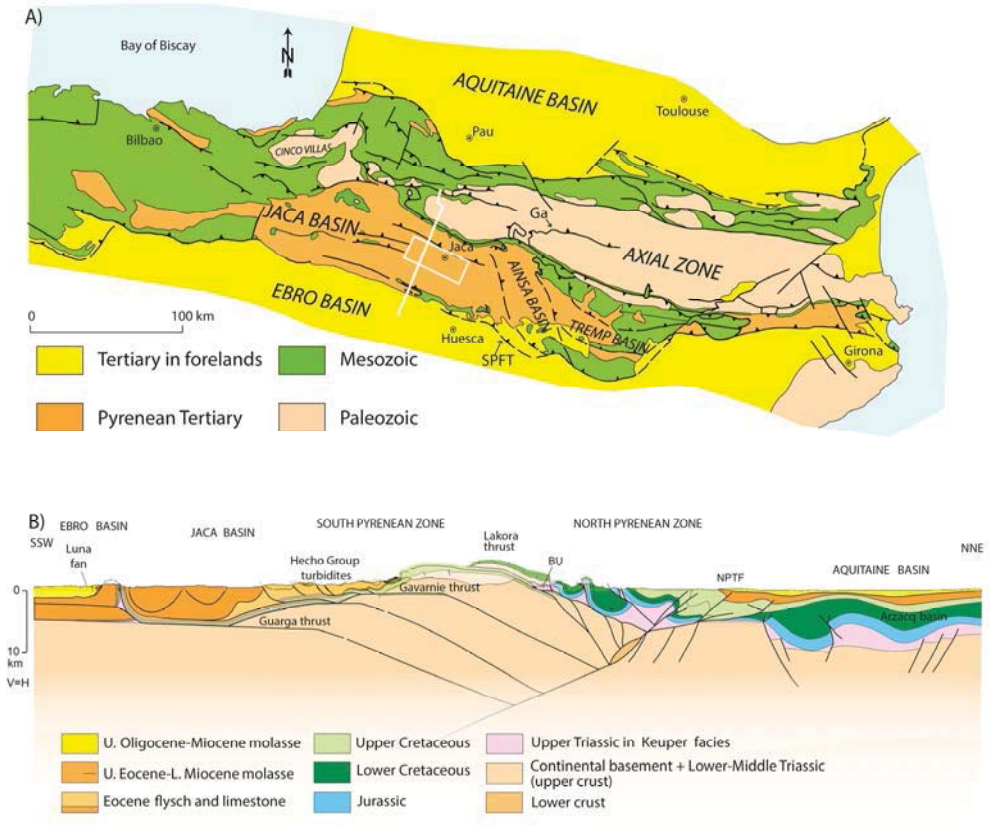

Figure 1. (A) Simplified geological map of the Pyrenees (redrawn from Teixell, 1996), showing the location of the study area (white frame). White line indicates cross-section in Figure 1B. Lk: Lakora thrust, Ga: Gavarnie thrust, SPTF: South Pyrenean Frontal Thrust. (B) Crustal cross-section of the west-central Pyrenees (simplified from Teixell et al., 2016), showing both the South Pyrenean Zone and the North Pyrenean Zone. NPFT: North-Pyrenean Frontal Thrust; BU: Bedous Triassic Unit.

Most of provenance studies have been focused in the northern sector of basin (Fontana *et al.*, 1989; Gupta and Pickering, 2008; Roigé *et al.*, 2016; Coll *et al.*, 2017), where the fluvial and alluvial sedimentation is mostly sourced from northern areas, mainly composed by the former turbidite deposits (Puigdefàbregas, 1975; Roigé *et al.*, 2017). Nonetheless, less is known about the petrologic signatures and the evolution of the different source areas in the southern sector of the basin.

In this sector of the basin, axially-fed fluvial systems were accumulated, where fruitful works have been dedicated to characterize the stratigraphy, sedimentology and deformation of these deposits (Mutti *et al.*, 1972; Soler-Sampere and Puigdefàbregas, 1970; Puigdefàbregas, 1975; Lafont, 1994; Millán-Garrido *et al.*, 1995; Barnolas and Gil-Pena, 2002; Montes, 2002; Pueyo *et al.*, 2002; Castelltort *et al.*, 2003; Castelltort *et al.*, 2004; Huyghe *et al.*, 2012) together with magnetostratigraphic and paleontological studies (Canudo, 1990; Hogan, 1993; Hogan and Burbank, 1996; Bentham *et al.*, 1992; Costa *et al.*, 2010; Rodríguez-Pintó *et al.*, 2012; Oliva-Urcia *et al.*, 2015). The proximal time equivalents for these axial drainage systems are located in the nearby Ainsa basin, and are mainly represented by the fluvial Escanilla Formation which progrades westwards entering the Jaca basin, being strongly controlled by the growing tectonic structures (Fig. 1) (Puigdefàbregas, 1975; Jolley, 1988; Bentham *et al.*, 1992; Montes, 2002). These sedimentary systems show an important lateral variability and diachrony along the basins which complicates correlation and provenance interpretations between them.

In this work, we aim to unravel the compositional nature of these deposits in order to constrain the interplay between the different active source areas that yielded to a competition of the axially-fed systems against the transverse-fed systems. In order to achieve this goal here we present a provenance study based on sedimentary petrography for the transitional to alluvial environments of the southern edge of the Jaca basin. We also analyse the petrographic composition of the fluvial system from the Escanilla Formation (Ainsa basin) to test its connectivity with the Campodarbe Formation. Moreover, we incorporate the fluvial to alluvial deposits located to the south of the External Sierras thrust front, in the Ebro basin, in order to compare it with the petrologic signatures from the Jaca thrust-sheet-top basin, achieving more insights into the last stages of the terrestrial sedimentation.

2. Geological setting

The study area is located in the southern part of the South Pyrenean foreland basin, involving the southwestern corner of the Ainsa basin, the southern part of the Jaca basin, and the northern edge of the Ebro basin, in the culmination of the External Sierras thrust front (Fig. 1, 2).

The Pyrenean mountain belt was formed as a doubly-vergent orogenic prism due to the collision between the European and Iberian plates during late Cretaceous-early Miocene times (Roure *et al.*, 1989; Puigdefàbregas *et al.*, 1992; Teixell, 1998; Vergés *et al.*, 2002). The northern side of the belt, known as North Pyrenean Zone (Fig. 1) is constituted by inverted extensional Mesozoic basins, that are flanked by the Aquitaine basin to the north (Lagabrielle *et al.*, 2010). The southern side (South Pyrenean Zone) is characterised by a south-verging basement-involved thrust stack that includes the Axial Zone, the Paleogene South Pyrenean basin and the South Pyrenean Frontal thrust. In the west-central Pyrenees, four main thrust sheets compose the South Pyrenean Zone, flanked to the south by the Ebro basin: The Lakora-Eaux-Chaudes, Gavarnie, Broto and Guarga thrust sheets (Fig. 1B). These thrust sheets involve Paleozoic basement and a cover assemblage with preorogenic Mesozoic rocks and a foreland basin sequence of late Cretaceous-early Miocene rocks. The Paleozoic basement constitutes the core of the belt, known as the Axial Zone, and is mainly constituted by Variscan low-grade metamorphic rocks and granitoids, that are unconformably overlain by Permo-Triassic red beds, or directly by Cretaceous limestones. The preorogenic Mesozoic succession is constituted, when complete, by Triassic Keuper facies, which constitute the detachment level for the synorogenic basins, followed by a thick carbonate and sandstone-shale successions (Jurassic and Cretaceous). Synorogenic rocks from late Santonian to early Miocene constitute the South Pyrenean foreland basin, which during Eocene times concentrated the fluvio-deltaic sedimentation in the Àger and Tremp Graus basins, to the east, that funneled sediments to the west, in the slope and deep-marine Ainsa and Jaca basins (Nijman and Nio, 1975; Mutti, 1985; Bentham *et al.*, 1992; Caja *et al.*, 2010). The deep-marine sedimentation, represented by the Hecho Group turbidites (Mutti, 1985), was progressively replaced from east to west by middle to late Eocene deltaic and alluvial deposits which marked the overfilled foreland basin stage (Puigdefàbregas, 1975; Dreyer *et al.*, 1999).

In the Ainsa basin, the deep-marine sedimentation is replaced by the Sobrarbe delta Formation (Lutetian) and the fluvial Escanilla Formation (Bartonian-Priabonian) (Mochales *et al.*, 2012), which were fed from the central Pyrenees, through the Sis and Gurp-Pobla paleovalleys (Bentham *et al.*, 1992; Michael, 2013). These systems prograde westward into the Jaca basin, entering through its southeastern edge. The Graus Formation conglomerates (Chattian-Aquitanian) represent the last preserved deposits of the Ainsa basin, lying unconformably over the Escanilla deposits (Reynolds, 1987).

The time equivalents of all these deposits are found in the Jaca basin, where the Sabiñánigo Sandstone (Bartonian), Belsué-Atarés (Bartonian-Priabonian), Campodarbe (Bartonian-Oligocene) and the Bernués (Oligocene-Miocene) Formations represent the transitional and terrestrial environments of the basin. The transition from marine to terrestrial environments in the basin is diachronic, following the main westward progradation of the sedimentary systems, which ends with generalised continental sediments marking the

closure and the initiation of a endorheic basin stage, dated to occur at 36 Ma (Ortí *et al.*, 1986; Payros *et al.*, 1999; Barnolas and Gil-Pena, 2002; Costa *et al.*, 2010).

At the same time that north to south directed folds started to grow, the Belsué-Atarés delta prograded from east to west with depocenters in synclines producing a strong diachrony clearly observed in the southern margin of the basin (Fig. 2, 3). In the northwestern Jaca basin, a subordinated system known as Martés sandstone (Puigdefàbregas, 1975) irrupts above marine distal facies. These delta sediments are followed by coastal and terrestrial deposits of the Campodarbe and Bernués Formations, which constitute the so-called Campodarbe Group (Mutti *et al.*, 1972).

The Campodarbe Formation is mainly constituted by fluvial to alluvial deposits which display the interference of two main sediment routings can be identified (Puigdefàbregas, 1975): an east-derived axial fluvial system that enters through the southeastern margin of the basin, and a north-derived transverse alluvial fan system that characterizes the northern part of the basin, controlled by the activity of the Gavarnie thrust. The overlying Bernués Formation deposits are mainly represented by alluvial fan deposits sourced from northen provenance areas, which mark the later stages of the basin infill (Puigdefàbregas, 1975). As proposed by (Puigdefàbregas, 1975; Arenas, 1993) and by the results obtained in Roigé et al. (*in prep. this thesis*), the Bernués Formation deposition can be attributed to Chattian-Aquitanian.

During Oligocene-Miocene times, the growing of the External Sierras thrust front (Soler-Sampere and Puigdefàbregas, 1970; Labaume *et al.*, 1985; Teixell, 1996; Oliva-Urcia *et al.*, 2015) caused that the Campodarbe Formation deposits were dissected and separated into the Jaca basin, to the north, and into the Ebro basin, to the south (Fig. 2, 3). In the Ebro basin, the top of the Campodarbe Formation deposits, has been dated at 24.5 Ma (Oliva-Urcia *et al.*, 2015). Above, the Uncastillo Formation fluvial/alluvial deposits (Chattian-Aquitanian) represent north sourced alluvial systems eroding part of the Jaca basin and areas further to the north (Internal Sierras and Axial Zone) (Puigdefàbregas, 1975; Friend *et al.*, 1989; Arenas *et al.*, 2001). In the study area, the Uncastillo Formation deposits are represented by the Luna alluvial fan. The Uncastillo and Bernués Formations represent the dominance of alluvial fan systems originated from the north, related to the activity of the Guarga thrust sheet (Puigdefàbregas, 1975).

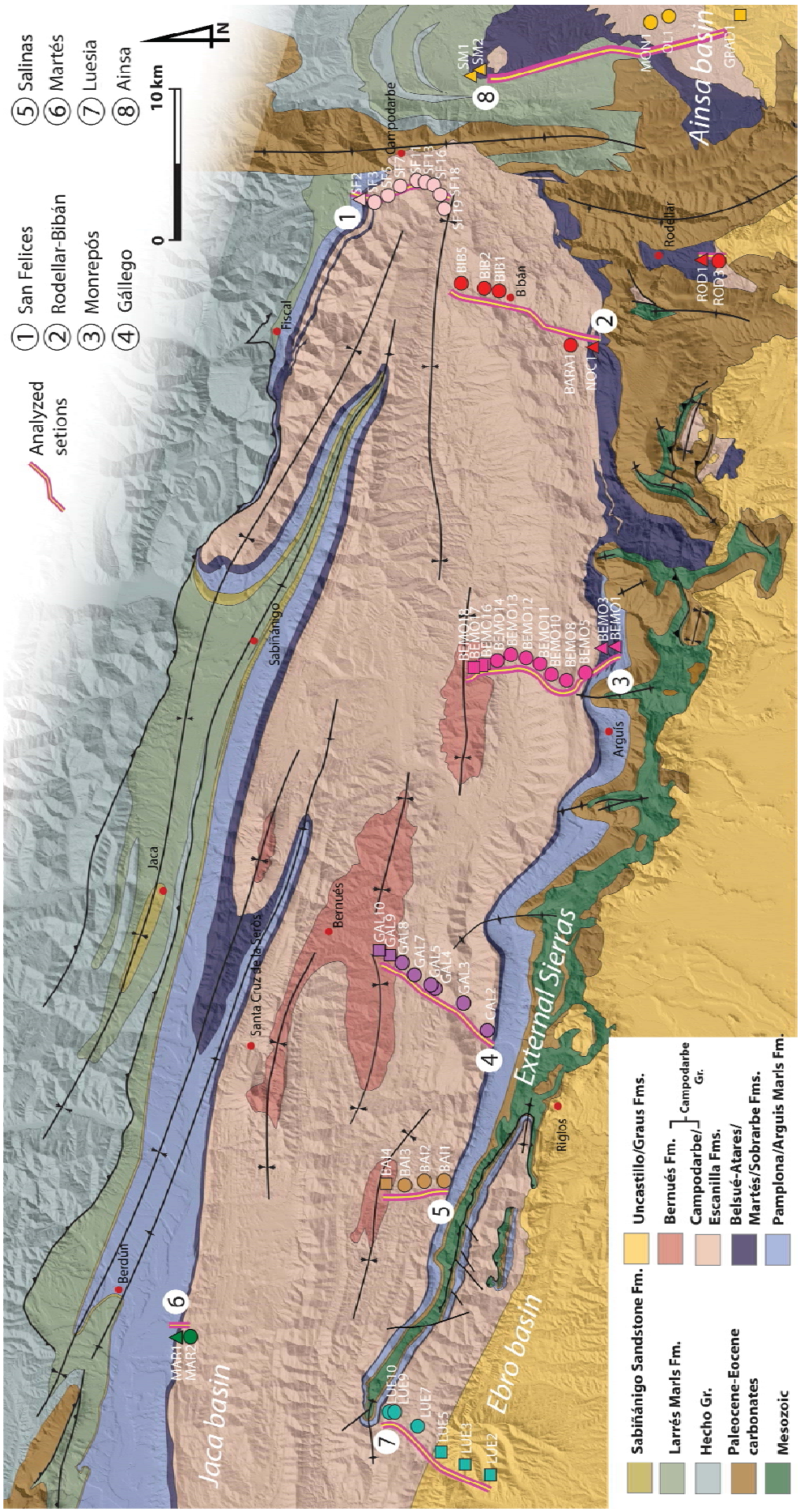

Figure 2. Geological map of the of the Jaca basin (modified from Puigdefàbregas, 1975). Yellow-purple lines show the location of the analysed sections. Numbers refer to each section: (1) San Felices section; (2) Rodellar-Bibán section; (3) Monrepós section, (4) Gállego section, (5) Salinas section, (6) Martés section, (7) Luesia section and (8) Ainsa section. Numbers and symbols refer to each of the analysed samples for sandstone petrography analyses.

3. Samples and methods

Samples from deltaic to fluvial/alluvial environments were collected from the southern part of the Jaca basin, in the San Felices, Rodellar-Bibán, Monrepós, Gállego, Salinas and Martés sections, which include the Belsué-Atarés, Campodarbe and Bernués Formations (Fig. 2, 3). In addition, two sections in the Ebro basin (Luesia section, involving the Campodarbe and Uncastillo Formations) and in the Ainsa basin (Ainsa section, involving the Sobrarbe, Escanilla and Graus Formations) were also sampled in the order to compare the compositional features between the time equivalents systems from the Jaca basin (Fig. 2).

Ninety-four sandstone and conglomerate samples were collected for a sandstone petrography analysis. The number and spacing of samples were established according to the representativeness of each analysed sedimentary system along the stratigraphic logs. Fifty-three samples were chosen for quantification of the detrital modes through point counting analysis under the polarizing microscope. Thin sections were prepared and stained using Na-cobaltinitrite (Chayes, 1952) for suitable identification of feldspar, and Alizarine red-S staining for distinction of carbonate composition, such as dolomite, ankerite and calcite.

Detrital modes were calculated following the Gazzi-Dickinson point counting method (Gazzi, 1966; Dickinson, 1970; Ingersoll et al., 1984; Zuffa, 1985). Three hundred to five hundred points were counted for each thin section (Dryden, 1931), and classified as framework grains, diagenetic minerals, matrix and porosity. All the framework grains were labeled according to the main four classes established by Zuffa (1980): non-carbonate extrabasinal (NCE), non-carbonate intrabasinal (NCI), carbonate extrabasinal (CE), and carbonate intrabasinal (CI). Metamorphic rock fragments were classified according to Garzanti and Vezzoli (2003), while classification of volcanic grains was performed following the criteria of Marsaglia and Ingersoll (1992) and Critelli and Ingersoll (1995). According to Zuffa (1985), samples were plotted and classified into first to fourth order ternary diagrams. Petrofacies were represented in ternary diagrams, calculating the mean confidence regions (90%) with the “CoDaPack” software (Comas-Cufí and Thió-Henestrosa, 2011).

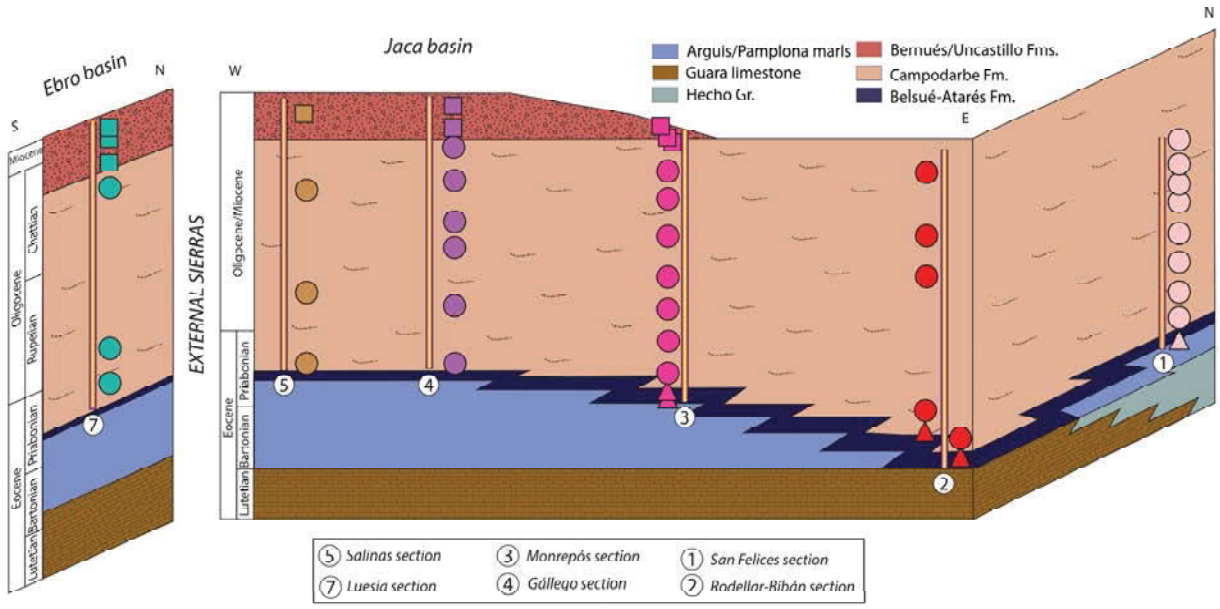

Figure 3. General stratigraphic cross-section sketch summarizing the relationships of the analyzed formations in the Jaca and Ebro basins. Stratigraphic ages extracted from (Labaume et al., 1985; Canudo and Molina, 1988; Oms et al., 2003; Mochales et al., 2012; Oliva-Urcia et al., 2015). Yellow-purple bars indicate the relative position of the analyzed sections, and symbols represent the relative position of the analyzed samples (see map on Figure 2 for sample location).

4. Results

Analysed samples are here described and classified in the four classes referred above (NCE, CE, NCI and CI). Framework grains are here described in order to establish their most probable provenance. Non-framework grains are authigenic minerals, related to cementation and replacing processes in most of the cases where calcite is the main cement typology. All percentages here described are referred over total framework grains.

4.1Grain types

4.1.1 NCE

Quartz is widely represented, with proportions ranging from 7% to 42.8%. It has been distinguished as monocrystalline, polycrystalline (with 2-3 or >3 subgrains) or contained in a rock fragment. Characteristic quartz with evaporitic inclusions (anhydrite and halite) occurs in proportions over 1-3%. Feldspar grains (Fig. 4A) appear in proportions up to 10% as orthoclase (<5%), microcline (<2%) and plagioclase (<5%). K-feldspar occurs non-altered while plagioclase usually shows higher degrees of alteration.

Lithic grains (Fig. 4B, C) are the most dominant components in many samples, as metamorphic, volcanic, non-carbonate sedimentary or plutonic rock fragments. Metamorphic rock fragments are highly represented in most of the samples (up to 48%), and have been classified as: (i) very low to low-grade (metapelites and phyllites), (ii) medium-grade (mica schists, schists and chloritic schists), and (iii) high-grade (meta-quartzite). Igneous grains are granitoid rock fragments (<2.5%) and volcanic lithics. Three textures of paleovolcanic lithics have been identified: (i) lathwork texture made of plagioclase and altered augite crystals, (ii) microlithic texture made of plagioclase microlites and, in lower proportions, (iii) vitric texture.

Non-carbonate sedimentary rock fragments are sandstone, hybrid sandstone (Fig. 4D), siltstone, hybrid siltstone and silicified rock fragments. Silicified rock fragments have been also subdivided into radiolarite rock fragments and silicified limestones. Heavy minerals are mainly zircon, tourmaline, titanite and epidote (<1%).

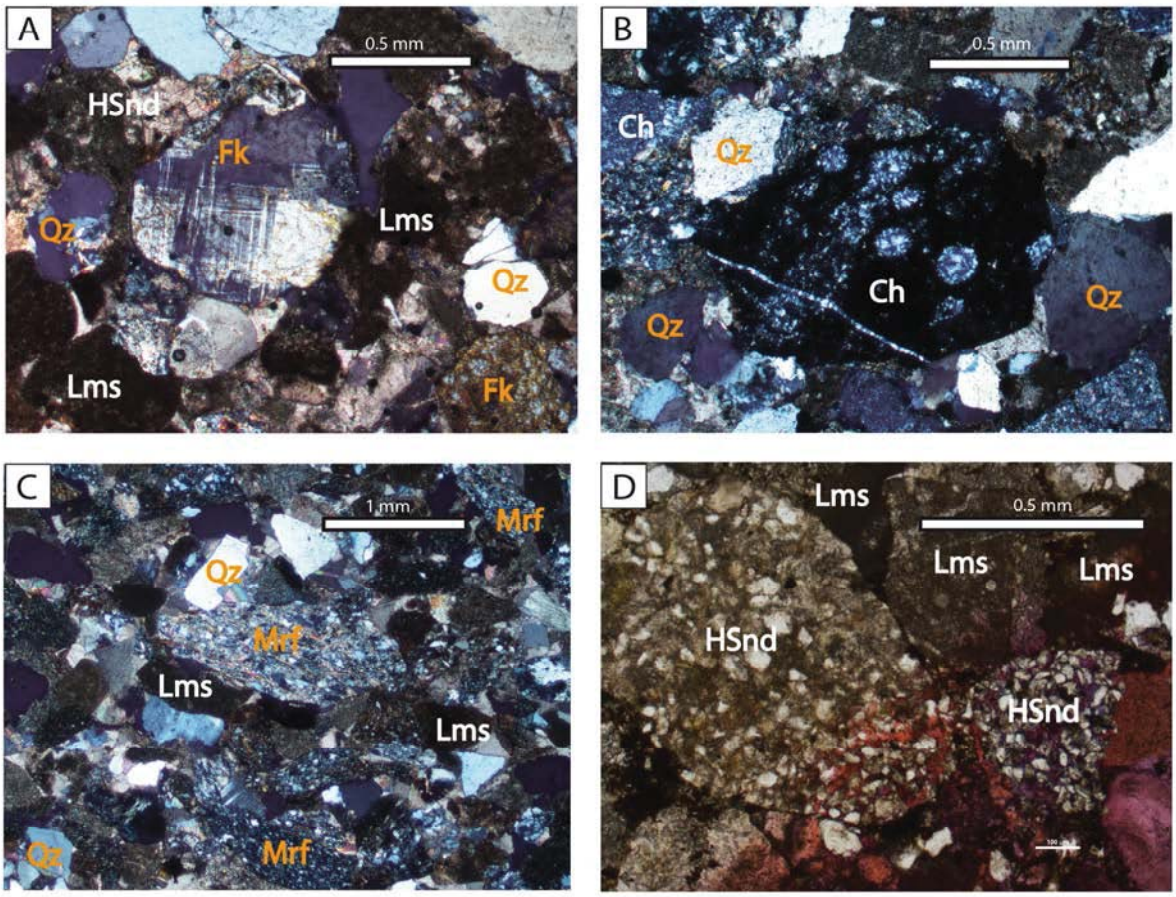

Figure 4. Optical photomicrographs of distinct extrabasinal grains. (A) Sample of the Belsué-Atarés Formation in the Rodellar section: feldspar (microcline) grain partially replaced (Fk), limestone rock fragments (Lms) and quartz grains (Qz) (cross-polarized, XPL); (B) Sample of the Martés sandstone: Radiolarite rock fragment (Ch) and quartz grains (Qz) (XPL); (C) Sample of the Campodarbe Formation (Gállego section): metamorphic rock fragments (Mrf), limestone rock fragments (Lms) and quartz grains (Qz) (XPL); (D) Sample from the Campodarbe Formation (San Felices section): Hybrid sandstone rock fragments (HSnd) and limestone rock fragments (Lms) (XPL).

4.1.2 NCI

Non-carbonate intrabasinal grains are scarce, appearing always as glauconite or argillaceous rip-up-clasts.

4.1.3 CE

Carbonate extrabasinal grains occur showing a wide variety of textures, and can reach proportions up to 65%. Distinction has been made into (i) bioclastic and sparitic limestones, (ii) dolostones, and (iii) dolomitic and dolomitized limestones. Most common components contained in these rock fragments are bioclasts as foraminifera (nummulitids, discocyclinids, miliolids, aveolinids), red algae or bivalves.

Dolostone fragments (<7%) have been recognized as dolomicrite, polycrystalline sparitic fragments and single-grain dolomite.

4.1.4 CI

Carbonate intrabasinal grains are sporadic (<4%), and appear as micritic intraclasts and caliche concretions, or as bioclasts (red algae, bivalves and benthic foraminifera).

4.2Modal sandstone composition

Sandstone detrital modes of the analysed systems have been plotted using ternary diagrams, in order to classify and illustrate compositional trends and potential shifts in the source areas. A first-order compositional classification (Fig. 5A) has been applied according to Zuffa (1980), which represents the relative content on “Non-carbonate extrabasinal” (NCE), “Carbonate extrabasinal” (CE) and “Carbonate intrabasinal” (CI) components, and distinguishes between lithic arenites, calclithites and hybrid arenites. The Quartz-Feldspar-Lithics (Q-F-L) diagram is used as second-order classification ternary diagram (Figs. 5B) (according to Dickinson *et al.*, 1983), while Lithic metamorphic-Lithic volcanic-Lithic sedimentary (Lm-Lv-Ls) is used as third-order ternary diagram (Fig. 5C).

All the analysed samples belonging to transitional environments (i.e. Belsué-Atarés Fm.) from the Jaca basin can be classified as lithic arenites, while deltaic samples from the Sobrarbe Formation in the Ainsa basin are calclithites (Fig. 5A). Regarding to the fluvial deposits of the Campodarbe Formation, only samples from the northeastern part of the basin (San Felices section) are calclithites pointing out the high content on limestone fragments. From east to west an increasing trend on the proportion of NCE grains occur, yielding to a sample

population corresponding to lithic arenites (Fig. 5A). Alluvial to fluvial samples from the overlying Uncastillo, Bernués and Graus Formations can also be classified as lithic arenites (Fig. 5A).

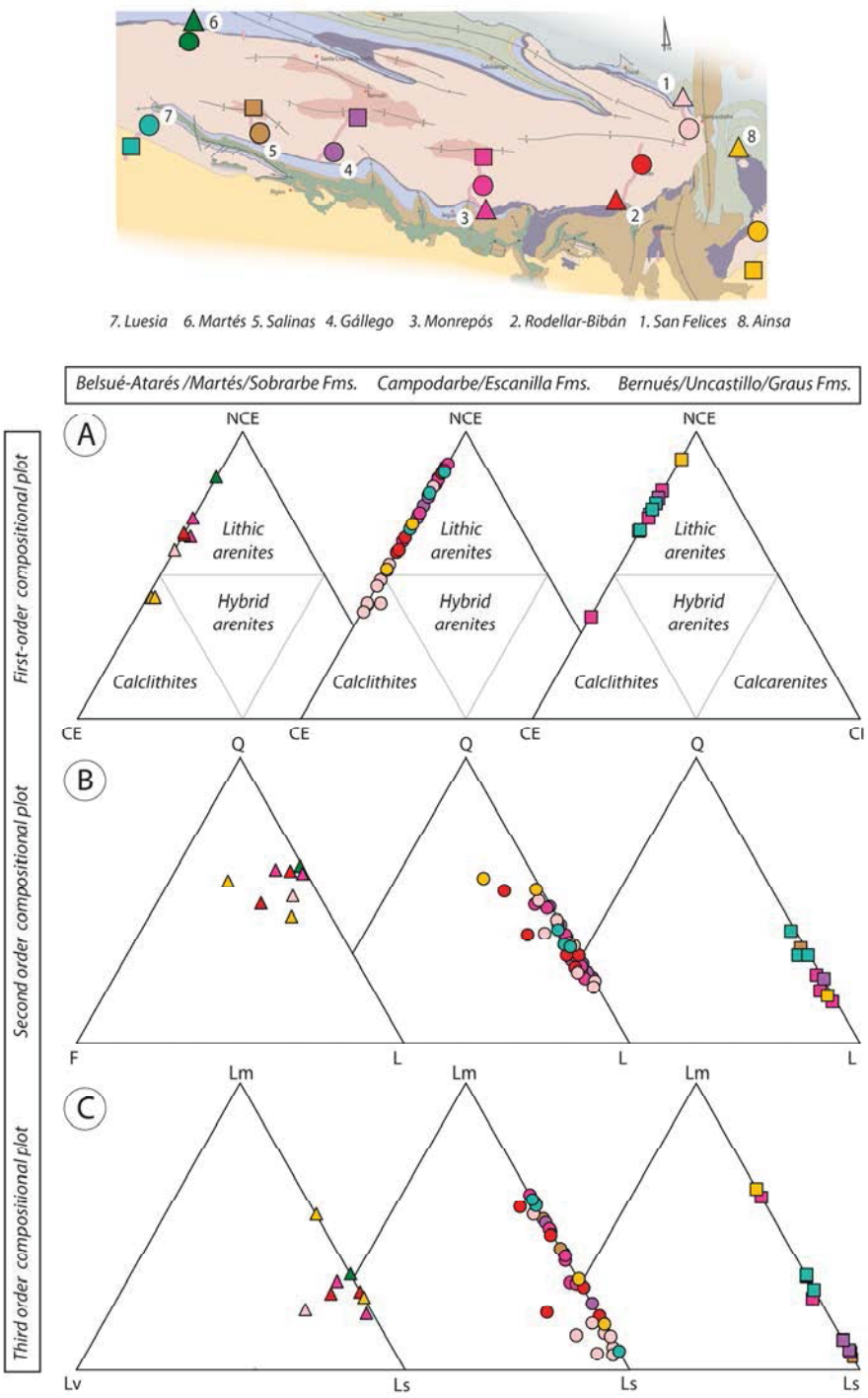

Figure 5. Top: Geological map from Figure 2, with symbols of the sample groups, in order to facilitate the interpretation of the ternary diagram located below (see Figure 2 for full geological map). Bottom: Compositional plots for all the analysed samples. Diagrams are arranged from left to right according their sedimentary environment (from deltaic to alluvial). (A) First order compositional plots (Zuffa, 1980) where NCE, Non-Carbonate Extrabasinal grains; CE, Carbonate Extrabasinal; and CI, Carbonate Intrabasinal; (B) Second order QFL compositional plots (Dickinson et al., 1983) where Q, Quartz; F, Feldspar; and L, Lithic fragments, and (C) Third order compositional plots where Lm, Lithic metamorphic grains; Lv, Lithic volcanic grains; and Ls, Lithic sedimentary grains.

The Q-F-L diagrams allow to distinguish a generalized increasing trend of lithic grains from the deltaic formations to the alluvial deposits (Fig. 5B). Deltaic deposits from Rodellar-Bibán section show a similar content on quartz and feldspar to those from the fluvial Escanilla Formation (Fig. 5B). The highest proportion of lithic fragments are contained in the last alluvial deposits from the Bernués and Graus Formations. In the Campodarbe Formation, sedimentary lithic grains dominate the northeastern part of the basin (San Felices section) while to the west the metamorphic ones increase (i.e. Luesia and Gállego sections) (Fig. 5C).

4.2.1 Petrofacies

A fourth-order ternary diagram is here presented in order to discriminate among the the petrofacies described in Roigé *et al.* (2017) for the northern Jaca basin, which compares hybrid sandstone fragments (Hybrid Snd), feldspar and lithic fragments, excluding hybrid sandstone fragments (F+L) and CE (Fig. 6). These petrofacies reflect the basin evolution and depict the interplay of different source areas.

4.2.2 Carbonate extrabasinal enriched petrofacies

Carbonate grains are the most dominant rock fragment (Fig. 7A, 8A) in this petrofacies (>45%). Mudstone and wackestone rock fragments widely occur among the carbonatic grains, while grainstone, packstone and dolostone rock fragments are also widespread. This petrofacies shows significant content on microcline, orthoclase, plagioclase and plutonic rock fragments, and lacks hybrid sandstone fragments.

This petrofacies occurs in the oldest analysed sedimentary systems, which are the Sobrarbe and Escanilla Formations in the Ainsa basin, and the Belsué-Atarés Formation and the basal Campodarbe Formation in the Jaca basin (Fig. 6).

In the Sobrarbe Formation (samples SM1 and SM3 in Figure 2) this petrofacies show the highest content of carbonate grains, displaying a wide range of mudstone, packstone and grainstone rock fragments, with subordinate granite, schists and feldspar grains. The overlying Escanilla Formation (samples MO1 and OL1) displays the same compositional features, although a slight increase of lithic fragments is observed (Fig. 6).

In the Jaca basin, this petrofacies are representative of the Belsué-Atarés deposits from San Felices, Rodellar-Bibán and Monrepós sections, which display a very close composition to that observed in the Escanilla Formation in the Ainsa basin. In the Rodellar-Bibán section this petrofacies (samples ROD1 and ROD3) display remarkable proportion of feldspar grains (up to 18% among framework grains).

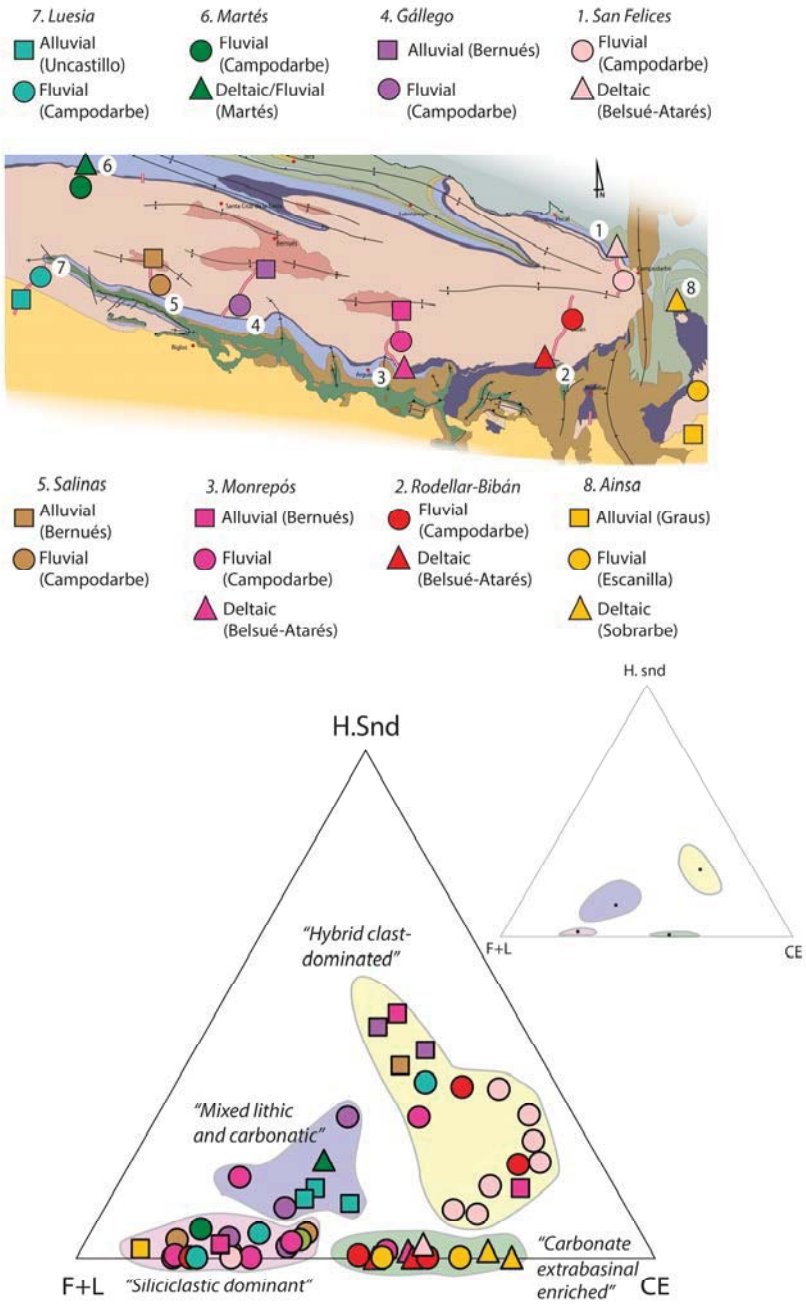

Figure 6. Top: Geological map from Figure 2, with symbols of the sample groups, in order to facilitate the interpretation of the ternary diagram located below. Bottom: Compositional plot where Hybrid Snd, Hybrid Sandstone fragments; FL, Feldspar and Lithic grains excluding hybrid sandstone fragments; and CE, Carbonate Extrabasinal grains. Compositional plot discriminates the four main groups of petrofacies described for all the analysed samples, while the small ternary diagram on the right side shows the mean confidence regions (90%) for each petrofacies. Yellow-coloured fields correspond to "Hybrid clast-dominated" petrofacies, green-coloured fields to "Carbonate extrabasinal enriched" petrofacies, blue-coloured fields to "Mixed lithic and carbonatic" petrofacies and pink coloured fields to "Siliciclastic dominant" petrofacies.

4.2.3 Siliciclastic dominant petrofacies

In this petrofacies siliciclastic components are the most dominant grain type (Fig. 7B, 8B, 8C), always with less than 30% of carbonatic grains and less than 5% of hybrid sandstone rock fragments. Shales, schists and quartzites are always present in this petrofacies, together with significant amounts of quartz grains, as well as radiolarite rock fragments and quartz-rich sandstone rock fragments. Other subordinate sandstone/siltstone rock fragments that usually appear are those with mica and opaques.

In the Ainsa basin, siliciclastic dominant petrofacies are represented in the Graus Formation conglomerates (sample GRAD1), where metamorphic rock fragments like metasiltstones, slate and phyllite lithic fragments, together with epidote grains are overwhelming (Fig. 6).

Similar components of this petrofacies are observed in the Campodarbe and Bernués Formations of the Jaca basin. In the Rodellar-Bibán and San Felices sections only few samples show siliciclastic dominant petrofacies while to the west they represented most of the Campodarbe Formation deposits Monrepós, Gállego, Martés, Salinas and Luesia sections (Fig. 6). In the Bernués Formation, only one sample from the Monrepós section shows this kind of petrofacies (sample BEMO18).

4.2.4 Hybrid clast-dominated petrofacies

The main feature of this petrofacies (Fig. 7C, 8D) is the high content of hybrid sandstone/siltstone rock fragments (>10%). Hybrid rock fragments are considered to be those that contain both extrabasinal and intrabasinal carbonate components, in similar proportions. Hybrid sandstone rock fragments are usually accompanied by limestone rock fragments, which are commonly the second most important component in this petrofacies. This petrofacies is also characterized by a low content of siliciclastic components (metamorphic and siliciclastic sandstone rock fragments).

Hybrid clast dominated petrofacies are representative of the entire Campodarbe Formation deposits in the San Felices section, while to the south-west of the basin they only occur in the upper parts of these formations (Rodellar-Bibán, Monrepós, Gállego and Luesia). The overlying Bernués Formation deposits maintain these compositional features and are therefore included in this petrofacies (Fig. 6).

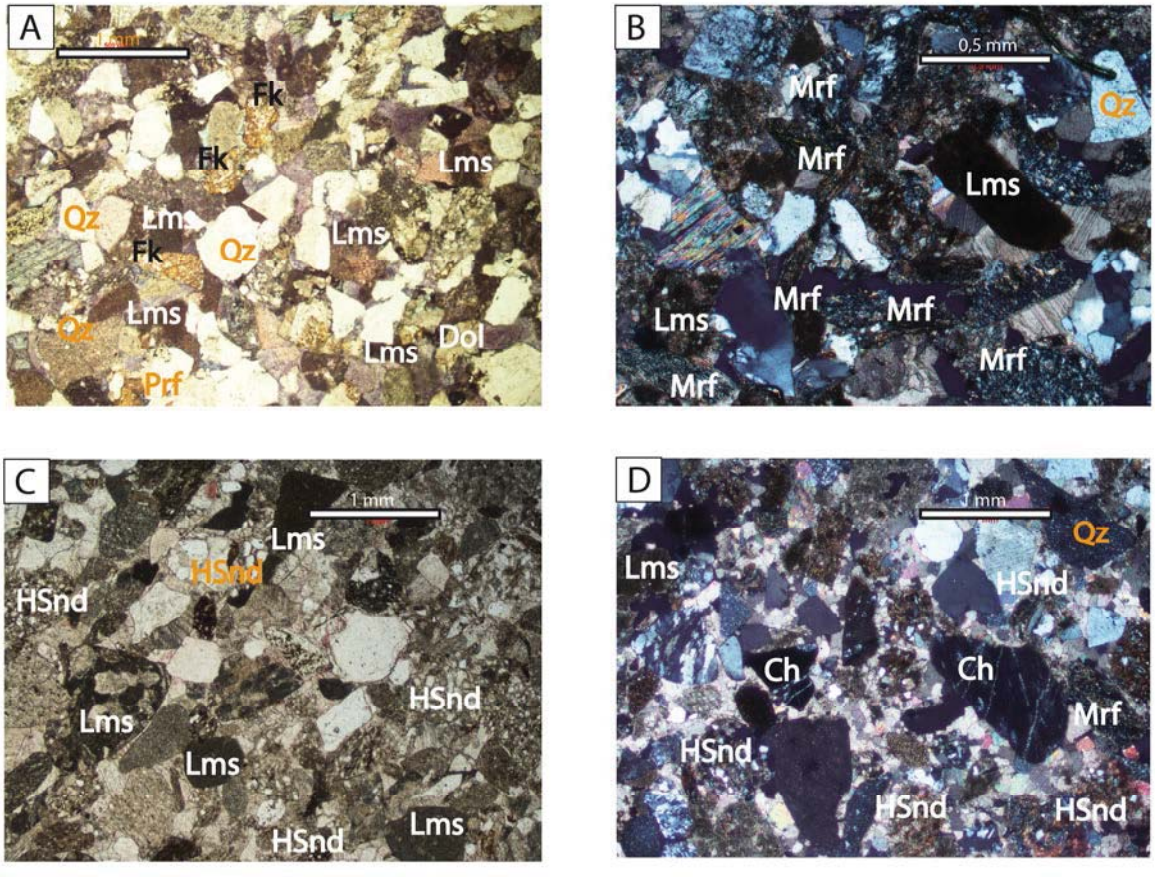

Figure 7. Optical photomicrographs of the described petrofacies: (A) General view of "Carbonate extrabasinal enriched" petrofacies, with abundant micritic and bioclastic limestone (Lms) fragments and quartz (Qz), K-feldpar (FdK), plutonic rock fragments (Prf) and dolomite grains (Dol) (XPL). Sample ROD1, Belsué-Atarés Formation; (B) "Siliciclastic dominant" petrofacies characterized by the highest contents of quartz (Q), metamorphic rock fragments (Mrf) and limestone grains (Lms) and by the absence of hybrid sandstone rock fragments (XPL). Sample GAL4, Campodarbe Formation; (C) General view of "Hybrid clast-dominated" petrofacies showing the large amount of hybrid sandstone rock fragments (HSnd), and limestone rock fragments (Lms) (PPL); and (D) Appearance of "Mixed lithic and carbonatic" petrofacies, showing the coexistence of hybrid sandstone rock fragments (HSnd) with abundant carbonatic (Lms) and siliciclastic grains radiolarite (Ch), quartz (Qz) and metamorphic grains (Mrf) (XPL).

4.2.5 Mixed lithic and carbonatic petrofacies

The "Mixed lithic and carbonatic" petrofacies is characterised by 15-40% carbonate grains (Fig. 7D, 8E, EG), hybrid sandstone rock fragments (up to 30 %) and higher proportions of lithic grains (25-35%, excluding hybrid sandstone fragments). Non-carbonatic grains are mainly represented by quartz, K-feldspar, radiolarite rock fragments, siliciclastic sandstones and volcanic lithic grains.

This petrofacies is recorded in a limited number of samples (Fig. 6), and shows two different sub-groups that can be identified in function of the lithic fragments type. In the Campodarbe Formation it appears in the Monrepós and Gállego sections (samples BEMO14, GAL7 and GAL8), and shows some proportions of hybrid

sandstone fragments and metamorphic lithic grains. In contrast, in the transitional Martés deposits (sample MAR1) and in the alluvial Uncastillo Formation (samples LUE2, LUE3 and LUE5) it appears lithic grains are dominated by abundant siliciclastic sandstones and radiolarite rock fragments.

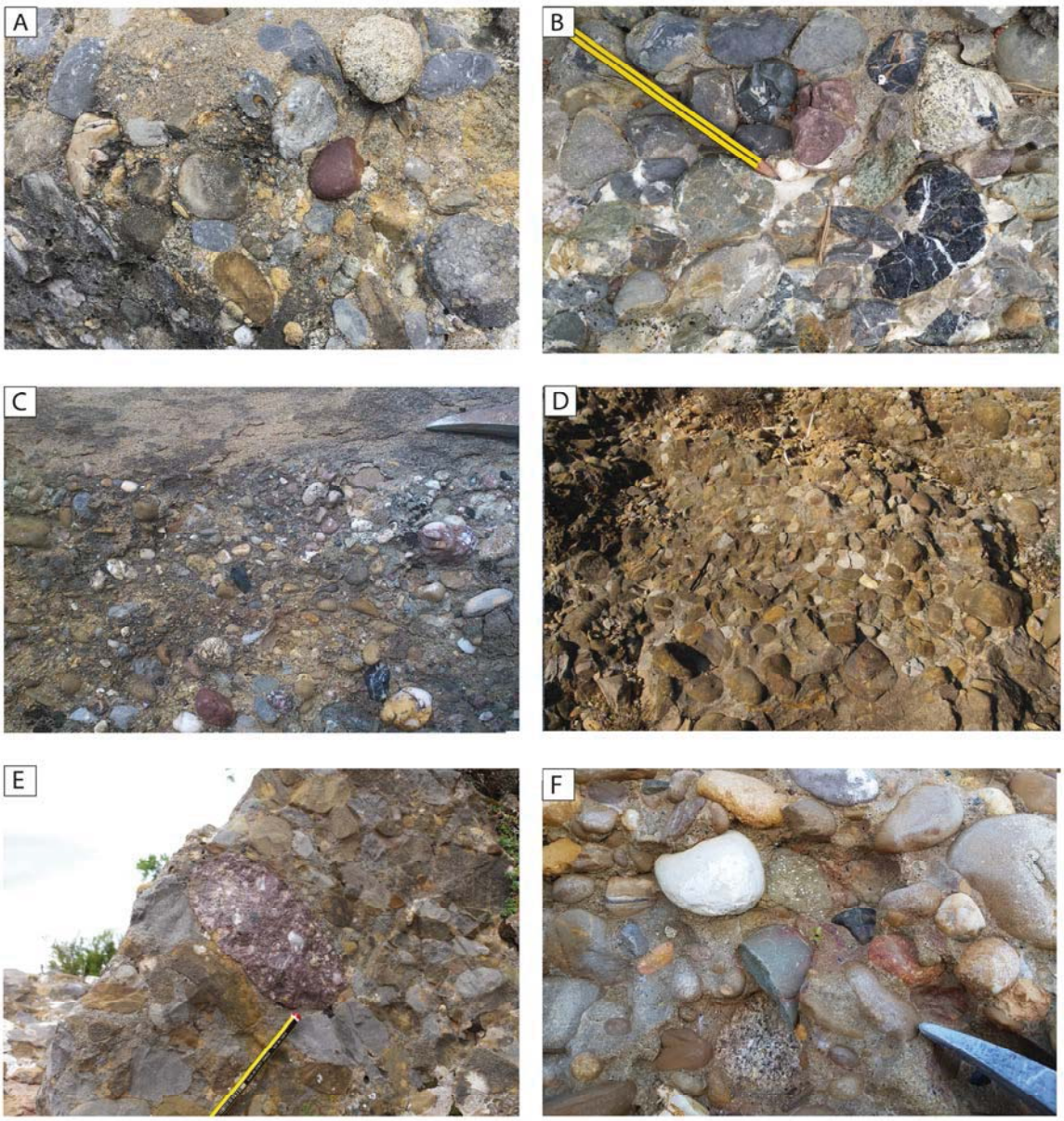

Figure 8. Images of the appearance of each of the described petrofacies in the conglomerate-sized deposits. (A) "Carbonate extrabasinal enriched" petrofacies: dominant proportion of the grey limestone clasts with few granitic white clasts. Image from the Escanilla Formationin the Ainsa section; (B) "Siliciclastic dominant" petrofacies: clasts from dolerites (green clasts at the center), granites (white clasts), radiolarite chert (dark clasts) and from permo-triassic sandstones (red clasts). Image from the Campodarbe Formation in the San Felices section; (C) "Siliciclastic dominant" petrofacies: quartz white clasts and Buntsandstein red clasts (Triassic) surrounded by other siliciclastic components (schists, radiolarite, sandstone clasts). Image from the Campodarbe Formation in the Bibán section; (D) "Hybrid clast-dominated" petrofacies: dominance of hybrid sedimentary clasts (i.e., all the brownish clasts) with few grey carbonatic clasts. Image from the Campodarbe Formation in the Gállego section; (E) "Mixed lithic and carbonatic" petrofacies: Grey limestone and hybrid sedimentary clasts clast (northern sources) and a Triassic red pebble, evidencing the mixing with axially-fed components. Image from the Campodarbe Formation in the San Felices section; and (F) "Mixed lithic and carbonatic" petrofacies: brownish sandstone clasts together with volcanic, radiolarite, granitic and limestone with black bedded chert clasts derived from the western Pyrenees. Image from the Uncastillo Formation in the Luesia section.

5. Provenance implications and evolution of the source areas

5.1 Petrofacies provenance

Sandstone detrital modes indicate multiple source areas, evidencing the interplay between systems of diverse provenance from Eocene to Miocene times. The four identified petrofacies allow for a better discrimination of these source areas and their evolution through time, which are here discussed in order to constrain the provenance of the analysed deposits.

As shown in Figure 9, the Belsué-Atarés Formation represents the first deltaic deposits represented in the southern border of the Jaca basin (Rodellar-Bibán section). "Carbonatic extrabasinal enriched" petrofacies are distinctive of this formation. Their compositional features, characterized by the dominance of carbonate grains with subordinate plutonic rock fragments, together with paleocurrent and facies architecture (Soler-Sampere and Puigdefàbregas, 1970; Puigdefàbregas, 1975) support a provenance from the east, located in the central Pyrenees. This source area would have been constituted by the Paleozoic basement of the Axial Zone, which provided significant amounts of plutonic components, together with the Mesozoic and Paleocene formations, which delivered a wide range of carbonate grains. The similarity with the composition of these deposits with the fluvial Escanilla Formation (Figs. 6, 7), allow to define this formation as the proximal time equivalents for the Belsué-Atarés deposits in this part of the basin, which is agreement with the results obtained in Roigé *et al.* (2017) by the same formations in the northern part of the Jaca basin.

The fluvial deposits of the Campodarbe Formation display three of the four petrofacies described, evidencing the interplay and evolution of different source areas. The lowermost part of this formation is only recorded in the eastern part of the basin (Rodellar section), as to west it passes to the Belsué-Atarés Formation and to the Arguis marls (Fig. 9) and as expected, all of them display the same "Carbonatic extrabasinal enriched" petrofacies as its marine time equivalents (Fig. 9). This petrofacies is progressively replaced upsection by "Siliciclastic dominant" petrofacies, which becomes the most represented petrofacies in the southern border of the Jaca basin. Paleocurrent directions and facies architecture continue indicating an eastern provenance for the Campodarbe Formation, but a change on the petrofacies thypology evidences a shift in the source rocks. This switch consists on the increase of metamorphic rock fragments, which evidences the persisting input from the Paleozoic basement, but highlights a major change in the nature of the source lithologies of the Axial Zone. This change has been identified also in the upper part of the Escanilla Formation, in the Ainsa basin (Michael, 2013). This shift could be linked to a reorganization of the drainage area in the Axial Zone caused by uplift or thrust emplacement in the source area. The dominance of these metamorphic lithologies in the source area is also recorded in the Graus Formation conglomerates (Fig. 6) evidencing the continuous

contribution of this source rocks through time. Therefore, the Rodellar-Bibán and Monrepós sections record the evolution of the eastern sources, which in the Axial Zone evolved from a plutonic dominated towards a metamorphic dominated source area (Fig. 9).

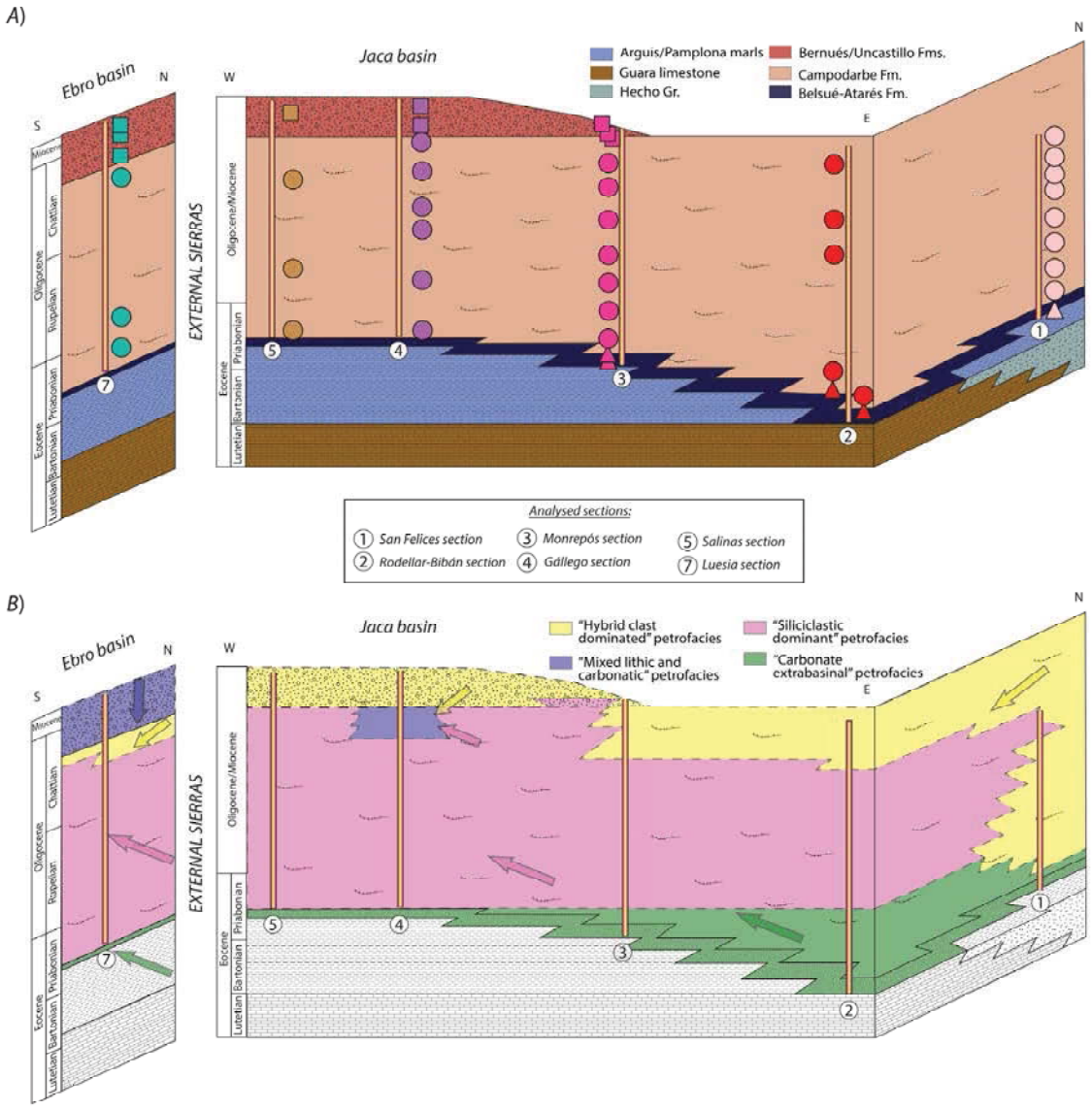

Figure 9. Top: General stratigraphic cross-section sketch with symbols representing the relative position of the analyzed samples presented in Figure 3, used here to understand the petrofacies scheme below. Bottom: Coloured stratigraphic cross-section sketch in order to illustrate the distribution of the petrofacies laterally and through time. Yellow-colour correspond to "Hybrid clast-dominated" petrofacies, green-colour to "Carbonate extrabasinal enriched" petrofacies, blue-colour to "Mixed lithic and carbonatic" petrofacies and pink colour to "Siliciclastic dominant" petrofacies. Coloured arrows are used to facilitate reading of the provenance information. Dashed lines represent the boundaries between petrofacies

Nonetheless, these two petrofacies associated with the eastern provenance of this axial-fed system are replaced upsection by the irruption of "Hybrid clast-dominated" petrofacies which evidences the entering of north-sourced systems in the Jaca basin (transverse-fed system). To the western part of the basin, the replacement of this petrofacies by the "Hybrid clast-dominated" petrofacies occurs in younger parts of the Campodarbe Formation, or even between this formation and the Bernués Formation, evidencing the competition of these sources in different positions of the basin (Fig. 9). In contrast, in the San Felices section (northeastern part of the basin) this north-derived petrofacies rules almost all the section, with punctual irruptions of "Siliciclastic dominant" petrofacies (Fig. 9).

"Mixed lithic and carbonatic" petrofacies with metamorphic components recorded in the Campodarbe Formation, would be the result of interference between "Siliciclastic dominant" petrofacies and "Hybrid clast dominated" petrofacies evidencing the interference between the axial-fed system with the transverse one (Fig. 9).

Much more to the west, in the Luesia section, the Campodarbe Formation does not show significant variations with its equivalents located in the easternmost part of Jaca basin. In contrast, the alluvial deposits of the Luna fan (Uncastillo Formation, in the Ebro basin) do not display the "Hybrid clast-dominated" petrofacies that occurs in its time equivalent Bernués Formation, which characterizes the north-derived alluvial sedimentation. Instead the Luna conglomerates show "Mixed lithic and carbonatic" petrofacies (Fig. 9). Although some components are common, the relatively high content of siliciclastic sandstone, radiolarite and volcanic rock fragments allow to infer a distinctive source area for the conglomerates of the Luna fan.

Moreover, the abundant siliciclastic content of the Luna fan cannot be derived from the Axial Zone located to the north of the Jaca basin, where the catchment drainage areas of the San Juan de la Peña and Peña Oroel were located (Roigé *et al*. 2017). In this sense, we propose that the source area of the Luna fan were located in the western Pyrenees, near the Cinco Villas massif (Fig. 1), in order to provide this distinctive petrologic signature. The work by Hirst and Nichols (1986) already pointed to this western source, according to the heavy mineral assemblages recorded in this fan. This is consistent with the thermochronologic results from the Axial Zone of the western Pyrenees, which show older exhumation ages than the Axial Zone of the west-central Pyrenees (Vacherat *et al.*, 2016; Bosch *et al.*, 2016; Hart *et al.*, 2017).

The "mixed and lithic" petrofacies recorded in the Martés sandstone, in the nortwestern part of the Jaca basin, imply a challenging interpretation. The siliciclastic content of these deposits is very close to the composition described in the Luna alluvial fan, that could indicate the same source area for both, located to the northwest, in the western Pyrenees. This interpretation would discard an eastern source area from the

central Pyrenees, as assumed before, according to the low content on metamorphic rock fragments. Nonetheless, this interpretation is not in accordance with north-west paleocurrent directions described for the Martés deposits (Puigdefàbregas, 1975), which imply a south-west directed paleoflow, probably derived from eastern source areas according to late Eocene basin paleogeography. As none of the samples described in the southern sector of the basin show the compositional features described in the Martés deposits, the most plausible explanation would be that reworking and consequent destruction of labile components such as metamorphic fragments, could cause the compositional differences between the Martés sandstones and the Campodarbe Formation most probable time and proximal equivalents.

5.2 General considerations

During Lutetian to Bartonian times, deltaic sedimentation in the southern Jaca basin was mainly derived from eastern source areas. This eastern provenance area was placed in the central Pyrenees, where the Mesozoic and Paleocene deposits and the Paleozoic basement composed the source area. The Paleozoic source rocks contributed by delivering plutonic components for the first stage of deltaic sedimentation (Bartonian), evolving to a much more dominant metamorphic source that persisted from Priabonian times until at least Oligo-Miocene times, as demonstrated by the compositional features of the Graus Formation.

Northern sources, mainly composed by the Hecho Group turbidites, were uplifted by the activity of the Gavarnie thrust. Transverse north-derived alluvial systems progressively replaced the axial-fed fluvial systems, from east to west, and from north to south. Therefore, the onset of transverse alluvial sedimentation in the northern margin competed against the axial fluvial systems, producing a westward and southward displacement of the axial fluvial network.

The later stages of the Jaca basin were controlled by the activity of the Guarga thrust that produced the uplift of the basin avoiding that the axial fluvial network could enter the basin. Therefore, only north-derived sediments filled the basin during Chattian-Aquitanian times (Bernués Formation).

Since the emersion of the External Sierras, the last fluvial deposits of the Campodarbe Formation (Oligocene) in the Ebro basin started to record the erosion of this new emerged domain. The overlying Luesia fan (Uncastillo Formation) represented the onset of the north-derived systems in this sector of the Ebro basin, concomitantly with the persistent sedimentation of the Bernués Formation in the Jaca basin. Therefore, the Chattian to Aquitanian period was mainly represented by two main north-derived systems with two distinctive source areas. For the Bernués Formation, the source area was situated immediately to the north of the Jaca basin, composed by the Hecho Group turbidites and the North Pyrenean Zone (Roigé *et al.*, 2017).

In contrast, the source area for the Uncastillo Formation was situated in the western Pyrenees, composed by the Paleozoic basement massifs and the previous foreland deposits (Hecho Group and Campodarbe Formations)

6. Conclusions

New sandstone petrography results allow to constraint the interplay of diverse sediment routing systems in the transitional to terrestrial environments of the Jaca thrust-sheet-top basin, and also from the Ebro basin during Lutetian to Miocene times. Additional analysis of the equivalent sedimentary systems in the Ainsa basin (Sobrarbe, Escanilla and Graus Formations) allow to obtain a better characterization of the evolution of eastern source areas.

Petrologic signatures allow to define four main petrofacies for the Belsué-Atarés, Campodarbe, Bernués and Uncastillo Formations, which are: “Carbonatic extrabasinal enriched”, “Siliciclastic dominant”, “Hybrid clast-dominated” and “Mixed lithic and carbonatic” petrofacies.

“Carbonatic extrabasinal enriched” petrofacies are distinctive from the Belsué-Atarés deltaic deposits. By contrast, the overlying Campodarbe Formation deposits show “Siliciclastic dominant”, “Hybrid clast-dominated” and “Mixed lithic and carbonatic” petrofacies, evidencing the interplay of source areas. The time equivalents Bernués and Uncastillo Formation show “Hybrid clast-dominated” and “Mixed lithic and carbonatic” petrofacies, respectively.

According to each recorded petrofacies we can infer that the deltaic sedimentation in the southern Jaca basin (Bartonian-Priabonian) was mainly derived from eastern source areas, located in the central Pyrenees, in which the Paleozoic basement contributed by delivering dominant plutonic components. A change in this source area during Priabonian times yielded to the evolution of a Paleozoic source area richer in metamorphic rocks that persisted until at least Oligo-Miocene times. Transverse north-derived systems progressively replaced the axial-fed systems, from east to west. The onset of alluvial sedimentation in the northern margin competed against the fluvial systems, producing a westward displacement of the axial fluvial network. During Chattian to Aquitanian times two main north-derived systems coexisted in the Jaca and Ebro basins. The Bernués Formation was derived from source areas located to the north of the Jaca basin, composed by the Hecho Group turbidites and the deposits of the North Pyrenean Zone. In contrast, the Uncastillo Formation was sourced from the western Pyrenees, composed by the Paleozoic basement massifs and the previous foreland deposits (Hecho Group and Campodarbe Formations).

7. References

Arenas, C., 1993. Sedimentologia y paleogeografia del Terciario del margen pirenaico y sector central de la Cuenca del Ebro (zona aragonesa occidental): Universidad de Zaragoza, 858 p.

Arenas, C., Millán, H., Pardo, G. and Pocoví, A., 2001. Ebro Basin continental sedimentation associated with late compressional Pyrenean tectonics(north-eastern Iberia): controls on basin margin fans and fluvial systems: *Basin Research*, **13**, p. 65–89, doi: 10.1046/j.1365-2117.2001.00141.x.

Barnolas, A. and Gil-Pena, I., 2002. Ejemplos de relleno sedimentario multiepisodico en una cuenca de antepais fragmentada: La Cuenca Surpirenaica: *Boletin Geologico y Minero*, **112**, p. 17–38.

Bentham, P.A., Burbank, D.W. and Puigdefabregas, C., 1992. Temporal and spatial controls on the alluvial architecture of an axial drainage system: late Eocene Escanilla formation, southern Pyrenean foreland basin, spain: *Basin Research*, **4**, p. 335–352, doi: 10.1111/j.1365-2117.1992.tb00052.x.

Bosch, G. V., Teixell, A., Jolivet, M., Labaume, P., Stockli, D., Domènech, M. and Monié, P., 2016. Timing of Eocene-Miocene thrust activity in the Western Axial Zone and Chaînons Béarnais (west-central Pyrenees) revealed by multi-method thermochronology: *Comptes Rendus - Geoscience*, **348**, p. 246–256, doi: 10.1016/j.crte.2016.01.001.

Caja, M.A., Marfil, R., Garcia, D., Remacha, E., Morad, S., Mansurbeg, H., Amorosi, A., Martínez-Calvo, C. and Lahoz-Beltrá, R., 2010. Provenance of siliciclastic and hybrid turbiditic arenites of the Eocene Hecho Group, Spanish Pyrenees: Implications for the tectonic evolution of a foreland basin: *Basin Research*, **22**, p. 157–180, doi: 10.1111/j.1365-2117.2009.00405.x.

Canudo, 1990. Los foraminíferos planctónicos del Paleoceno– Eoceno del Prepirineo oscense en el sector de Arguis.: Universidad de Zaragoza.

Canudo, J.I. and Molina, E., 1988. Biocronología de foraminíferos planctónicos de la secuencia deposicional de Jaca (Pirineo Aragonés): Eoceno medio y superior. In: *II Cong. Geol. Esp.* SGE, Granada, p. 273–276.

Castelltort, S., Guillocheau, F., Robin, C., Rouby, D., Nalpas, T., Lafont, F. and Eschard, R., 2003. Fold control on the stratigraphic record: a quantified sequence stratigraphic study of the Pico del Aguila anticline in the south-western Pyrenees (Spain): *Basin Research*, **15**, p. 527–551.

Castelltort, S., Pochat, S. and Van den Driessche, J., 2004. How reliable are growth strata in interpreting short-term (10 s to 100 s ka) growth structures kinematics? *Comptes Rendus Geoscience*, **336**, p. 151–158,

doi: 10.1016/j.crte.2003.10.020.

Chayes, F., 1952. The finer-grained calcalkaline granites of New England: *The Journal of Geology*, **60**, p. 207–254.

Coll, X., Gómez-Gras, D., Roigé, M. and Mestres, N., 2017. Heavy-mineral assemblages as a provenance indicator in the Jaca basin (Middle-Late Eocene, southern Pyrenees): *Geogaceta*, **61**.

Comas-Cufí, M. and Thió-Henestrosa, S., 2011. CoDaPack 2.0: a stand-alone, multi-platform compositional software. In: *CoDaWork'11: 4th InternationalWorkshop on Compositional Data Analysis* (Tolosana-Delgado, R., and Ortego, M.I., eds.) Sant Feliu de Guíxols.

Costa, E., Garcés, M., López-Blanco, M., Beamud, E., Gómez-Paccard, M. and Larrasoaña, J.C., 2010. Closing and continentalization of the South Pyrenean foreland basin (NE Spain): Magnetochronological constraints: *Basin Research*, **22**, p. 904–917, doi: 10.1111/j.1365-2117.2009.00452.x.

Critelli, S. and Ingersoll, R. V, 1995. Interpretation of neovolcanic versus paleovolcanic sand grains: an example from Miocene deep marine sandstones of the Topanga Group (southern California): *Sedimentology*, **42**, p. 783–804.

Dickinson, W.R., 1970. Interpreting detrital modes of graywacke and arkose: *Journal of Sedimentary Research*, **40**, p. 695–707.

Dickinson, W.R., Beard, L.S., Brakenridge, G.R., Erjavec, J.L., Ferguson, R.C., Inman, K.F. and Ryberg, P.T., 1983. Provenance of North American Phanerozoic sandstones in relation to tectonic setting: *Geological Society of America Bulletin*, **94**, p. 222–235.

Dreyer, T., Corregidor, J., Arbues, P. and Puigdefabregas, C., 1999. Architecture of the tectonically influenced Sobrarbe deltaic complex in the Ainsa Basin, northern Spain: *Sedimentary Geology*, **127**, p. 127–169, doi: 10.1016/S0037-0738(99)00056-1.

Dryden, J.A.L., 1931. Accuracy in percentage representation of heavy mineral frequencies: *Proceedings of the National Academy of Sciences*, **17**, p. 233–238.

Fontana, D., Zuffa, G.G. and Garzanti, E., 1989. The interaction of eustacy and tectonism from provenance studies of the Eocene Hecho Group Turbidite Complex (South-Central Pyrenees, Spain): *Basin Research*, **2**, p. 223–237, doi: 10.1111/j.1365-2117.1989.tb00037.x.

Friend, P.F., Hirst, J.P., Hogan, P.J., Jolley, D.W., Mcelroy, R., Nichols, G.J. and Rodriguez-Vidal, J., 1989.

Pyrenean tectonic control of Oligo-Miocene river systems, Huesca, Aragon, Spain:

Garzanti, E. and Vezzoli, G., 2003. A Classification of Metamorphic Grains in Sands Based on their Composition and Grade: *Journal of Sedimentary Research*, **73**, p. 830–837, doi: 10.1306/012203730830.

Gazzi, P., 1966. Le arenarie del flysh sopracretaceo dell'Apenino modenese; correlazioni con il flysh Monghidoro: *Mineral. Petrogr. Acta*, **12**, p. 69–97.

Gupta, K. Das and Pickering, K.T., 2008. Petrography and temporal changes in petrofacies of deep-marine Ainsa-Jaca basin sandstone systems, Early and Middle Eocene, Spanish Pyrenees: *Sedimentology*, **55**, p. 1083–1114, doi: 10.1111/j.1365-3091.2007.00937.x.

Hart, N.R., Stockli, D.F., Lavier, L.L. and Hayman, N.W., 2017. Thermal evolution of a hyperextended rift basin, Mauléon Basin, western Pyrenees: *Tectonics*, **36**, p. 1103–1128, doi: 10.1002/2016TC004365.

Hirst, J.P. and Nichols, G.J., 1986. Thrust tectonic controls on Miocene alluvial distribution patterns, southern Pyrenees: *IAS Special Publications*, **8**, p. 247–258, doi: 10.1002/9781444303810.

Hogan, P.J., 1993. Geochronologic, Tectonic and Stratigraphic Evolution of the Southwest Pyrenean Foreland Basin, Northern Spain.: University of Southern California, 208 p.

Hogan, P.J. and Burbank, D.W., 1996. Evolution of the Jaca piggyback basin and emergence of the External Sierra, southern Pyrenees: *Tertiary basins of Spain the stratigraphic record of crustal kinematics*, **1**, p. 153–160, doi: 10.1017/CBO9781107415324.004.

Huyghe, D., Castelltort, S., Mouthereau, F., Serra-Kiel, J., Filleaudeau, P.Y., Emmanuel, L., Berthier, B. and Renard, M., 2012. Large scale facies change in the middle Eocene South-Pyrenean foreland basin: The role of tectonics and prelude to Cenozoic ice-ages: *Sedimentary Geology*, **253–254**, p. 25–46, doi: 10.1016/j.sedgeo.2012.01.004.

Jolley, J., 1988. Thrust tectonics and alluvial architecture of the Jaca Basin, southern Pyrenees: University of Wales, Cardiff, 365 p.

Labaume, P., Séguret, M. and Seyve, C., 1985. Evolution of a turbiditic foreland basin and analogy with an accretionary prism: Example of the Eocene South-Pyrenean Basin: *Tectonics*, **4**, p. 661–685.

Lafont, F., 1994. Influences relatives de la subsidence et de l'eustatisme sur la localisa- tion et la géometrie des reservoirs d'un système deltaique. Exemple de l'Eocene du bassin de Jaca (Pyrenees espagnoles): University of Rennes, France, 264 p.

Lagabrielle, Y., Labaume, P. and Saint-Blanquat, M., 2010. Mantle exhumation, crustal denudation, and gravity tectonics during Cretaceous rifting in the Pyrenean realm (SW Europe): Insights from the geological setting of the lherzolite bodies: *Tectonics*, **29**, doi: 10.1029/2009TC002588.

Marsaglia, K.M. and Ingersoll, R. V, 1992. Geological Society of America Bulletin reassessment of magmatic-arc provenance: , doi: 10.1130/0016-7606(1992)104<1637.

Michael, N., 2013. Functioning of an ancient routing system, the Escanilla Formation, South Central Pyrenees: Imperial College London, 318 p.

Millán-Garrido, H., Pocoví, A. and Casas, A.M., 1995. El frente cabalgamiento surpirenaico en el extremo occidental de las Sierras Exteriores: *Revista de la Sociedad Geologica de España*, **8**, p. 73–90.

Mochales, T., Barnolas, A., Pueyo, E.L., Serra-Kiel, J., Casas, A.M., Samsó, J.M., Ramajo, J. and Sanjuán, J., 2012. Chronostratigraphy of the Boltaña anticline and the Ainsa Basin (southern pyrenees): *Bulletin of the Geological Society of America*, **124**, p. 1229–1250, doi: 10.1130/B30418.1.

Montes, M., 2002. Estratigrafia del Eoceno-Oligoceno de la Cuenca de Jaca (Sinclinorio del Guarga): Universitat de Barcelona, 365 p.

Mutti, E., 1985. Turbidite systems and their relations to depositional sequences. In: *Provenance of Arenites* (Zuffa, G.G., ed.) NATO ASI Ser., p. 65–93.

Mutti, E., Luterbacher, H., Ferrer, J. and Rosell, J., 1972. Schema stratigrafico e lineamenti di facies del Paleogeno Marino della zona centrale sudpirenaica tra Tremp (Catalogna) e Pamplona (Navarra): *Memorie della Società Geologica Italiana*, **11**, p. 391–416.

Nijman, W. and Nio, S.-D., 1975. *The Eocene Montañana Delta (Tremp-Graus Basin, provinces of Lérida and Huesca, Southern Pyrenees, N Spain)*: Field trip B guidebook (The sedimentary evolution of the Paleogene south Pyrenean Basin), XI International SedimentologicalCongress, International Association of Sedimentologists, Nice, Excursion Guidebook.

Oliva-Urcia, B., Beamud, E., Garces, M., Arenas, C., Soto, R., Pueyo, E.L. and Pardo, G., 2015. New magnetostratigraphic dating of the Palaeogene syntectonic sediments of the west-central Pyrenees: tectonostratigraphic implications: *Palaeomagnetism in Fold and Thrust Belts: New Perspectives. Geological Society, London, Special Publications*, **425**, p. 107–128, doi: 10.1144/SP425.5.

Oms, O., Dinarès-Turell, J. and Remacha, E., 2003. Magnetic stratigraphy from deep clastic turbidites: An example from the Eocene Hecho group (Southern Pyrenees): *Studia Geophysica et Geodaetica*, **47**, p.

275–288, doi: 10.1023/A:1023719607521.

Ortí, F., Salvany, J.M., Rosell, L., Pueyo, J.J. and Inglés, M., 1986. Evaporitas antiguas (Navarra) y actuales (Los Monearos) de la Cuenca del Ebro. In: *Guía de las Excursiones del XI Congreso Español de Sedimentologia* (Anadón, P., and Cabrera, L., eds.) Generalitat de Catalunya, Comissió Interdepartamental de Recerca i Innovació Tecnològica (CIRIT), Barcelona., p. 21–24.

Payros, A., Pujalte, V. and Orue-Etxebarria, X., 1999. The South Pyrenean Eocene carbonate megabreccias revisited: New interpretation based on evidence from the Pamplona Basin: *Sedimentary Geology*, **125**, p. 165–194, doi: 10.1016/S0037-0738(99)00004-4.

Pocoví, A., Millan, H., Navarro, J.J. and Martinez, M.B., 1990. Rasgos estructurales de la Sierra de Salinas y zona de los Mallos (Sierras Exteriores, Prepirineo, provincias de Huesca y Zaragoza): *Geogaceta*, **8**, p. 36–39.

Pueyo, E.L., Millán, H. and Pocoví, A., 2002. Rotation velocity of a thrust: A magnetotectonic study in the Pico del Aquila anticlina (southern Pyrenees, Spain): *Sedimentary Geology on Growth Strata*, **146 (1-2)**, p. 191–208.

Puigdefàbregas, C., 1975. La sedimentación molásica en la cuenca de Jaca: *Pirineos*, **104**, p. 1–188.

Puigdefàbregas, C., Muñoz, J.A. and Verges, J., 1992. Trusting and foreland basin evolution in the southern Pyrenees. In: *Thrust Tectonics* Springer Netherlands, p. 247–254.

Reynolds, A., 1987. Tectonically Controlled Fluvial Sedimentation in the South-Pyrenean Foreland Basin: University of Liverpool, Liverpool.

Rodríguez-Pintó, A., Pueyo, E.L., Serra-Kiel, J., Samsó, J.M., Barnolas, A. and Pocoví, A., 2012. Lutetian magnetostratigraphic calibration of larger foraminifera zonation (SBZ) in the Southern Pyrenees: The Isuela section: *Palaeogeography, Palaeoclimatology, Palaeoecology*, **333–334**, p. 107–120, doi: 10.1016/j.palaeo.2012.03.012.

Roigé, M., Gómez-Gras, D., Remacha, E., Boya, S., Viaplana-Muzas, M. and Teixell, A., 2017. Recycling an uplifted early foreland basin fill: An example from the Jaca basin (Southern Pyrenees, Spain): *Sedimentary Geology*, **360**, p. 1–21, doi: 10.1016/j.sedgeo.2017.08.007.

Roigé, M., Gómez-Gras, D., Remacha, E., Daza, R. and Boya, S., 2016. Tectonic control on sediment sources in the Jaca basin (Middle and Upper Eocene of the South-Central Pyrenees): *Comptes Rendus - Geoscience*, **348**, p. 236–245, doi: 10.1016/j.crte.2015.10.005.

Roure, F., Choukroune, P., Berastegui, X., Muñoz, J.A., Villien, A. and Matheron, P., 1989. ECORS deep seismic data and balanced cross sections: Geometric constrains on the evolution of the Pyrenees: *Tectonics*, **8**, p. 41–50.

Soler-Sampere, M. and Puigdefàbregas, C., 1970. Líneas generales de la geología del Alto Aragón Occidental: *Pirineos*,, p. 5–20.

Teixell, A., 1998. Crustal structure and orogenic material budget in the west central Pyrenees: *Tectonics*, **17**, p. 395–406.

Teixell, A., 1996. The Anso transect of the southern Pyrenees: basement and cover thrust geometries: *Journal of the Geological Society*, **153**, p. 301–310, doi: 10.1144/gsjgs.153.2.0301.

Teixell, A. and García-Sansegundo, J., 1995. Estructura del sector central de la Cuenca de Jaca (Pirineos meridionales): *Rev. Soc. Geol. España*, **8**, p. 215–228.

Vacherat, A., Mouthereau, F., Pik, R., Bellahsen, N., Gautheron, C., Bernet, M., Daudet, M., Balansa, J., Tibari, B., Pinna Jamme, R. and Radal, J., 2016. Rift-to-collision transition recorded by tectonothermal evolution of the northern Pyrenees: *Tectonics*, **35**, p. 907–933, doi: 10.1002/2015TC004016.

Vergés, J., Fernàndez, M. and Martínez, A., 2002. The Pyrenean orogen: pre-, syn-, and post-collisional evolution: *Journal of the Virtual Explorer*, **8**, p. 57–76, doi: 10.3809/jvirtex.2002.00058.

Zuffa, G.G., 1980. Hybrid arenites: their composition and classification: *Journal of Sedimentary Petrology*, **50**, p. 21–29.

Zuffa, G.G., 1985. Optical analyses of arenites: influence of methodology on compositional results. In: *Provenance of Arenites* (Zuffa, G.G., ed.) Boston, p. 165–189.

Supplementary information. Table 1 Sandstone compositional data (point counting analyses).

	SF2 %	SF3%	SF5%	SFE7%	SFE11%	SFE13%	SFE16%	SFE18%	SFE19%	ROD1%	ROD3 %	NOC1 %	BARA1 %	BIB1 %	BIB2 %	BIB5 %	BEMO1 %	BEMO3 %	BEMO5%	BEMO8%	BEMO10%	BEMO11%	BEMO12%	BEMO13%	BEMO14%	BEMO16%	BEMO17%	BEMO18%
Total siliciclastic extrabasinal	42.68	24.93	36.89	29.45	36.79	26.56	33.33	56.88	26.54	47.78	42.38	47.48	44.79	48.36	26.93	40.00	47.59	47.47	48.54	60.82	58.79	49.11	69.93	45.08	52.26	20.12	43.41	56.31
Total detrital quartz	21.97	9.57	15.85	6.41	12.58	6.56	16.67	19.88	5.25	23.42	16.16	28.62	23.93	14.93	7.12	12.33	28.92	28.16	23.62	28.84	22.36	14.88	17.97	7.52	6.35	4.19	3.30	2.77
Qtz monocrystalline	11.78	5.51	10.67	4.66	8.81	3.13	11.73	11.62	4.63	11.08	11.59	16.98	16.56	7.76	3.41	11.33	21.39	15.51	17.15	13.79	12.46	6.55	7.52	6.35	4.19	3.30	3.29	2.77
Monocrystal. und. qtz	0.32	-	0.30	0.29	-	-	0.62	0.31	-	2.53	0.30	0.94	2.15	0.60	-	-	0.90	0.63	-	0.31	-	0.30	-	-	-	-	-	-
Qtz inherited syntaxial cement	0.32	-	-	-	-	-	-	-	-	-	0.30	-	-	-	-	-	-	0.32	-	-	-	-	-	-	-	-	-	-
Qtz polycristall. 2-3 subgrains	2.23	0.58	0.61	1.17	0.63	1.54	3.06	-	-	2.53	0.91	2.20	1.84	0.30	-	0.33	0.60	0.95	1.29	2.51	2.56	1.19	0.65	0.95	-	-	-	0.62
Qtz polycristall. >3 subgrains	4.46	2.03	1.83	-	2.20	0.31	0.93	0.61	0.31	2.53	0.91	5.97	1.53	1.79	1.24	0.67	3.61	4.43	1.94	6.27	2.24	1.79	3.27	2.54	0.32	1.20	1.20	2.77
Quartz keuper	1.91	-	0.30	0.29	-	0.31	-	-	-	0.95	0.91	-	0.92	0.30	0.31	-	0.60	0.95	0.32	0.63	0.32	0.30	0.98	-	0.32	-	-	0.92
Quartz in plutonic r.f.	0.32	0.29	-	-	-	-	-	-	-	3.16	-	-	0.31	0.30	-	-	0.60	0.95	-	0.31	-	-	-	-	-	-	-	-
Quartz in metamorphic r.f.	-	-	-	-	-	-	-	-	-	-	-	-	-	-	-	-	-	-	-	-	-	-	-	-	-	-	-	-
Quartz in sandstone r.f.	0.64	1.16	1.52	-	0.94	2.19	1.85	4.28	0.31	0.63	1.22	2.52	0.61	3.88	2.17	-	1.20	4.43	2.91	5.02	4.79	4.76	5.56	1.59	6.77	0.30	0.60	3.38
Quartz in hybrid sandstone r.f.	-	-	0.61	-	-	-	-	-	-	-	-	-	-	-	-	-	-	-	-	-	-	-	-	0.63	0.32	-	1.20	-
Cc replacement on quartz	-	-	-	-	-	-	-	-	-	-	-	-	-	-	-	-	-	-	-	-	-	-	-	-	-	-	-	-
Total detrital feldspar	3.50	1.74	0.30	-	0.94	0.93	0.61	0.31	9.18	5.18	2.20	5.21	1.79	0.93	-	4.22	0.63	2.27	0.94	0.32	0.60	1.31	0.63	1.29	0.30	0.60	1.54
Detrital K-feld	0.96	0.29	0.30	-	0.94	0.93	0.61	0.31	4.43	2.74	0.94	1.84	1.49	0.93	-	1.81	-	1.62	0.31	-	0.30	1.31	0.63	1.29	0.30	0.30	1.54	
K-feld in plutonic r.f.	-	-	-	-	-	-	-	-	-	0.32	0.91	-	0.31	-	-	-	-	-	-	-	-	-	-	-	-	-	-	-
Detrital plagioclase	1.59	0.58	-	-	-	-	-	-	-	2.53	1.22	1.26	3.07	0.30	-	-	1.20	0.32	0.65	0.31	-	0.30	-	-	-	0.30	-	-
Plagioclase in plutonic r.f.	-	-	-	-	-	-	-	-	-	0.32	-	-	-	-	-	-	-	-	-	-	-	-	-	-	-	-	-	-
Detrital Microcline	0.96	0.87	-	-	-	-	-	-	-	1.58	0.30	-	-	-	-	-	1.20	0.32	-	0.31	0.32	-	-	-	-	-	-	-
Microcline in plutonic r.f	-	-	-	-	-	-	-	-	-	-	-	-	-	-	-	-	-	-	-	-	-	-	-	-	-	-	-	-
Total fine lithics	17.20	13.62	20.73	23.03	24.21	19.06	15.74	36.39	20.99	15.19	21.04	16.67	15.64	31.64	18.89	27.67	14.46	18.67	22.65	31.03	36.10	33.63	50.65	32.38	39.03	15.02	36.53	44.31
Phyllites	0.64	-	2.13	-	0.31	0.94	0.93	12.54	-	0.32	2.13	2.20	3.68	5.97	1.55	2.00	0.90	0.32	4.21	3.13	7.35	5.36	15.36	0.63	2.90	1.20	0.60	6.46
Schists	2.23	-	0.91	-	0.31	1.25	1.23	5.81	1.85	0.63	1.22	1.57	0.92	5.97	2.48	2.67	2.41	1.27	1.29	6.90	10.22	8.04	13.40	2.86	7.10	1.50	1.20	13.85
Chloritochists lithic	-	-	-	-	-	-	-	-	-	-	-	0.31	-	-	-	-	-	-	-	-	-	-	-	-	-	-	-	-
Quartzite	0.96	0.87	0.61	1.75	0.63	0.31	-	3.98	0.62	1.90	0.91	0.94	3.99	4.18	1.86	0.33	0.60	2.53	1.62	2.82	1.92	1.49	4.58	1.59	3.55	0.90	0.30	5.85
Plutonic r.f.	-	-	-	-	-	-	-	0.31	-	1.27	-	0.63	0.61	-	-	-	-	-	-	-	-	-	-	-	-	-	-	-
Cc replacement on plut. r.f.	-	-	-	-	-	-	-	-	-	-	-	-	-	-	-	-	-	-	-	-	-	-	-	-	-	-	-	-
Volcanic r.f.	-	-	0.30	-	0.31	1.88	-	-	-	-	-	-	0.61	-	0.31	0.67	0.30	-	-	0.31	-	-	0.65	-	-	-	-	0.62
Volcanic chert	-	-	-	-	-	-	-	-	-	-	-	-	-	-	-	-	-	-	-	-	-	-	-	-	-	-	-	-
Vitric volcanic lithic	-	-	-	-	-	-	-	-	-	-	-	-	-	-	-	-	-	-	-	-	-	-	-	-	-	-	-	-
volcanic lithic with microlitic	0.96	-	-	-	-	-	-	-	-	-	-	-	-	-	-	-	-	-	-	0.63	-	0.30	-	-	-	-	-	0.62
volcanic lithic lathwork texture	-	-	-	-	-	-	0.62	-	-	2.22	2.44	-	-	-	-	-	0.30	0.95	0.65	0.63	-	-	-	1.27	0.32	-	0.60	0.92
sandstone r.f.	1.27	0.29	-	0.29	0.31	1.25	0.93	2.14	0.31	1.90	0.61	2.20	0.92	2.39	-	0.33	0.60	0.63	0.32	0.31	0.64	0.89	2.29	1.27	3.23	-	0.60	-
Hybrid sandstone r.f.	-	2.32	0.30	6.41	7.23	1.88	0.93	-	3.09	-	-	-	-	-	4.64	3.00	-	-	-	-	-	-	-	1.27	1.61	1.50	4.49	0.62
Siltstone r.f.	5.10	0.29	1.83	0.87	1.26	3.44	4.94	9.48	3.09	4.75	9.15	5.35	3.37	7.46	1.55	1.67	5.12	6.65	7.12	5.64	7.03	9.52	5.88	3.49	9.03	2.10	5.69	7.38
Hybrid Siltstone r.f.	1.27	7.54	7.62	11.66	11.32	2.81	3.09	-	12.04	-	0.30	-	-	-	6.50	15.67	0.30	0.63	0.65	-	-	1.49	0.33	15.24	6.13	5.41	21.26	0.62
Chlorite	-	-	-	-	-	-	-	-	-	-	-	-	-	-	-	-	1.20	-	-	-	-	-	-	-	-	0.30	-	0.31
Chert	1.27	-	-	-	-	-	-	-	-	1.27	1.22	0.31	0.31	0.90	-	-	1.51	1.58	1.62	0.63	0.32	0.30	0.65	0.95	0.97	0.60	0.60	1.54
Muscovite	0.64	-	-	-	-	0.31	-	-	-	-	0.30	0.63	0.31	0.30	-	-	0.30	-	-	-	-	-	-	0.32	-	-	-	-
Biotite	-	-	0.61	-	-	-	-	-	-	-	-	0.31	-	-	-	-	-	-	-	0.31	0.32	-	-	-	-	-	-	-
Heavy minerals	-	-	-	-	-	-	-	-	-	-	-	-	-	-	-	-	-	-	0.32	-	0.32	-	-	0.32	-	-	-	-
Silicified r.f.	1.91	2.32	1.52	1.46	2.20	5.00	0.31	0.61	-	-	0.30	1.57	0.92	0.60	-	1.00	0.90	1.58	4.21	2.82	1.60	1.19	-	1.90	-	0.30	1.20	0.31
Cc replacement silificied r.f.	-	-	-	-	-	-	-	-	-	-	-	-	-	-	-	-	-	-	-	-	-	-	-	-	-	-	-	-
Fe-oxid replacement r.f.	0.64	-	4.88	0.58	-	1.54	0.31	-	-	1.83	0.31	-	2.69	-	0.33	-	-	-	-	2.82	3.83	3.27	2.94	0.32	3.87	1.20	-	3.38
Silificied limestone	-	-	-	-	-	-	-	-	-	-	-	-	-	-	-	-	-	-	-	-	-	-	-	-	-	-	-	-
Radiolarite r.f.	-	-	-	-	0.31	0.31	0.93	1.22	-	0.32	0.61	0.31	-	1.19	-	-	-	2.53	0.65	4.08	2.56	1.79	4.58	0.95	0.32	-	-	1.85
Alterite	0.32	-	-	-	-	-	-	-	-	0.63	-	-	-	-	-	-	-	-	-	-	-	-	-	-	-	-	-	-
Total carbonate extrabasinal	29.62	37.39	39.63	41.11	31.76	30.94	31.17	13.76	44.75	25.95	24.70	26.42	32.52	8.36	40.87	27.67	20.48	25.32	28.16	13.79	7.35	19.35	10.78	27.94	10.65	36.64	18.26	14.77
Mono. esparitic limestone	-	0.29	0.61	0.87	0.63	-	0.62	0.31	-	1.27	1.83	0.63	3.99	0.90	0.31	-	3.01	2.22	0.32	0.31	0.32	0.60	-	1.27	-	0.90	0.90	0.31
Poli. Esparitic r.f.	2.23	0.87	0.91	0.29	0.63	0.31	2.16	0.92	2.16	4.43	0.91	5.35	4.91	0.30	0.62	1.00	1.51	1.90	4.53	1.57	0.64	0.60	1.63	-	-	0.60	-	2.15
Dolomitized polycrystal. r.f.	-	-	-	-	-	-	-	-	0.31	-	0.91	-	-	-	-	-	-	0.32	-	-	-	-	-	-	-	-	-	-
Biomicritic	2.23	-	3.05	2.04	2.20	4.69	0.62	1.53	3.09	0.32	3.05	0.63	1.53	-	1.55	2.67	3.01	1.90	0.32	-	-	-	0.65	-	-	-	-	0.62
Biosparitic	-	-	-	-	0.31	-	-	-	0.31	-	-	0.31	-	-	-	0.33	-	-	0.32	-	-	-	-	-	-	0.60	-	-
Dolomicrite r.f	-	-	-	-	-	-	-	-	-	0.32	0.30	0.31	0.31	-	-	-	1.20	0.32	0.65	-	-	-	0.33	-	-	-	-	-
Dolomite monocrystalline	-	-	-	-	-	0.93	-	-	-	0.61	1.26	2.45	-	-	-	-	-	2.22	1.29	-	-	0.30	0.65	-	-	-	-	-
Dolostone r.f. (sacaroidea)	0.32	-	-	-	-	4.32	0.61	-	1.58	1.83	2.52	2.45	-	-	0.93	-	-	2.22	1.94	1.25	-	0.30	0.98	-	-	-	-	0.92
Bioclastic grainstone r.f.	5.73	3.48	6.40	7.58	1.89	1.25	1.23	1.22	4.32	1.90	1.52	0.31	0.31	-	2.79	0.67	0.30	2.53	-	1.25	0.32	0.60	-	1.27	4.84	5.41	0.90	0.62
Dolom. bioclast. grainstone r.f.	-	-	-	-	-	-	-	-	-	-	-	-	-	-	-	-	-	-	-	-	-	-	-	-	-	-	-	-
Bioclastic Packes-Wackes r.f.	5.73	19.42	18.90	17.78	18.87	15.00	7.72	3.98	18.83	5.70	7.01	3.46	3.37	0.90	15.79	10.33	2.41	2.85	5.50	3.13	0.96	7.44	3.59	16.83	5.81	18.02	9.58	5.23
Dolom. Packes-Wackes r.f.	-	-	-	-	-	-	-	-	-	-	-	-	-	0.30	-	-	-	-	-	-	-	-	-	-	-	-	-	-
Biomicritic mudstone r.f.	13.38	7.83	8.84	6.41	6.60	9.38	13.27	5.20	14.81	10.44	6.71	11.64	13.19	5.97	18.89	12.67	9.04	11.08	13.27	6.27	5.11	9.52	2.94	8.57	-	11.11	6.29	4.92
Dolomitized mudstone	-	-	-	-	0.94	-	-	-	-	-	-	-	-	-	-	-	-	-	-	-	-	-	-	-	-	-	-	-
Extrabasinal bioclasts	-	5.51	0.91	6.12	-	-	0.31	-	0.93	-	-	-	-	-	-	-	-	-	-	-	-	-	-	-	-	-	0.60	-
Total carbonate intrabasinal	-	-	-	2.92	-	-	-	-	0.31	-	-	-	-	-	-	-	-	1.90	-	-	-	-	-	-	-	0.30	-	-
Reworked calcrete clasts	-	-	-	2.92	-	-	-	-	0.31	-	-	-	-	-	-	-	-	-	-	-	-	-	-	-	-	0.30	-	-
Coated grains	-	-	-	-	-	-	-	-	-	-	-	-	-	-	-	-	-	-	-	-	-	-	-	-	-	-	-	-
Bioclasts	-	-	-	-	-	-	-	-	-	-	-	-	-	-	-	-	-	1.90	-	-	-	-	-	-	-	-	-	-
Non-carbonate intrabasinal	-	-	-	-	-	-	-	-	-	-	-	-	-	-	-	-	-	-	-	-	-	-	-	-	-	-	-	-
Total matrix	-	-	-	2.04	-	-	-	-	-	-	-	-	-	-	-	-	0.90	-	-	-	-	-	-	-	-	-	-	-
Diagenetics minerals	27.71	37.68	23.48	24.49	31.45	42.50	35.49	29.36	28.40	26.27	32.93	26.10	22.70	43.28	32.20	32.33	31.02	25.32	22.65	25.39	33.87	31.55	19.28	26.98	37.10	43.24	38.02	27.38
Total porosity	-	-	-	-	-	-	-	-	-	-	-	-	-	-	-	-	-	-	0.65	-	-	-	-	-	-	-	-	1.54
TOTAL	100.00	100.00	100.00	100.00	100.00	100.00	100.00	100.00	100.00	100.00	100.00	100.00	100.00	100.00	100.00	100.00	100.00	100.00	100.00	100.00	100.00	100.00	100.00	100.00	100.00	100.00	100.00	100.00

	GAL2%	GAL3%	GAL4%	GAL5%	GAL7%	GAL8%	GAL9%	GAL10%	BAI1%	BAI2%	BAI3%	BAI4%	MARTES1%	MARTES2%	LUE10%	LUE9%	LUE7%	LUE5%	LUE3%	LUE2%	SM1%	SM3%	MO1%	OL1%	GRAD1 %
Total siliciclastic extrabasinal	47.19	53.73	61.04	58.99	50.92	50.00	43.96	59.54	55.38	64.56	46.87	46.77	67.37	58.88	65.09	57.10	47.98	43.35	50.94	55.20	26.02	31.29	46.75	36.16	52.71
Total detrital quartz	13.13	25.78	17.86	13.56	12.58	20.70	9.91	18.42	20.57	17.41	21.38	15.69	41.62	21.81	25.79	19.75	16.20	13.29	20.13	17.05	11.60	17.84	26.93	19.50	8.73
Qtz monocrystalline	8.13	14.91	10.06	5.36	8.90	14.33	5.57	12.17	16.77	9.49	14.80	12.92	18.86	13.08	16.35	14.51	13.08	8.86	14.78	10.69	6.58	13.16	21.05	14.78	6.33
Monocrystal. und. qtz	-	-	0.32	-	-	-	-	-	-	-	0.99	-	1.50	-	0.94	0.31	0.62	-	0.63	-	0.63	1.75	0.31	0.94	-
Qtz inherited syntaxial cement	-	-	-	-	-	-	-	-	-	-	-	-	-	-	-	-	-	0.32	-	-	0.31	-	-	-	-
Qtz polycristall. 2-3 subgrains	0.31	0.93	0.32	0.95	0.31	-	0.31	0.99	0.63	0.32	0.33	0.31	7.49	1.25	0.94	1.23	0.62	0.32	0.31	1.16	0.31	1.17	2.48	0.63	1.20
Qtz polycristall. >3 subgrains	2.50	2.80	2.92	0.95	0.61	2.23	0.93	1.32	0.63	4.75	0.99	0.92	6.59	2.80	3.14	1.54	1.87	0.95	1.57	3.18	0.94	0.88	2.48	1.89	-
Quartz keuper	0.31	1.24	0.32	-	0.92	1.59	0.31	-	0.32	-	0.66	-	-	-	0.63	-	-	-	0.31	0.58	1.25	0.58	0.31	0.31	-
Quartz in plutonic r.f.	-	-	-	-	0.31	-	-	0.33	-	-	-	-	1.80	-	-	-	-	0.32	-	-	0.63	0.29	-	-	-
Quartz in metamorphic r.f.	-	-	-	-	-	-	-	-	-	-	-	-	5.39	-	-	-	-	-	-	-	-	-	-	-	-
Quartz in sandstone r.f.	1.88	5.90	3.90	-	1.53	2.55	2.79	2.63	2.22	2.85	3.62	1.54	-	4.67	3.77	2.16	-	2.53	2.20	1.45	0.94	-	0.31	0.94	1.20
Quartz in hybrid sandstone r.f.	-	-	-	6.31	-	-	-	0.99	-	-	-	-	-	-	-	-	-	-	0.31	-	-	-	-	-	-
Cc replacement on quartz	-	-	-	-	-	-	-	-	-	-	-	-	-	-	-	-	-	-	-	-	-	-	-	-	-
Total detrital feldspar	0.31	0.31	1.95	-	0.31	0.64	-	0.99	0.32	1.27	0.33	0.62	0.60	0.62	1.26	1.54	0.62	1.58	0.63	0.29	3.13	7.89	7.43	0.63	0.90
Detrital K-feld	-	0.31	0.97	-	0.31	0.64	-	0.99	-	0.95	-	0.62	-	-	0.31	0.62	0.62	-	0.63	0.29	2.51	2.05	3.10	-	0.60
K-feld in plutonic r.f.	-	-	-	-	-	-	-	-	-	-	-	-	-	-	-	-	-	0.32	-	-	-	-	-	-	-
Detrital plagioclase	0.31	-	0.97	-	-	-	-	-	0.32	0.32	0.33	-	0.60	0.62	0.63	0.93	-	1.27	-	-	0.31	4.09	1.24	0.31	-
Plagioclase in plutonic r.f.	-	-	-	-	-	-	-	-	-	-	-	-	-	-	-	-	-	-	-	-	-	-	-	-	-
Detrital Microcline	-	-	-	-	-	-	-	-	-	-	-	-	-	-	0.31	-	-	-	-	-	0.31	1.46	3.10	0.31	0.30
Microcline in plutonic r.f	-	-	-	-	-	-	-	-	-	-	-	-	-	-	-	-	-	-	-	-	-	0.29	-	-	-
Total fine lithics	33.75	27.64	41.23	45.43	38.04	28.66	34.06	40.13	34.49	45.89	29.93	30.46	25.15	36.45	38.05	35.80	31.15	28.48	30.19	37.86	11.29	5.56	12.38	16.04	43.07
Phyllites	6.25	6.21	7.79	13.56	7.67	1.27	0.31	0.33	5.06	4.11	4.93	0.31	0.30	6.23	7.55	7.10	0.62	0.32	1.89	2.31	1.88	-	0.93	-	12.05
Schists	12.19	8.70	10.71	10.73	11.96	3.50	1.24	1.64	13.29	15.19	5.59	-	1.80	9.03	13.21	11.11	0.31	5.38	5.03	5.20	2.51	0.88	1.55	0.94	13.55
Chloritochists lithic	-	-	-	-	-	-	-	-	0.32	-	-	-	-	-	0.31	-	-	-	-	-	-	-	-	-	-
Quartzite	1.88	1.24	2.60	4.10	2.15	2.23	0.93	2.30	2.53	4.43	2.96	0.92	1.20	0.93	2.52	3.70	0.93	2.22	2.83	4.91	1.88	-	0.62	1.57	1.20
Plutonic r.f.	-	-	-	-	-	-	-	-	-	-	-	-	-	-	-	-	-	-	-	-	-	0.88	-	-	-
Cc replacement on plut. r.f.	-	-	-	-	-	-	-	-	-	-	-	-	-	-	-	-	-	-	-	-	-	-	-	-	-
Volcanic r.f.	-	-	-	-	-	-	-	-	-	-	-	-	-	-	-	-	-	-	-	-	-	-	-	-	-
Volcanic chert	-	-	-	-	-	-	-	-	-	0.32	-	-	-	-	-	-	-	0.32	-	-	-	-	-	-	-
Vitric volcanic lithic	-	-	-	-	-	-	-	-	-	-	-	-	-	-	-	-	-	-	-	-	-	-	-	-	-
volcanic lithic with microlitic	-	-	1.30	-	-	-	-	-	-	-	-	-	0.90	-	-	-	-	-	-	-	-	-	-	-	-
volcanic lithic lathwork texture	0.31	0.62	-	0.95	0.31	-	0.31	0.33	-	0.95	0.33	-	0.60	0.31	0.31	0.93	-	1.27	0.31	-	0.31	0.29	-	-	0.30
sandstone r.f.	-	0.62	0.65	-	-	-	1.24	0.33	0.63	0.63	0.33	-	-	0.62	0.94	1.23	0.31	3.80	1.26	2.02	0.31	0.29	-	0.31	2.11
Hybrid sandstone r.f.	0.63	0.31	0.65	-	2.45	0.96	3.72	6.91	-	0.32	0.66	2.77	2.10	-	-	1.23	-	1.27	-	0.29	-	-	-	-	0.60
Siltstone r.f.	3.44	6.83	7.47	8.83	5.21	6.69	1.86	4.93	6.01	10.44	4.93	3.38	4.19	9.35	7.23	5.25	4.36	3.16	4.40	8.38	3.45	2.05	3.41	4.40	8.73
Hybrid Siltstone r.f.	1.25	0.62	1.62	1.58	3.07	11.15	19.50	19.41	0.32	1.58	2.63	16.00	5.39	2.49	-	1.23	19.31	4.11	5.97	6.07	0.63	-	-	-	-
Chlorite	0.31	0.31	-	-	-	-	-	-	-	-	-	-	-	-	-	-	-	-	-	-	-	-	0.31	-	-
Chert	0.63	0.93	-	0.95	1.23	0.64	-	0.66	-	2.22	1.32	0.31	2.69	-	-	-	1.25	0.95	2.20	1.45	-	-	1.24	-	0.30
Muscovite	-	-	-	0.32	-	-	0.31	-	0.32	-	-	-	-	-	-	-	-	-	-	-	0.31	0.88	0.93	0.63	-
Biotite	-	-	-	-	-	-	-	-	-	-	-	-	-	-	-	-	-	-	-	-	-	-	0.31	-	-
Heavy minerals	-	-	-	-	-	-	-	-	-	-	-	-	-	0.62	-	-	-	-	-	-	-	-	-	0.31	1.20
Silicified r.f.	2.19	-	1.30	1.26	-	1.27	2.48	2.63	1.27	2.22	2.30	6.15	2.99	0.62	1.89	1.23	4.05	2.22	3.46	1.73	-	-	1.24	1.26	-
Cc replacement silificied r.f.	-	-	-	1.89	-	-	-	-	-	-	-	-	-	-	-	-	-	-	-	-	-	-	-	-	-
Fe-oxid replacement r.f.	4.06	-	5.52	-	3.07	0.64	-	0.33	4.75	2.53	2.30	0.31	-	6.23	3.77	1.85	-	0.32	0.31	0.58	-	-	1.86	6.60	2.41
Silificied limestone	-	-	-	-	-	-	-	-	-	-	-	-	-	-	-	-	-	-	-	-	-	-	-	-	-
Radiolarite r.f.	0.63	1.24	1.62	1.26	0.92	0.32	2.17	0.33	-	0.95	1.64	0.31	2.99	-	0.31	0.93	-	3.16	2.52	4.91	-	0.29	-	-	0.60
Alterite	-	-	-	-	-	-	-	-	-	-	-	-	-	-	-	-	-	-	-	-	-	-	-	-	-
Total carbonate extrabasinal	20.00	15.53	13.96	11.67	17.48	14.65	23.53	18.09	12.66	8.86	25.66	18.77	12.87	8.72	10.38	15.74	24.30	22.47	16.98	20.23	34.80	40.94	22.29	33.02	5.42
Mono. esparitic limestone	0.31	0.62	0.32	-	1.23	0.32	0.31	-	0.63	-	0.33	-	-	-	0.94	0.62	0.31	-	-	0.29	-	2.92	0.31	0.63	-
Poli. Esparitic r.f.	-	0.62	-	0.32	1.23	-	0.31	-	0.32	-	-	-	-	0.62	0.31	-	-	-	0.63	0.29	-	4.39	-	0.94	-
Dolomitized polycrystal. r.f.	-	-	-	-	-	-	-	-	-	-	-	-	-	-	-	-	-	-	-	-	-	0.58	-	-	-
Biomicritic	-	-	-	-	-	-	-	-	-	-	-	-	-	-	0.31	-	-	-	-	-	6.27	-	3.41	-	-
Bioesparitic	-	-	-	-	-	-	-	-	-	-	-	-	-	-	-	0.62	-	-	0.63	0.29	-	-	-	-	-
Dolomicrite r.f	-	-	-	-	-	-	-	-	-	-	-	-	-	-	-	-	-	-	-	-	-	-	-	0.94	-
Dolomite monocrystalline	0.31	-	-	-	-	-	-	-	-	-	-	-	-	-	-	-	-	-	-	-	1.25	-	0.31	2.52	-
Dolostone r.f. (sacaroidea)	0.63	-	-	0.32	-	-	-	-	-	-	-	-	-	-	-	0.62	-	-	-	0.58	-	2.63	0.31	0.94	-
Bioclastic grainstone r.f.	0.63	1.86	4.22	1.58	1.53	-	1.24	0.33	-	0.95	3.62	-	-	0.62	0.31	2.16	0.62	6.33	0.31	0.29	0.94	1.17	0.31	2.52	-
Dolom. bioclast. grainstone r.f.	-	-	-	-	-	-	-	-	-	-	-	-	-	-	-	-	-	-	-	-	-	-	-	-	-
Bioclastic Packes-Wackes r.f.	8.13	2.80	5.19	2.84	5.21	7.96	12.38	14.80	2.22	5.70	14.14	10.15	8.68	3.43	0.63	3.40	8.72	10.76	7.23	9.83	10.97	14.33	5.26	7.55	1.51
Dolom. Packes-Wackes r.f.	-	-	-	-	-	-	-	-	-	-	-	-	-	-	-	-	-	-	-	-	-	-	-	-	-
Biomicritic mudstone r.f.	10.00	9.63	4.22	6.62	7.98	5.10	7.12	2.96	8.86	1.90	7.57	5.54	4.19	4.05	7.86	8.33	13.71	4.11	7.55	7.51	15.36	14.91	12.38	16.98	3.92
Dolomitized mudstone	-	-	-	-	-	-	-	-	-	-	-	-	-	-	-	-	-	-	-	-	-	-	-	-	-
Extrabasinal bioclasts	-	-	-	-	0.31	1.27	2.17	-	0.63	0.32	-	3.08	-	-	-	-	0.93	1.27	0.63	1.16	-	-	-	-	-
Total carbonate intrabasinal	-	-	-	-	-	-	-	-	-	-	-	-	-	-	0.31	-	-	-	-	-	0.63	1.46	-	-	-
Reworked calcrete clasts	-	-	-	-	-	-	-	-	-	-	-	-	-	-	-	-	-	-	-	-	-	-	-	-	-
Coated grains	-	-	-	-	-	-	-	-	-	-	-	-	-	-	-	-	-	-	-	-	-	-	-	-	-
Bioclasts	-	-	-	-	-	-	-	-	-	-	-	-	-	-	0.31	-	-	-	-	-	0.63	1.46	-	-	-
Non-carbonate intrabasinal	-	-	-	-	-	-	-	-	-	-	-	-	-	-	-	3.70	-	-	-	-	-	4.09	-	-	-
Total matrix	-	-	-	-	-	-	-	-	-	-	-	-	-	-	-	-	-	-	-	2.02	-	-	-	-	-
Diagenetics minerals	32.81	30.75	25.00	29.34	31.60	35.35	32.51	22.37	31.96	26.58	22.70	34.46	19.76	32.40	24.21	23.46	27.73	34.18	32.08	22.54	38.56	22.22	30.96	30.82	41.87
Total porosity	-	-	-	-	-	-	-	-	-	-	-	-	-	-	-	-	-	-	-	-	-	-	-	-	-
TOTAL	100.00	100.00	100.00	100.00	100.00	100.00	100.00	100.00	100.00	100.00	100.00	100.00	100.00	100.00	100.00	100.00	100.00	100.00	100.00	100.00	100.00	100.00	100.00	100.00	100.00

Capítol 9

Discussió integrada: Evolució composicional i paleogeogràfica dels sistemes sedimentaris de la conca de Jaca

En els anteriors capítols s'han exposat els resultats referents a l'anàlisi de procedència dels sistemes sedimentaris de la conca de Jaca, els qual han estat presentats en ordre d'acord a la seva edat (del Lutecià a l'Aquitanià), i la seva posició en la conca (de nord a sud). En aquest capítol es procedeix a discutir aquestes dades per tal d'integrar-les en referència als objectius plantejats en el capítol 2.

La varietat de signatures composicionals distinctives observades evidencia la continua evolució de les àrees font, fortament controlades per la tectònica, que es transmeten a la conca mitjançant múltiples punts d'aport. La interacció entre les diverses àrees font complica la definició de la procedència dels sistemes sedimentaris. Per tal de facilitar la comprensió de l'evolució de la conca, la definició d'unes petrofàcies (Fig. 9.1) basades en l'estudi composicional detallat dels sistemes permet distingir i obtenir una imatge simplificada de l'evolució de cada àrea font en el temps i en l'espai en la conca de Jaca (Fig. 9.2).

Tal i com s'ha exposat en els capítols 6 i 8, les petrofàcies definides en aquesta tesi es basen en els continguts relatius dels components més significatius, com són els fragments de gresos híbrids, els grans feldspàtics i lítics (excloent els fragments de gresos híbrids), i els fragments de calcàries (Fig. 9.1). Les quatre petrofàcies que se'n deriven són: (a) petrofàcies dominada per fragments de gresos híbrids, (b) petrofàcies enriquida en fragments carbonàtics, (c) petrofàcies dominada per components siliciclàstics, i (d) petrofàcies mixta en fragments de roca carbonàtics i lítics.

En la conca de Jaca, de la sedimentació turbidítica del Grup Hecho a la sedimentació al·luvial posterior es pot observar una clara diversificació de les signatures petrològiques (Fig. 9.1A, B). Així, la sedimentació del Grup Hecho durant els sistemes turbidítics de Banastón s'inicia amb un clar predomini de la petrofàcies enriquida en fragments de roca carbonàtics que evoluciona a un increment en components lítics per als sistemes turbidítics de Jaca (Fig. 9.1C). Els últims dipòsits turbidítics, corresponents al canal del Rapitán, registren un primer augment de fragments de gresos (Fig. 9.1C), evidenciant un primer gran canvi composicional en la conca relacionat amb l'aixecament tectònic de noves àrees font al nord. És a partir d'aquest moment en que en la evolució a la sedimentació deltaica suprajacent, hi juguen diverses petrofàcies indicatives de múltiples procedències (Fig. 9.1C).

1. Jaca 2. Santa Orosia 3. Canciás 4. San Felices 5. Abenilla 6. Sabiñánigo 7. Peña Oroel

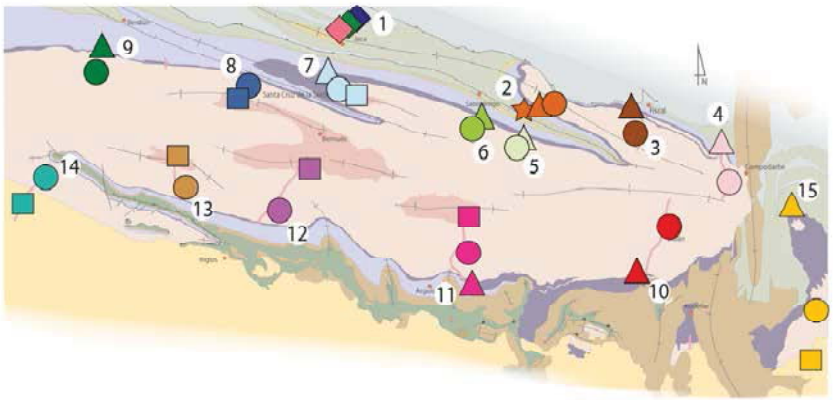

8. San Juan 9. Martés 10. Rodellar-Bibán 11. Monrepós 12. Gállego 13. Salinas 14. Luesia 15. Ainsa de la Peña

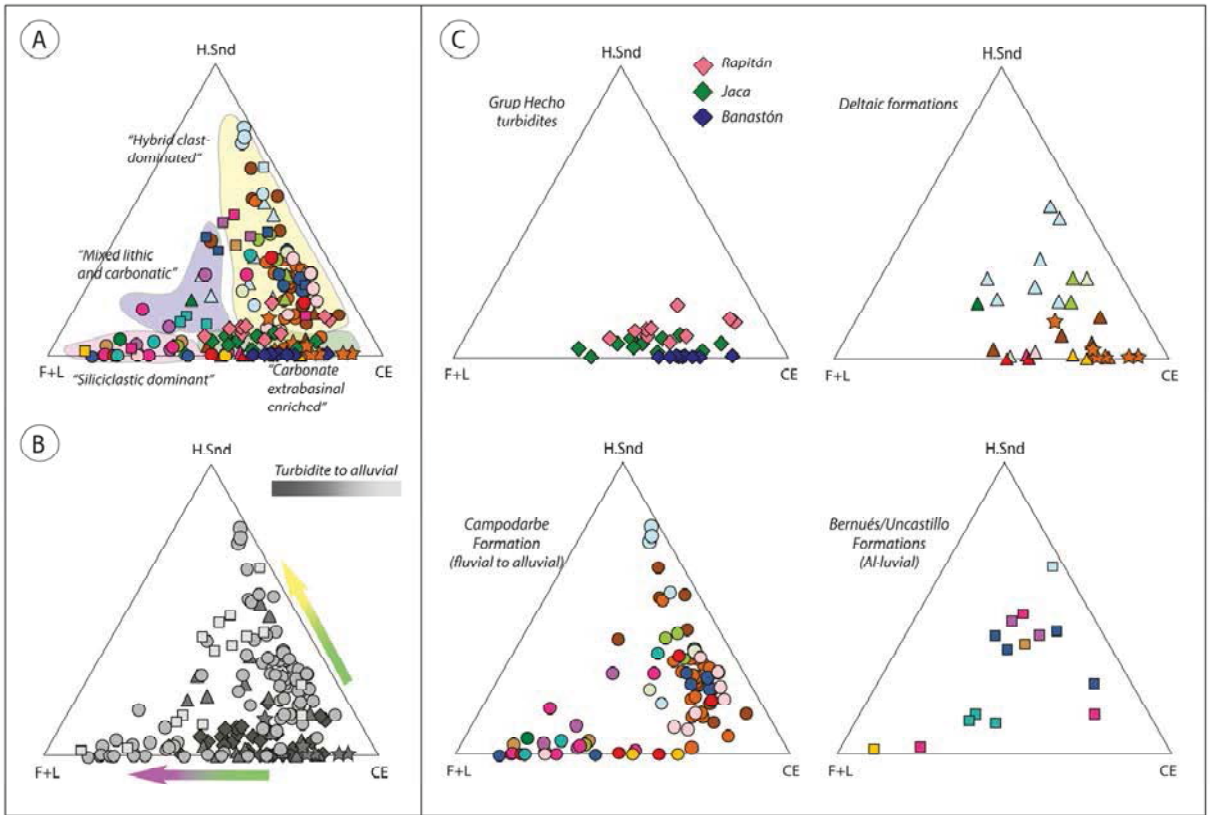

Figura 9.1. En la part superior, es mostra un mapa simplificat de la zona d'estudi amb la situació orientativa de les mostres analitzades en les diferents seccions estratigràfiques que es representen en els diagrames ternari composicionals. La simbologia de les turbidites i els ambients deltaics ha canviat respecte a la presentada en el capítol 4 (veure Annex 3 per situació de les mostres). A) Diagrama ternari representant les quatre petrofàcies definides en la tesi que s'extreuen de la representació de totes les mostres analitzades, on H.Snd, fragments de gresos híbrids, F+L, feldspats i lítics excloent els gresos híbrids, i CE, carbonàtics extraconcals. B) Diagrama ternari anterior en escala de grisos per a visualitzar la diferenciació de les àrees font d'ambients turbidítics a ambients al·luvials. C) Diagrames ternaris de petrofàcies per a les diferents formacions estudiades.

Tal i com es pot observar en el mapa de la Figura 9.2, durant la sedimentació deltaica (Formació Gres de Sabiñánigo i Belsué-Atarés) la petrofàcies enriquida en fragments carbonàtics es concentra a la part sud de la conca. Al mateix temps, al nord de la conca, aquesta petrofàcies només queda representada a la part est (zona pròxima a l'anticlinal de Boltaña), i és substituida progressivament per la petrofàcies dominada per fragments de gresos híbrids, produïnt-se en determinats sectors una clara interferència entre ambdues petrofàcies.

Durant la sedimentació continental posterior (Formació Campodarbe), és quan els sistemes mostren la major diversitat de petrofàcies (Fig. 9.1C), la qual es manifesta amb l'aparició d'una nova petrofàcies de procedència est, dominada per components siliciclàstics, la qual és sistemàticament reemplaçada d'est a oest i de nord a sud per la petrofàcies dominada per fragments de gresos híbrids, seguint la direcció de progradació dels sistemes en la conca (Fig. 9.2). Finalment, els dipòsits conglomeràtics al·luvials de la conca de Jaca registren generalment la petrofàcies dominada per fragments de gresos híbrids, mentre que simultàniament, a la conca de l'Ebre mostren petrofàcies dominades per siliciclàstics en la Formació Graus (sector est), i petrofàcies mixtes en lítics i carbonàtics en el ventall al·luvial de Luna, de la Formació Uncastillo (sector oest de la zona d'estudi).

La identificació d'aquestes diferents petrofàcies permet definir la composició de les àrees font, i els canvis que succeeixen en elles durant el temps. No obstant, és important tenir en consideració que les petrofàcies s'estableixen d'acord a les variacions de proporció en certs components, o grup de components, i que, encara que un grup de mostres siguin classificades en una mateixa petrofàcies, això no és indicatiu d'una mateixa procedència. Aquest efecte és produeix pel fet que en els diagramens ternaris només es representen tres components. Així, es pot donar el cas en que mostres que cauen projectades dins de l'àrea d'una mateixa petrofacies poden tenir diferents procedències com a consequència del seu contingut en els components que no han estat considerats en el diagrama. A més, tal i com es mostra en les projeccions de la Figura 9.1, els canvis entre petrofàcies sovint són graduals, amb mostres que es troben just al límit entre àrees de petrofàcies, evidenciant l'evolució composicional entre elles. Per aquests motius, a continuació es discuteix la procedència de cada petrofàcies per tal de contribuir en el coneixement de l'evolució paleogeogràfica dels sistemes des del Bartonià fins al Miocè inferior (Fig. 9.3, 9.4).

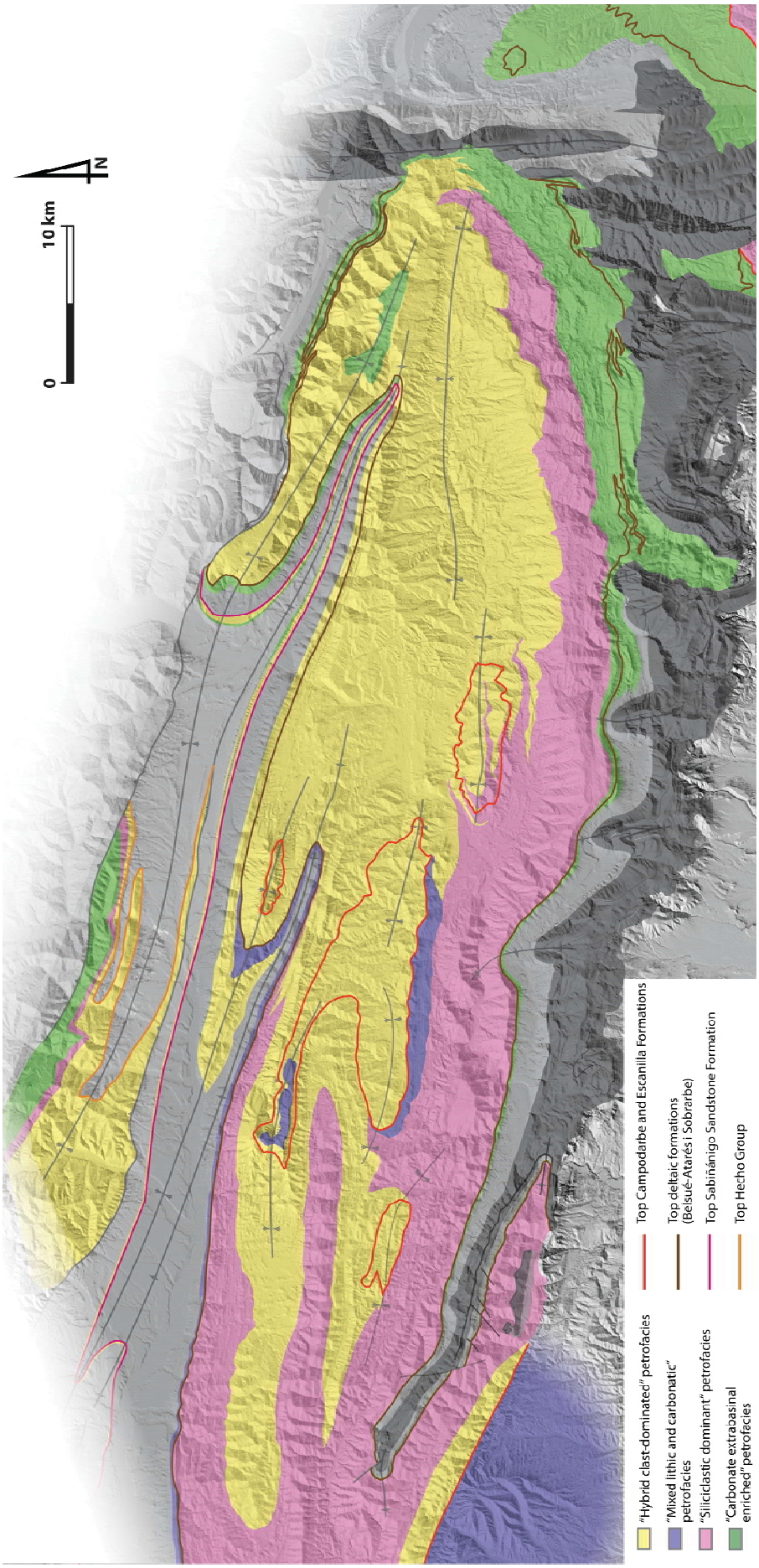

Figura 9.2. Mapa de petrofàcies de la conca de Jaca i sector oest d'Àinsa i nord de l'Ebre. ELs colors corresponen a cada una de les petrofàcies (d'acord amb els colors emprats en la resta de la tesi), i les línies al sostre de les diferents formacions.

Tal i com s'ha descrit en els capítols anteriors, el pas de la sedimentació turbidítica del Grup Hecho a la sedimentació al·luvial posterior comporta un canvi en l'organització de les xarxes de drenatge (Puigdefàbregas, 1975; Jolley, 1988; Montes, 2002), el qual bàsicament consisteix en el reemplaçament de sistemes de drenatge axial procedents d'àrees font situades a l'est, per sistemes de drenatge transvers, que deriven de noves àrees font que s'estan originant al nord de la conca com a conseqüència de la tectònica d'encavalcaments.

Així, la sedimentació del Grup Hecho en general s'associa amb un sistema de drenatge axial, procedent d'àrees font situades a l'est i localitzades en els Pirineus centrals. Els sistemes turbidítics de Banastón s'inicien amb un clar predomini de la petrofàcies dominada per fragments carbonàtics, evolucionant composicionalment cap a un increment en components lítics a l'inici dels sistemes turbidítics de Jaca. Tant per les turbidites de Banastón com per les de Jaca, s'observen tendències composicionals de base a sostre del sistema, tant en la fracció gres, analitzada al microscopi petrogràfic, com en les distribucions de les edats d'U-Pb en zircons detrítics. Tal i com s'apunta en el capítol 4, aquests canvis són interpretats com a resultat de la ciclicitat tectonoestratigràfica, ja que es donen unes tendències semblants de base a sostre de cada Unitat Tectono-Sedimentaria (UTS-4, Banastón, i UTS-5, Jaca, de Remacha i Fernández, 2003), similar a les observades per Fontana *et al.* (1989) i Caja *et al.* (2010) ens els sistemes turbidítics equivalents en la conca d'Ainsa. En quan a la correlació dels sistemes turbidítics entre la conca de Jaca i la d'Ainsa, actualment limitades per l'anticlinal de Boltaña, diverses discrepàncies s'han fet paleses en diferents treballs a l'hora d'establir les equivalències entre aquests (Oms *et al.*, 2003; Remacha i Fernández, 2003; Gupta i Pickering, 2008). D'acord amb les dades obtingudes en aquesta tesi, i la seva comparació amb els treballs de Caja *et al.* (2010), per a l'anàlisis petrogràfic, i Thomson *et al.* (2017), per a l'anàlisi geocronològic en la conca d'Ainsa, aquí es proposen els sistemes turbidítics superiors de Morillo i Guaso com a possibles equivalents proximals dels sistemes de Banastón a la conca de Jaca, i el sistema deltaic de Sobrarbe com a equivalent proximal de la part baixa dels sistemes turbidítics de Jaca.

Els últims dipòsits turbidítics, corresponents al canal del Rapitán (part alta dels sistemes turbidítics de Jaca), registren un primer augment de gresos híbrids, que juntament amb un canvi composicional general, són interpretats com els primers indicis de creació d'una àrea font situada al nord provocada per l'activitat de l'encavalcament de Lakora/Eaux-Chaudes, fet molt rellevant ja que marca l'inici del drenatge transversal a la conca de Jaca durant el Bartonià (Fig. 9.3A). Aquest sistema representa el primer sistema turbidític sense connexió amb la conca d'Aínsa, evidenciant la creació de noves àrees font, que podien actuar al seu temps com a marge nord de la conca turbidítica, el qual avui en dia es troba totalment erosionat (Mutti *et al.*, 1972; Remacha *et al.*, 2005). Les distribucions d'U-Pb en zircons detrítics evidencien també aquest canvi de procedència, en que les distibucions dominades per signatures Varisques que es donen en el Grup Hecho

(Whitchurch *et al.*, 2011; Thomson *et al.*, 2017) són substituides per un increment en les senyals Cadomianes i de >700 Ma. Per tant, els sistemes turbidítics de Jaca són els primers dipòsits que registren la interacció entre el sistema de drenatge axial, alimentat desde la conca d'Aínsa, i el nou sistema de drenatge transversal de procedència nord que s'està instaurant a la conca de Jaca.

Després de la sedimentació dels sistemes turbidítics de Jaca, la conca es veu sotmessa a una somerització generalitzada que provoca que els ambients de sedimentació turbidítica siguin substituïts progressivament per ambients deltaics. Amb el final de la sedimentació turbidítica de drenatge transversal al marge nord de la conca, la sedimentació de drenatge axial, procedent de la conca d'Aínsa, representada per ambients deltaics, s'instala definitivament en el marge sudest (Fig. 9.3A). De forma sincrònica un seguit d'estructures de vergència nordoest-sudest comencen a créixer en aquesta part de la conca (Fig. 9.3A), condicionant de forma clara les direccions de dispersió del sediment (Puigdefàbregas, 1975; Dreyer *et al.*, 1999).

La coexistència de sediments procedents d'àrees font situades al nord, amb sediments derivats d'àrees font de l'est, no només es manté sinó ques'accentuant al llarg de tota la sedimentació deltaica en la conca.Les signatures d'ambdues procedències reflecteixen una evolució de les àrees font ben diferenciada. Mentre l'àrea font de l'est, situada al Pirineu central, subministra litologies resultants de l'exhumació i incisió continuada de materials Mesozoics i Paleozoics, l'àrea font del nord està dominada pels dipòsits turbidítics eocens, marcant els estadis inicials d'inversió del marge nord de la conca i de creació d'aquesta nova àrea font per l'activitat de l'encavalcament de Lakora-Eaux Chaudes.

Més endavant, durant els últims estadis de sedimentació deltaica (Formació Belsué-Atarés) aquesta diferent evolució de les àrees font queda remarcada per un increment considerable del contingut de fragments de gresos híbrids, sobretot pels sistemes situats al marge nord de la conca, mentre aquells situats a l'est i al sud, continuen enregistran l'erosió d'àrees dominades per roques sedimentàries carbonàtiques (Fig. 9.3B). Tal i com s'ha descrit en els capítols anteriors (capítols 5 i 8), l'activitat sintectònica d'estructures emergents en la conca (p. ex. anticlinals d'Atarés o Basa) controla en bona mesura la distribució de les petrofàcies durant el Bartonià i Priabonià.

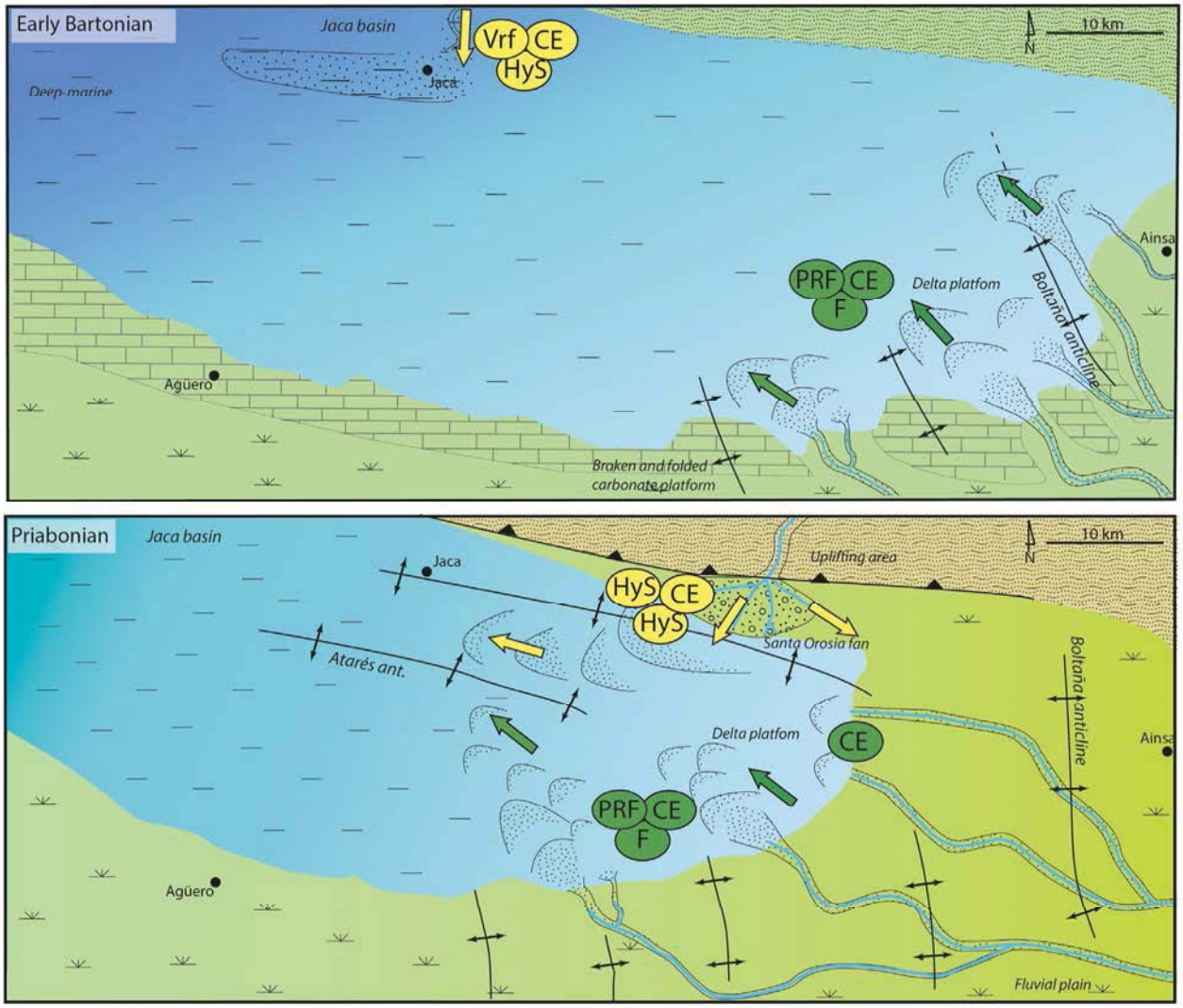

Figura 9.3. A) Mapa paleogeogràfic de la conca de Jaca durant el trànsit Lutecià-Bartonià. Les fletxes i cercles denoten la tipologia de petrofacies (color d'acord amb els descrits al mapa de la Figura 2). Els components representats corresponen a: H. Snd, fragments de gresos híbrids, VRF, fragments volcànics, CE, fragments carbonàtics, PRF, fragments plutònics, F, feldspats. B) Mapa paleogeogràfic de la conca de Jaca durant el Priabonià. Els components representats corresponen a: H. Snd, fragments de gresos híbrids, PRF, fragments plutònics, F, feldspats, i CE, fragments carbonàtics. Els mapes han estat reconstruits a partir de Puigdefàbregas (1975); Bentham et al. (1992); Hogan (1993); Montes (2002); Caja et al. (2010); Huyghe et al. (2012).

Els sistemes fluvials i al·luvials de la Formació Campodarbe enregistren una diversificació clara en quan a les signatures petrològiques.Els sistemes situats al marge nord de la conca són alimentats per una àrea font persistent al nord, la qual evoluciona cap a un increment en el reciclatge dels dipòsits turbidítics previs per l'activitat tectònica de l'encavalcament de Gavarnie, tal i com es descriu en els capítols 4 i 5. Pel contrari, en el marge sud de la conca, els sediments fluvials corresponents al sistema de drenatge axial derivat dels Pirineus centrals no enregistren aquest reciclatge dels gresos turbidítics i la petrofàcies carbonàtica típica és reemplaçada per un increment generalitzat en el contingut de fragments lítics, sobretot de naturalesa metamòrfica. Aquesta evolució en la preponderància d'una àrea font Paleozoica dominada per roques plutòniques cap a un àrea font dominada per roques metamòrfiques, té lloc essencialment en el moment

d'instauració de la sedimentació continental generalitzada en la conca (Fig. 9.4A). Aquest canvi també és enregistrat a la part superior de la Formació Escanilla a la conca d'Aínsa, tal com descriu Michael (2013), i assenyala com a possible causant d'aquest canvi l'expansió de les àrees de drenatge cap al nord de la Zona Axial, incorporant així el massisos metamòrfics Nordpirinencs. Al tractar-se d'una tendència evolutiva que es produeix en la mateixa àrea font, pot considerar-se com un bon marcador de correlació entre la conca d'Aínsa i de Jaca.

Fruit de l'activitat tectònica emergent al nord de la conca, els sistemes de drenatge transversal s'acaben imposant, i evolucionen, sobretot de nord a sud, guanyant espai en la conca d'acord amb el sentit d'avançament de les estructures, provocant el desplaçament del sistema de drenatge axial cap a posicions més occidentals (Fig. 9.4A). Tal i com es mostra en el capítol 5, l'àrea font per aquests sistemes procedents del nord està constituïda majoritàriament pels materials de la conca turbidítica precedent, i en les seves capçaleres pels materials de la Zona Nordpirinenca, la qual havia de constituir un veritable relleu que va ser erosionat durant la sedimentació eocena-oligocena. L'erosió dels materials de la Zona Nordpirinenca i la seva incorporació en els ventalls al·luvials de la conca de Jaca (zona Sudpirinenca) implica que la divisòria d'aigües estava situada molt més al nord durant l'Eocè-Miocè que la seva posició actual. Aquest fet evidencia una clara migració de la divisòria de nord a sud de l'orògen, almenys en el sector oest-central dels Pirineus.

Cal resaltar que els sistemes situats al nordest de la conca, com és el cas del ventall al·luvial de Canciás (Fig. 9.4A), experimenten una evolució diferenciada, que consiteix en un increment de components carbonàtics (fragments de calcàries i dolomies) en els nivells conglomeràtics superiors (Fig. 9.4A). Aquesta tendència composicional s'interpreta com el resultat de l'erosió del relleu que està creant l'activitat de les làmines encavalcants situades al nord d'Aínsa, que incorporen part de la cobertora Paleocena i Mesozoica (p.ex. l'encavalcament de Peña Montañesa o Cotiella). Les estructures tectòniques emergents segueixen condicionan la distribució dels sistemes en la conca, i la sedimentació es produeix preferenment en en els sinclinals, fet que facilita la confluència entre els sistemes transversals i axials, donant lloc a signatures petrològiques mixtes (Fig. 9.4A).

Durant els últims estadis de rebliment (Fig. 9.4B), els sistemes al·luvials de la conca de Jaca reflecteixen una única àrea font (veure capítol 5), la situada a la nord, subministrant predominantment fragments de gresos procedents de l'antiga conca turbidítica, amb contribucions menors de materials Mesozoics i Paleozoics. En aquest últim estadi, el sistema de drenatge axial queda totalment desplaçat, i ja no és capaç d'entrar a la conca de Jaca, degut a l'aixecament que aquesta experimenta com a resultat de l'activitat de l'encavalcament de Guarga (Cámara i Klimowitz, 1985; Teixell i García-Sansegundo, 1995; Millán *et al.*, 2006; Muñoz *et al.*, 2013). Aquests últims sistemes de drenatge transversal provoquen l'acumulació de dipòsits conglomeràtics,

preferenment en el sinclinals actius, la sedimentació dels quals hauria perdurat almenys fins a l'inici del Miocè, d'acord amb els resultats geocronològics presentats en el capítol 7. En aquest últim estadi, el creixement del relleu de les Serres Exteriors exerceix de barrera física entre la conca de Jaca, que es comporta com a *piggy-back,* i la conca de l'Ebre, la qual esdevé la conca *foreland* principal .Així doncs, la sedimentació activa passa a produir-se a la conca de l'Ebre, on els grans sistemes al·luvials de procedència pirinenca (ventalls de Luna i Huesca) es desenvolupen, simultaneament amb petits ventalls al·luvials de procedència més local, que contenen només litologies de les Serres Exteriors (Fig. 9.4B) (Friend *et al.*, 1989; Hirst i Nichols, 1986; Nichols i Hirst, 1998; Arenas *et al.*, 2001).

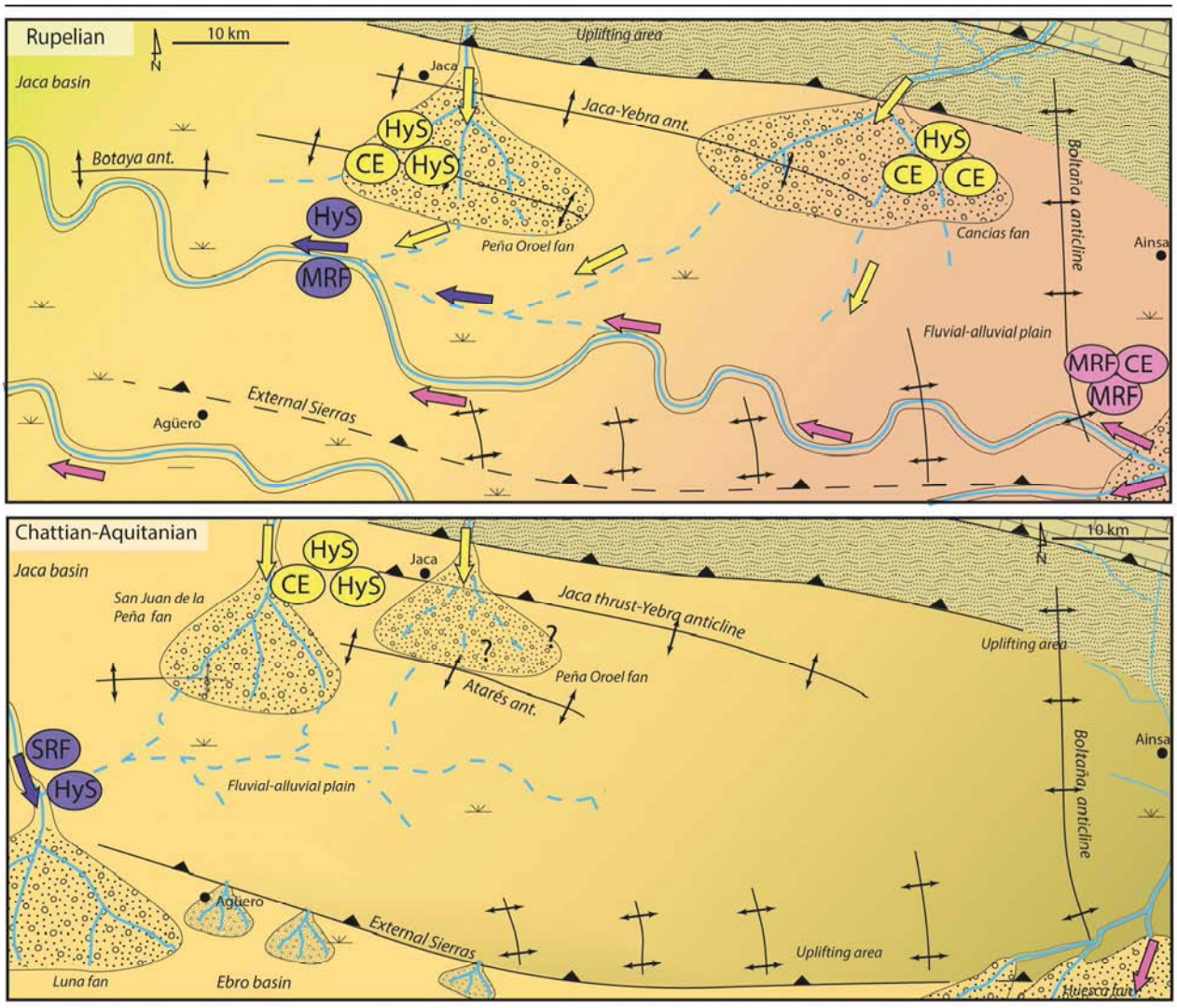

Figura 9.4. A) Mapa paleogeogràfic de la conca de Jaca i de l'Ebre durant el Rupelià. Les fletxes i cercles denoten la tipologia de petrofacies (color d'acord amb els descrits al mapa de la Figura 2). Els components representats corresponen a: H. Snd, fragments de gresos híbrids, MRF, fragments metamòrfics, i CE, fragments carbonàtics B) Mapa paleogeogràfic de la conca de Jaca i de l'Ebre durant el Chattià-Aquitanià. Els components representats corresponen a: H. Snd, fragments de gresos híbrids, MRF, fragments de metamòrfics, SRF, fragments de lítics sedimentaris, i CE, fragments carbonàtics. Els mapes han estat reconstruits a partir de Hirst i Nichols (1986) Puigdefàbregas (1975); Friend et al. (1986); Arenas (1993); Nichols i Hirst (1998); Jones (2004).

En aquest estadi es dóna una situació característica, que consisteix en que la conca de Jaca està sent parcialment erosionada pels grans ventalls de Huesca i Luna, al mateix temps que encara es produeix acumulació de sediment en el marge nord de la conca, essencialment en el ventall de San Juan de la Peña (Fig. 9.4B). Per tant, durant el Chattià i Aquitanià tres àrees font diferenciades i situades al nord subministrarien sediments tant la conca de Jaca com el marge nord de la conca de l'Ebre, donant lloc a la sedimentació d'est a oest, de:

(a) El sistema que conforma el ventall de Huesca (Hirst i Nichols, 1986; Friend *et al.*, 1989; Jones *et al.*, 2001; Arenas *et al.*, 2001; Yuste *et al.*, 2004). Aquest sistema s'hauria alimentat a través de les paleovalls del Sis i Gurp, amb materials de naturalesa Paleozoica dominanment, amb abundants contribucions dels materials de cobertora Mesozoica de les unitats envalcants de la Unitat Central Sud-Pirinenca (Séguret, 1972) i del reciclatge dels material dipositats en la conca de Jaca al ser incidits per la xarxa de drenatge i/o deformats per les estructures de les Serres Exteriors.

(b) El ventall de San Juan de la Peña, el qual evidencia que les àrees font situades al nord de la zona segueixent estant constituïdes majoritàriament per la conca turbidítica anterior, sense clares evidències d'exhumació de materials més antics (p. ex. basament Paleozoic) de la Zona Axial d'aquesta part dels Pirineu.

(c) I finalment a l'oest, el ventall al·luvial de Luna (Formació Uncastillo) mostra una composició diferenciada del de San Juan de la Peña. Encara que ambdós ventalls comparteixen components, com ara els fragments de gresos eocens reciclats, el ventall de Luna mostra una diversitat molt major de components derivats d'àrees font Paleozoiques i Mesozoiques. Per tant, l'àrea font Paleozoica i Mesoica per al ventall de Luna no podia estar situada al nord de Jaca, ja que aquesta encara es trobava recoberta pels materials eocens, tal i com demostren les litologies presents en el ventall de San Juan de la Peña. En aquesta tesi es proposa la zona oest dels Pirineus (massisos Vascos) com a la principal àrea font per al sistema de Luna, que d'igual manera seguia rebent també les litologies dels sediments sintectonics Pirinencs, com testimonia la composició mixta que presenta.

A escala de conca Sudpirinenca, les diferents reorganitzacions en les xarxes de drenatge i el creixement topogràfic de l'orògen, controlades essencialment per la tectònica, es donen de forma diacrònica com a resultat de la progradació de la deformació de l'orògen i el seu caràcter asimètric. En les conques situades al Pirineu central, com les de Tremp-Graus i Aínsa, es defineix una clara reorganització, que es produeix de forma progressiva des de finals del Cretaci fins a l'Eocè mitjà.Els sistemes de drenatge axial, procedents dels Pirineus Orientals i del Massís de l'Ebre, són reemplaçats per sistemes de drenatge transversal derivats de la

creació de noves àrees font localitzades en els Pirineus centrals (Fontana *et al.*, 1989; Caja *et al.*, 2010; Whitchurch *et al.*, 2011; Filleaudeau *et al.*, 2012; Thomson *et al.*, 2017),essent aquests últims els que alimentaríen els sistemes de drenatge axial a la conca de Jaca. Així mateix, aquests sistemes posteriorment també serien reemplaçats pels sistemes de drenatge transversal procedents del nord de la conca de Jaca, producte de la important reorganització de les àrees font.

Com la deformació de l'orogen pirinenc progressa d'est a oest, i de nord a sud, el canvis paleogeogràfics en les diferents conques també progressaran d'est a oest i de nord a sud. D'aquesta manera la sedimentació per sistemes de drenatge axial en les conques serà substituida d'est a oest i de nord a sud per sistemes transverals a l'orogen.

A banda de la clara diacronia en aquests majors canvis paleogeogràfics que succeixen en conques adjacents, és evident que les àrees font sofreixen evolucions molt diferents. Així doncs, mentre la instauració del drenatge transversal en la conca d'Aínsa produeix l'exhumació de roques del basament Paleozoic, en la conca de Jaca els sistemes transversals es nodreixen essencialment dels dipòsits sinorogènics precedents. Aquestes característiques es veuen igualment reflectides en les distribucions de les edats d'U-Pb en zircons detrítics, tant emprades recentment en els Pirineus, en que en major part de la conca Sudpirinenca s'ha definit el pas de direccions de transport de sediment axials a transverses en base a la substitució de senyals Cadomianes per senyals Varisques. Aquest patró és totalment oposat a l'observat en la conca de Jaca (capítol 6), en que els sistemes transversos substitueixen les senyals Varisques dominants per la reinserció de senyals Cadomianes, evidenciant així la resposta diferencial al creixement diacrònic topogràfic en un oròsen, d'est a oest, en que les àrees font són afectades per diferents patrons d'exhumació tenint una clara influència en les signatures petrològiques dels sistemes sedimentaris que se'n deriven. Així mentre el Pirineu central experimenta una història d'exhumació més prolongada, on s'erosionen des de materials Eocens fins a Paleozoics, el Pirineu oest-central sofreix una evolució totalment diferent i individualitzada, on els sediments sintectònics inhibeixen l'erosió dels nivells més profunds de la Zona Axial.

Amb tot, en aquesta tesi es fa palesa la necessitat d'integrar diferents tècniques d'anàlisi de la procedència, per tal de desxifrar senyals ambigües, que dificulten la caracterització de l'evolució de les àrees font, sobretot en contextos on no existeixen àrees font suficientment diferenciades. En la conca Sudpirinenca, les litologies susceptibles de formar part de l'àrea font són molt similars en tot el domini Pirinenc. Ara bé, l'exhumació diferencial d'aquestes litologies proporciona signatures composicionals prou distintives com per obtenir dades crucials per a contribuir a resoldre la història tectono-estratigràfica d'una conca d'avantpaís, com la de Jaca.

Capítol 10

Conclusions

A multidisciplinary approach integrating sandstone petrography, clast point counting, detrital zircon U-Pb geochronology, and geological field observations has allowed to constraint the compositional features and the source area evolution for the middle Eocene to early Miocene sedimentary systems of the Jaca basin.

Four petrofacies have been identified from a detailed petrographic analysis, which are: (a) “Hybrid clast-dominated, (b) “Carbonatic extrabasinal enriched”, (c) “Siliciclastic dominant”,” and (d) “Mixed lithic and carbonatic” petrofacies.

Integration of all the data contained in this thesis has permitted to produce a cartography displaying the petrofacies distribution along the basin, which contribute to reconstruct the paleogeographic evolution, summarized as follows:

- During Lutetian times, turbidite sedimentation (Hecho Group) was fed axially, derived from eastern source areas. The Banastón turbidites are dominated by carbonatic components, while the lowermost part of the Jaca turbidites show an increase of lithic components (i.e. plutonic rock fragments). Source areas delivered carbonatic grains sourced from the South Central Pyrenean Zona, and lithic grains from the Paleozoic basement of the Axial Zone. Detrital zircon U-Pb geochronology in these deposits show a dominant Variscan age distribution, indicative of supply from late Variscan granitoids from the central Pyrenees.

- The last turbiditic deposits (Bartonian), known as the Rapitán channel, record a compositional shift marked by the increase of sandstone and hybrid sandstone rock fragments, accompanied by an increase of Cadomian age signal in detrital zircon distributions. This main change is here interpreted as the first emersion of northern source areas caused by the activity of the Lakora/Eaux-Chaudes thrust, evidencing the initial stage of transverse drained drainage systems.

- Sandstone petrography and detrital zircon U-Pb geochronology for the Hecho Group turbidites show compositional trends from base to top of each Tectono-Stratigraphic Units (TSU). These trends are here interpreted as high-frequency tectono-stratigraphy cyclicity, which consist on the increase of the intrabasinal components and the decrease of the Variscan signals, from base to top of each TSU.

- The replacement of the turbiditic sedimentation by transitional environments took place during Bartonian times. At that time, axially drained deltaic systems derived from eastern sources coexisted with transverse drained deltaic systems sourced from northern sources. The eastern source delivered detritus derived from the exhumation of Mesozoic and Paleozoic materials to the Belsué-Atarés Formation delta located at the southern margin of the basin. In contrast, newly created northern sources fed the Sabiñánigo Sandstone delta.

- Growing of structures during deltaic sedimentation in the northern and Southern margin of the basin controlled sediment dispersal and caused a strong diachrony. During Priabonian times, these delta systems are fed by the Santa Orosia fan delta (transverse drained) to the north. In the southern margin, deltaic systems were fed by prograding fluvial environments from the Campodarbe Formation (axially drained). Syndepositional structures as the Yebra de Basa or Atarés anticlines controlled the interplay between these sedimentary systems.

- Generalised terrestrial environments in the basin record the interruption of the marine connection with the Atlantic ocean, dated to occur at 36 Ma. At that time, alluvial fan systems situated at the northern part of the basin were fed from a protracted northern source, which caused an increase of the recycling of the former turbiditic basin due to the activity of the Gavarnie thrust. These transverse drained systems were fed from a source area composed by the Hecho Group turbidites, and by material of the North Pyrenean Zone that cropped out in the headwaters. Erosion of North Pyrenean materials imply a water divide position located further north than its present day location, which lets to conclude that during Cenozoic times a migration from north to south of the water divide took place at least for in west-central Pyrenees.

- Detrital zircon U-Pb analysis in the north derived aluvial fans reveal a clear dominance of Cadomian and >700 Ma age populations. This contrasts with the expected age distribution, which was assumed to be dominated by Variscan age components due to the deep recycling of the Hecho Group turbidites. This effect demonstrates that propagation of provenance signatures involved in recycling processes can be complicated to constraint. Several factors such as source lithology, zircon fertility and intrinsic textural properties of source rocks can exhert a strong control on the compositional features of the resulting clastic deposits.

- During the endorheic basin stage, axially fed fluvial system from the Campodarbe Formation are affected by a change on the eastern source area. This shift consists on the introduction of large amounts of metamorphic rock fragments, while the plutonic ones decrease. This compositional change can also be identified in the fluvial Escanilla Formation, in the Ainsa basin. As this compositional evolution is interpreted to occur in the source area (central Pyrenees), it can be considered a good correlation stratigraphic marker.

- During Oligocene times, transverse drained systems prevail due to the increase on the tectonic activity in the northern hinterland. Therefore, axially drained systems are displaced from north to south, and from east to west, following the main progradation direction trend. This effect is interpreted as the consequence diachronous orogenesis of the Pyrenees, wich evolved from east to west, and from north so south, yielding to a strong diacrhony of the main paleogeographic changes taking place in the different subbasins of the South Pyrenean foreland basin.

- In addittion, during the Eocene and Oligocene, adjacent basins were sourced from source terrains with a clearly differientated evolution. Thus, transverse fed drained systems in the Ainsa basin were chiefly sourced from the Paleozoic basement while transverse fed systems from the Jaca basin rwere fed from the former synorogenic deposits.

- Miocene volcanic zircons in the San Juan de la Peña fan (Bernués Formation) dated through U-Pb and (U-Th)/He techniques allow to propose a Miocene age for this fan, discarding a lower Oligocene age as proporsed before. Thus, sedimentation of these alluvial deposits can be linked to the activity of the Guarga thrust.

- In this last stage of the Jaca basin evolution (Oligocene and Miocene), both the Jaca and the Ainsa basin are being eroded by th Luna and Huesca fans, located in the Ebro foreland basin. This erosive stage occurs concomitantly with the last stages of sedimentation in the Jaca basin. The Luna alluvial fan (Uncastillo Formation) is also sourced from Paleozoic and Mesozoic material of the western Pyrenees.

The methodology applied in the present thesis highlights the need for a Integration of different provenance techniques in order to resolve ambiguous provenance signals which hinder the characterization of the sediment routing evolution, chiefly in active tectonic settings, where diverse source areas can occur. In addition, compositional and petrofacies changes described here can be enhanced when coupled with a sequence stratigraphic framework, allowing to generate a model potentially applied to other case studies.

La integració de diverses tècniques de procedència, com són l'anàlisi petrogràfic, els comptatges de clasts en conglomerats, l'estudi geocronològic d'U-Pb en zircons detrítics, juntament amb les observacions pròpies del treball de camp han permès definir les característiques composicionals i l'evolució en les àrees font dels sistemes sedimentaris de la conca de Jaca des de l'Eocè mig fins al Miocè inferior.

A partir de l'estudi modal dels gresos s'han pogut identificar quatre petrofàcies: (a) petrofàcies dominada per fragments de gresos híbrids, (b) petrofàcies enriquida en fragments carbonàtics, (c) petrofàcies dominada per components siliciclàstics, i (d) petrofàcies mixta en fragments de roca carbonàtics i lítics.

A partir de la definició d'aquestes petrofàcies i de la integració de les tècniques d'anàlisi de procedència emprades en aquesta tesi, s'ha elaborat una cartografia de distribució de petrofàcies que ha permès establir més fàcilment les principals característiques de l'evolució paleogeogràfica de la conca, les quals es resumeixen a continuació:

- Durant el Lutecià mig, la sedimentació turbidítica (Grup Hecho) era alimentada per un sistema de drenatge axial, procedent d'àrees font situades a l'est de la conca. Els sistemes turbidítics de Banastón mostren un clar predomini dels components carbonàtics, mentre que la part basal dels sistemes turbidítics de Jaca mostren un increment en components lítics, sobretot de naturalesa plutònica. Les àrees font subministraven dominantment components carbonàtics, derivats majoritàriament de la Zona Sudpirinenca central, i també materials del basament paleozoic de la Zona Axial. L'anàlisi geocronològic U-Pb en zircons detrítics mostra una distribució d'edats dominada per signatures varisques, que és indicativa de l'erosió dels granits tardihercinians en el Pirineu central.

- A l'inici del Bartonià, els últims dipòsits turbidítics, corresponents al canal del Rapitán, registren un canvi composicional significatiu respecte als sistemes anteriors, destacant l'augment de fragments de gresos i de gresos híbrids, juntament amb un augment de les senyals cadomianes en els zircons detrítics en detriment de les senyals varisques. Aquest important canvi s'interpreta com els primers indicis de creació, d'una nova àrea font situada al nord, que comença a emergir per l'activitat de l'encavalcament de Lakora/Eaux-Chaudes, marcant l'inici del desenvolupament dels sistemes de drenatge transversal a la conca de Jaca.

- Tant per les turbidites de Banastón com per les del sistema de Jaca, s'observen tendències composicionals de base a sostre de cada Unitat Tectono-Sedimentària (UTS), tant en la fracció gres analitzada amb el microscopi petrogràfic, com en les distribucions de les edats d'U-Pb en zircons detrítics. Aquests canvis són interpretats com a resultat de la ciclicitat tectonoestratigràfica, en que de base a sostre de cada unitat augmenten els components carbonàtics d'origen intraconcal, i disminueix la senyal varisca en les poblacions de zircons detrítics.

- El final de la sedimentació turbidítica ve acompanyat per un estadi de somerització en la conca que s'inicia durant el Bartonià, amb el que s'instal·la definitivament la sedimentació deltaica. La coexistència de sediments procedents d'àrees font situades al nord, amb sediments derivats d'àrees font de l'est, s'amplia en general a tota la conca. L'àrea font de l'est, alimenta els sistemes deltaics del marge sud de la conca (Formació Belsué-Atarés), subministrant-los litologies resultants de l'exhumació i incisió continuada dels materials Mesozoics i Paleozoics. Per contra, l'àrea font del nord, alimenta essencialment el sistema deltaic de la Formació Gres de Sabiñánigo i li aporta majoritàriament gresos turbidítics, marcant els estadis inicials d'inversió del marge nord de la conca i de creació d'aquesta nova àrea font.

- Durant la sedimentació deltaica, el creixement d'estructures tant al marge nord com al marge sud de la conca controla la dispersió dels sistemes, provoca la seva forta diacronia . En el Priabonià, aquests sistemes deltaics són alimentats en el marge nord pel *fan delta* de Santa Orosia (sistema de drenatge transversal) i al sud pels dipòsits fluvial de la Formació Campodarbe (sistema de drenatge axial). Durant aquests estadis les estructures sintectòniques, com l'anticlinal del Basa o el d'Atarés, controlen la interacció entre els dos sistemes de drenatge.

- Durant la continentalització de la conca, la qual veu definitivament interrompuda la seva connexió marina amb l'oceà Atlàntic als 36 Ma, els sistemes situats al marge nord de la conca són alimentats per una àrea font persistent al nord, la qual evoluciona cap a un increment en el reciclatge dels dipòsits turbidítics previs per l'activitat tectònica de l'encavalcament de Gavarnie. Durant tota la sedimentació al·luvial, els sistemes de drenatge amb procedència nord travessaven una àrea font que estava constituïda majoritàriament pels materials de la conca turbidítica precedent, però que en les seves capçaleres afloraven els materials de la Zona Nordpirinenca. L'erosió dels materials de la Zona Nordpirinenca implica que la divisòria d'aigües estava situada molt més al nord que la seva posició actual, evidenciant així una clara migració de la divisòria de nord a sud, almenys en el sector oest-central dels Pirineus.

- L'anàlisi d'U-Pb en zircons detrítics en el ventalls al·luvials de procedència nord revela una clara dominància de les signatures cadomianes i >700 Ma, i no dominada per signatures varisques, com seria d'esperar degut al preponderant reciclatge de les turbidites del Grup Hecho. Aquesta situació evidencia la complexitat en la propagació de signatures en processos de reciclatge, els quals no tan sols poden estar afectats pel tipus de litologia o per la feritilitat de les roques de l'àrea font, sinó que també per les seves propietats texturals intrínsiques.

- En aquest mateix estadi de tancament endorreic de la conca, la sedimentació fluvial de la Formació Campodarbe, la qual es localitza sobretot al marge sud de la conca, també es veu afectada per un canvi en la naturalesa de les àrees font situades a l'est. Aquest canvi consisteix en un augment considerable dels fragments de roca metamòrfics en detriment dels frament plutònics i carbonàtics. Aquest canvi també és enregistrat a la part superior de la Formació Escanilla a la conca d'Aínsa. Al tractar-se d'una tendència evolutiva que es produeix en una mateixa àrea font que és comuna per ambdues formacions, pot considerar-se com un bon marcador de correlació entre les conques d'Aínsa i de Jaca.

- Fruit de l'activitat tectònica emergent al nord de la conca, durant l'Oligocè els sistemes de drenatge transversal s'acaben imposant als de drenatge axial i evolucionen, sobretot de nord a sud, ampliant la seva àrea deposicional en la conca d'acord amb el sentit d'avançament de les estructures i provocant el desplaçament del sistema de drenatge axial cap a posicions més occidentals. Aquest fet és conseqüència de la diacronia de la deformació de l'orogen pirinenc, la qual progressa d'est a oest, i de nord a sud, provocant que els canvis paleogeogràfics en les diferents conques progressin d'est a oest i de nord a sud.

- Durant l'Eocè-Oligocè, a banda de la clara diacronia en aquests canvis paleogeogràfics majors que succeixen en conques adjacents, és evident que les àrees font sofreixen evolucions molt diferents. Així doncs, la instauració del drenatge transversal en la conca d'Aínsa produeix l'exhumació generalitzada de les roques del basament Paleozoic, en canvi en la conca de Jaca, els sistemes transversals es nodreixen essencialment dels dipòsits sinorogènics precedents.

- La presència de zircons miocens al ventall al·luvial de San Juan de la Peña (Formació Bernués) datats mitjançant U-Pb, i associats a un episodi volcànic llunyà, tal i com revela l'anàlisi d'(U-Th)/He, permet establir una edat miocena per aquests dipòsits, descartant així la seva atribució a l'Oligocè inferior, com s'havia assumit fins ara per la majoria dels autors. Conseqüentment, la sedimentació d'aquest ventall al·luvial s'ha de relacionar amb l'activitat tectònica causada per l'encavalcament del Guarga.

- En aquest últim estadi (Oligocè-Miocè), part de les conques de Jaca i Aínsa estan sent erosionades pels ventalls de Luna i Huesca que es dipositen a la recent constituida conca de l'Ebre. Aquesta erosió es produeix coetàniament amb els últims estadis de sedimentació en la conca de Jaca. En particular, el ventall al·luvial de Luna (Formació Uncastillo) a banda d'erosionar part dels dipòsits sintectònics de la conca de Jaca, també es nodria d'àrees font paleozoiques i mesozoiques, situades a la zona oest dels Pirineus (massisos Vascos).

Finalment, s'ha de ressaltar que amb la consecució d'aquesta tesi s'ha fet palesa la necessitat d'integrar diferents tècniques d'anàlisi de la procedència, per tal de desxifrar senyals ambigües, que dificulten la caracterització de l'evolució de les àrees font, sobretot en contextos on no existeixen àrees font suficientment diferenciades. A més es desprèn la necessitat d'integrar aquests canvis composicionals i/o de petrofàcies amb un marc d'estratigrafia seqüencial, que permeti obtenir un model conceptual aplicable a altres casos d'estudi i a diferents escales de resolució.

Referències

Allen, P.A., 1997. *Earth Surface Processes*: Blackwell, Oxford, 404p.

Allen, P.A. i Allen, J.R., 2013. *Basin Analysis: Principles and Application to Petroleum Play Assessment*: Oxford, UK, Wiley-Blackwell.

Amorosi, A. i Zuffa, G.G., 2011. Sand composition changes across key boundaries of siliciclastic and hybrid depositional sequences: *Sedimentary Geology*, **236**, p. 153–163, doi: 10.1016/j.sedgeo.2011.01.003.

Andò, S., Garzanti, E., Padoan, M. i Limonta, M., 2012. Corrosion of heavy minerals during weathering and diagenesis: A catalog for optical analysis: *Sedimentary Geology*, **280**, p. 165–178, doi: 10.1016/j.sedgeo.2012.03.023.

Arenas, C., 1993. Sedimentologia y paleogeografia del Terciario del margen pirenaico y sector central de la Cuenca del Ebro (zona aragonesa occidental): Universidad de Zaragoza, 858 p.

Arenas, C., Millán, H., Pardo, G. i Pocoví, A., 2001. Ebro Basin continental sedimentation associated with late compressional Pyrenean tectonics(north-eastern Iberia): controls on basin margin fans and fluvial systems: *Basin Research*, **13**, p. 65–89, doi: 10.1046/j.1365-2117.2001.00141.x.

Arribas, J., Ochoa, M. and Mas, R., 2007. Sandstone petrofacies in the northwestern sector\rof the Iberian Basin\rPetrofacies arenosas en el sector noroccidental de la Cuenca Ibérica\r: *Journal of Iberian Petrology*, **33**, p. 191–206.

Barnolas, A. i Teixell, A., 1994. Platform sedimentation and collapse in a carbonate dominated margin of a foreland basin (Jaca basin, Eocene, southern Pyrenees): *Geology*, **22**, p. 1107–1110.

Beamud, E., Muñoz, J.A., Fitzgerald, P.G., Baldwin, S.L., Garcés, M., Cabrera, L. i Metcalf, J.R., 2011. Magnetostratigraphy and detrital apatite fission track thermochronology in syntectonic conglomerates: Constraints on the exhumation of the South-Central Pyrenees: *Basin Research*, **23**, p. 309–331, doi: 10.1111/j.1365-2117.2010.00492.x.

Bentham, P.A., Burbank, D.W. i Puigdefabregas, C., 1992. Temporal and spatial controls on the alluvial architecture of an axial drainage system: late Eocene Escanilla formation, southern Pyrenean foreland basin, spain: *Basin Research*, **4**, p. 335–352, doi: 10.1111/j.1365-2117.1992.tb00052.x.

Caja, M.A., Marfil, R., Garcia, D., Remacha, E., Morad, S., Mansurbeg, H., Amorosi, A., Martínez-Calvo, C. i Lahoz-Beltrá, R., 2010. Provenance of siliciclastic and hybrid turbiditic arenites of the Eocene Hecho Group, Spanish Pyrenees: Implications for the tectonic evolution of a foreland basin: *Basin Research*, **22**, p. 157–180, doi: 10.1111/j.1365-2117.2009.00405.x.

Cámara, P. i Klimowitz, J., 1985. Interpretación geodinámica de la vertiente centro-occidental surpirenaica: *Estudios geológicos*, **41**, p. 391–404.

Castelltort, S. i Van Den Driessche, J., 2003. How plausible are high-frequency sediment supply-driven cycles in the stratigraphic record? *Sedimentary Geology*, **157**, p. 3–13, doi: 10.1016/S0037-0738(03)00066-6.

Costa, E., Garcés, M., López-Blanco, M., Beamud, E., Gómez-Paccard, M. i Larrasoaña, J.C., 2010. Closing and continentalization of the South Pyrenean foreland basin (NE Spain): Magnetochronological constraints: *Basin Research*, **22**, p. 904–917, doi: 10.1111/j.1365-2117.2009.00452.x.

Davis, D. i Lin, S.F., 2003. Unraveling the geologic history of the Hemlo Archean gold deposit, Superior province, Canada: a U-Pb geochronological study.: *Economic Geology and Bulletin of the Society of Economic Geologists*, **70**, p. 335–348.

Dick, A.B., 1887. On zircon and other minerals contained in sands: *Nature*, **36**, p. 91–92.

Dickinson, W.R., 1970. Interpreting detrital modes of graywacke and arkose: *Journal of Sedimentary Research*, **40**, p. 695–707.

Dickinson, W.R., 1985. Interpreting provenance relations from detrital modes of sandstones: *Provenance of Arenites*,, p. 333–361, doi: 10.1007/978-94-017-2809-6_15.

Dickinson, W.R. i Gehrels, G.E., 2009. Use of U-Pb ages of detrital zircons to infer maximum depositional ages of strata: A test against a Colorado Plateau Mesozoic database: *Earth and Planetary Science Letters*, **288**, p. 115–125.

Dickinson, W.R. i Suczek, C.A., 1979. Plate tectonics and sandstone compositions: *AAPG Bulletin*, **63**, p. 2164–2182.

Dreyer, T., Corregidor, J., Arbues, P. i Puigdefàbregas, C., 1999. Architecture of the tectonically influenced Sobrarbe deltaic complex in the Ainsa Basin, northern Spain: *Sedimentary Geology*, **127**, p. 127–169,

doi: 10.1016/S0037-0738(99)00056-1.

Filleaudeau, P.Y., Mouthereau, F. i Pik, R., 2012. Thermo-tectonic evolution of the south-central Pyrenees from rifting to orogeny: Insights from detrital zircon U/Pb and (U-Th)/He thermochronometry: *Basin Research*, **24**, p. 401–417, doi: 10.1111/j.1365-2117.2011.00535.x.

Fillon, C., Gautheron, C. i van der Beek, P., 2013. Oligocene-Miocene burial and exhumation of the Southern Pyrenean foreland quantified by low-temperature thermochronology: *Journal of the Geological Society*, **170**, p. 67–77, doi: 10.1144/jgs2012-051.

Fitzgerald, P.G., Muñoz, J.A., Coney, P.J. i Baldwin, S.L., 1999. Asymmetric exhumation across the Pyrenean orogen: Implications for the tectonic evolution of a collisional orogen: *Earth and Planetary Science Letters*, **173**, p. 157–170, doi: 10.1016/S0012-821X(99)00225-3.

Fontana, D., Zuffa, G.G., Garzanti, E. i Pyrenees, C., 1989. The Eocene Hecho Group Turbidite Complex (south - central Pyrenees , Spain): , p. 223–237.

Friend, P.F., Hirst, J.P., Hogan, P.J., Jolley, D.W., Mcelroy, R., Nichols, G.J. i Rodriguez-Vidal, J., 1989. *Pyrenean tectonic control of Oligo-Miocene river systems, Huesca, Aragon, Spain*:

Friend, P.F., Hirst, J.P. i Nichols, G.J., 1986. Sandstone-body structure and river pro-cesses in the Ebro Basin of Aragon, Spain. In: *Cuadernos de Geología Ibérica: Sedimentación Continental en España* p. 9–30.

Garzanti, E., 2015. From static to dynamic provenance analysis – sedimentary petrology upgraded: *Sedimentary Geology*, **336**, p. 3–13, doi: 10.1016/j.sedgeo.2015.07.010.

Garzanti, E., 1991. Non-Carbonate Intrabasinal Grains in Arenites: Their Recognition, Significance, and Relationship to Eustatic Cycles and Tectonic Setting: *Journal of Sedimentary Research*, **61**, p. 959–975, doi: 10.1306/D4267816-2B26-11D7-8648000102C1865D.

Garzanti, E., Doglioni, C., Vezzoli, G. i Andò, S., 2007a. Orogenic Belts and Orogenic Sediment Provenance: *The Journal of Geology*, **115**, p. 315–334, doi: 10.1086/512755.

Garzanti, E., Limonta, M., Resentini, A., Bandopadhyay, P.C., Najman, Y., Andò, S. i Vezzoli, G., 2013. Sediment recycling at convergent plate margins (indo-burman ranges and andaman-nicobar ridge): *Earth-Science Reviews*, **123**, p. 113–132, doi: 10.1016/j.earscirev.2013.04.008.

Garzanti, E., Vezzoli, G., Andò, S., Lavé, J., Attal, M., France-Lanord, C. i DeCelles, P., 2007b. Quantifying sand provenance and erosion (Marsyandi River, Nepal Himalaya): *Earth and Planetary Science Letters*, **258**, p. 500–515, doi: 10.1016/j.epsl.2007.04.010.

Gazzi, P., 1966. Le arenarie del flysh sopracretaceo dell'Apenino modenese; correlazioni con il flysh Monghidoro: *Mineral. Petrogr. Acta*, **12**, p. 69–97.

Gómez-Gras, D., Roigé, M., Fondevilla, V., Oms, O., Boya, S. i Remacha, E., 2016. Provenance constraints on the Tremp Formation paleogeography (southern Pyrenees): Ebro Massif VS Pyrenees sources. Cretac. Res. 57. https://doi.org/10.1016/j.cretres.2015.09.: *Cretaceous Research*, **57**, doi: 10.1016/j.cretres.2015.09.010.

Gupta, K. Das i Pickering, K.T., 2008. Petrography and temporal changes in petrofacies of deep-marine Ainsa-Jaca basin sandstone systems, Early and Middle Eocene, Spanish Pyrenees: *Sedimentology*, **55**, p. 1083–1114, doi: 10.1111/j.1365-3091.2007.00937.x.

Haughton, P., TODD, S.P. i Morton, A.C., 1991. Sedimentary provenance studies: *Geological Society, London, Special Publications*, **57**, p. 1–11.

Hehuwat, F.A., 1970. The transition from Marine to Continental Sedimentation in the Eocene of the Guarga Synclinorium Huesca province. Spain: Utrecht.

Hirst, J.P. i Nichols, G.J., 1986. Thrust tectonic controls on Miocene alluvial distribution patterns, southern Pyrenees: *IAS Special Publications*, **8**, p. 247–258, doi: 10.1002/9781444303810.

Hogan, P.J., 1993. Geochronologic, Tectonic and Stratigraphic Evolution of the Southwest Pyrenean Foreland Basin, Northern Spain.: University of Southern California, 208 p.

Howard, J.L., 1993. The statistics of counting in rudites: a review, with examples from the Upper Palaeogene of southern California, USA.: *Sedimentology*, **40**, p. 157–174.

Huyghe, D., Castelltort, S., Mouthereau, F., Serra-Kiel, J., Filleaudeau, P.Y., Emmanuel, L., Berthier, B. i Renard, M., 2012. Large scale facies change in the middle Eocene South-Pyrenean foreland basin: The role of tectonics and prelude to Cenozoic ice-ages: *Sedimentary Geology*, **253–254**, p. 25–46, doi: 10.1016/j.sedgeo.2012.01.004.

Ingersoll, R. V., Bullard, T.F., Ford, R.L., Grimm, J.P., Pickle, J.D. i Sares, S.W., 1984. The Effect of Grain Size on Detrital Modes: A Test of the Gazzi-Dickinson Point-Counting Method: *SEPM Journal of Sedimentary Research*, **Vol. 54**, p. 103–116, doi: 10.1306/212F83B9-2B24-11D7-8648000102C1865D.

Jolley, J., 1988. Thrust tectonics and alluvial architecture of the Jaca Basin, southern Pyrenees: University of Wales, Cardiff, 365 p.

Jones, S.J., 2004. Tectonic controls on drainage evolution and development of terminal alluvial fans, southern Pyrenees, Spain: *Terra Nova*, **16**, p. 121–127, doi: 10.1111/j.1365-3121.2004.00539.x.

Jones, S.J., Frostick, L.E. i Astin, T.R., 2001. Braided stream and flood plain architecture: The Rio Vero formation, Spanish Pyreness: *Sedimentary Geology*, **139**, p. 229–260, doi: 10.1016/S0037-0738(00)00165-2.

Labaume, P., Meresse, F., Jolivet, M., Teixell, A. i Lahfid, A., 2016. Tectonothermal history of an exhumed thrust-sheet-top basin: An example from the south Pyrenean thrust belt: *Tectonics*, **35**, p. 1280–1313, doi: 10.1002/2016TC004192.

Labaume, P., Séguret, M. i Seyve, C., 1985. Evolution of a turbiditic foreland basin and analogy with an accretionary prism: Example of the Eocene South-Pyrenean Basin: *Tectonics*, **4**, p. 661–685.

Lagabrielle, Y., Labaume, P. i Saint-Blanquat, M., 2010. Mantle exhumation, crustal denudation, and gravity tectonics during Cretaceous rifting in the Pyrenean realm (SW Europe): Insights from the geological setting of the lherzolite bodies: *Tectonics*, **29**, doi: 10.1029/2009TC002588.

Lévy, M., 1978. Note sur quelques minéraux contenus dans les sables du Mesvrin, près Autun.: *Bulletin de la Société Française de Minéralogie et de Crystallographie*, **1**, p. 39–41.

Malusà, M.G., Resentini, A. i Garzanti, E., 2016. Hydraulic sorting and mineral fertility bias in detrital geochronology: *Gondwana Research*, **31**, p. 1–19, doi: 10.1016/j.gr.2015.09.002.

Mange, M. i Maurer, H.F.W., 1992. *Heavy Minerals in Colour*: Chapman & Hall, London.

Metcalf, J.R., Fitzgerald, P.G., Baldwin, S.L. i Muñoz, J.A., 2009. Thermochronology of a convergent orogen: Constraints on the timing of thrust faulting and subsequent exhumation of the Maladeta Pluton in the Central Pyrenean Axial Zone: *Earth and Planetary Science Letters*, **287**, p. 488–503, doi:

10.1016/j.epsl.2009.08.036.

Michael, N., 2013. Functioning of an ancient routing system, the Escanilla Formation, South Central Pyrenees: Imperial College London, 318 p.

Michael, N.A., Whittaker, A.C., Carter, A. i Allen, P.A., 2014. Volumetric budget and grain-size fractionation of a geological sediment routing system: Eocene Escanilla Formation, south-central Pyrenees: *Bulletin of the Geological Society of America*, **126**, p. 585–599, doi: 10.1130/B30954.1.

Millán, H., Urcia, B. i Juan, A., 2006. La transversal de Gavarnie-Guara. Estructura y edad de los mantos de Gavarnie, Guara-Gèdre y Guarga (Pirineo centro-occidental): *Geogaceta*,, p. 35–38.

Montes, M., 2002. Estratigrafia del Eoceno-Oligoceno de la Cuenca de Jaca (Sinclinorio del Guarga): Universitat de Barcelona, 365 p.

Mouthereau, F., Filleaudeau, P.Y., Vacherat, A., Pik, A., Lacombe, O., Fellin, M.G., Castelltort, S., Christophoul, F. i Masini, E., 2014. Placing limits of shortening evolution in the Pyrenees: role fo margin architecture and implications for the Iberia/Europe convergence: *Tectonics*, **33**, p. 2283–2314.

Muñoz, J.A., 1992. Evolution of a continental collision belt: ECORS-Pyrenees crustal balanced cross-section. In: *Thrust Tectonics* (McClay, K.R., ed.) Chapman & Hall, London, U.K., p. 235–246.

Muñoz, J.A., Beamud, E., Fernández, O., Arbués, P., Dinarés-Turell, J. i Poblet, J., 2013. The Ainsa Fold and thrust oblique zone of the central Pyrenees: Kinematics of a curved contractional system from paleomagnetic and structural data: *Tectonics*, **32**, p. 1142–1175, doi: 10.1002/tect.20070.

Mutti, E., 1985. Turbidite systems and their relations to depositional sequences. In: *Provenance of Arenites* (Zuffa, G.G., ed.) NATO ASI Ser., p. 65–93.

Mutti, E., Luterbacher, H., Ferrer, J. i Rosell, J., 1972. Schema stratigrafico e lineamenti di facies del Paleogeno Marino della zona centrale sudpirenaica tra Tremp (Catalogna) e Pamplona (Navarra): *Memorie della Società Geologica Italiana*, **11**, p. 391–416.

Nagtegaal, P.J.C. i Weerd, T., 1985. Provenance of Cambro-Ordovician to Oligocene sandstones in the Southern Pyrenees, Spain. Geol. Mqnb., 64, 2540.: *Geol. Mijnb.*, **64**, p. 25–40.

Nichols, G.J. i Hirst, J.P., 1998. Alluvial fans and fluvial distributary systems, Oligo-Miocene, northern Spain; contrasting processes and products: *Journal of Sedimentary Research*, **68**, p. 879–889, doi: 10.2110/jsr.68.879.

Nie, J., Horton, B.K., Saylor, J.E., Mora, A., Mange, M., Garzione, C.N., Basu, A., Moreno, C.J., Caballero, V. i Parra, M., 2012. Integrated provenance analysis of a convergent retroarc foreland system: U-Pb ages, heavy minerals, Nd isotopes, and sandstone compositions of the Middle Magdalena Valley basin, northern Andes, Colombia: *Earth-Science Reviews*, **110**, p. 111–126, doi: 10.1016/j.earscirev.2011.11.002.

Nijman, W. i Nio, S.-D., 1975. *The Eocene Montañana Delta (Tremp-Graus Basin, provinces of Lérida and Huesca, Southern Pyrenees, N Spain)*: Field trip B guidebook (The sedimentary evolution of the Paleogene south Pyrenean Basin), XI International SedimentologicalCongress, International Association of Sedimentologists, Nice, Excursion Guidebook.

Oms, O., Dinarès-Turell, J. i Remacha, E., 2003. Magnetic stratigraphy from deep clastic turbidites: An example from the Eocene Hecho group (Southern Pyrenees): *Studia Geophysica et Geodaetica*, **47**, p. 275–288, doi: 10.1023/A:1023719607521.

Ortí, F., Salvany, J.M., Rosell, L., Pueyo, J.J. i Inglés, M., 1986. Evaporitas antiguas (Navarra) y actuales (Los Monearos) de la Cuenca del Ebro. In: *Guía de las Excursiones del XI Congreso Español de Sedimentologia* (Anadón, P., and Cabrera, L., eds.) Generalitat de Catalunya, Comissió Interdepartamental de Recerca i Innovació Tecnològica (CIRIT), Barcelona., p. 21–24.

Paola, C., Heller, P.L. i Angevine, C.L., 1992. The large scale dynamics of grain size variation in alluvial basins: *Basin Research*, **4**, p. 73–90.

Puigdefàbregas, C., 1975. La sedimentación molásica en la cuenca de Jaca: *Pirineos*, **104**, p. 1–188.

Puigdefàbregas, C., Muñoz, J.A. i Verges, J., 1992. Trusting and foreland basin evolution in the southern Pyrenees. In: *Thrust Tectonics* Springer Netherlands, p. 247–254.

Puigdefàbregas, C. i Souquet, P., 1986. Tecto-sedimentary cycles and depositional sequences of the Mesozoic and Tertiary from the Pyrenees: *1986*, **129**, p. 173–203.

Remacha, E. i Fernández, L.P., 2003. High-resolution correlation patterns in the turbidite systems of the

Hecho Group (South-Central Pyrenees, Spain): *Marine and Petroleum Geology*, **20**, p. 711–726, doi: 10.1016/j.marpetgeo.2003.09.003.

Remacha, E., Fernández, L.P. i Maestro, E., 2005. The Transition Between Sheet-Like Lobe and Basin-Plain Turbidites in the Hecho Basin (South-Central Pyrenees, Spain): *Journal of Sedimentary Research*, **75**, p. 798–819, doi: 10.2110/jsr.2005.064.

Remacha, E., Oms, O. i Coello, J., 1995. he Rapitán turbidite channel and its related eastern levee-overbank deposits, Eocene Hecho group, south-central Pyrenees, Spain. In: *Atlas of Deep Water Environments* Springer Netherlands, p. 145–149.

Romans, B.W., Castelltort, S., Covault, J.A., Fildani, A. i Walsh, J.P., 2016. Environmental signal propagation in sedimentary systems across timescales: *Earth-Science Reviews*, **153**, p. 7–29, doi: 10.1016/j.earscirev.2015.07.012.

Roure, F., Choukroune, P., Berastegui, X., Muñoz, J.A., Villien, A. i Matheron, P., 1989. ECORS deep seismic data and balanced cross sections: Geometric constrains on the evolution of the Pyrenees: *Tectonics*, **8**, p. 41–50.

Saylor, J.E., Stockli, D.F., Horton, B.K., Nie, J. i Mora, A., 2012. Discriminating rapid exhumation from syndepositional volcanism using detrital zircon double dating: Implications for the tectonic history of the Eastern Cordillera, Colombia: *Bulletin of the Geological Society of America*, **124**, p. 762–779, doi: 10.1130/B30534.1.

Séguret, M., 1972. Etude tectonique des nappes et séries décollées de la partie centrale du versant sud des Pyrenées: Universite Montpellier, 155 p.

Soler-Sampere, M. i Puigdefàbregas, C., 1970. Líneas generales de la geología del Alto Aragón Occidental: *Pirineos*,, p. 5–20.

Sømme, T.O., Helland-hansen, W., Martinsen, O.J. i Thurmond, J.B., 2009. Relationships between morphological and sedimentological parameters in source-to-sink systems: A basis for predicting semi-quantitative characteristics in subsurface systems: *Basin Research*, **21**, p. 361–387, doi: 10.1111/j.1365-2117.2009.00397.x.

Sorby, H.C., 1880. On the structure and origin of non-calcareus stratified rocks. Proc. Geol. Soc. London. 36,

46-92.: *Geological Society, London, Special Publications*, **36**, p. 46–92.

Teixell, A., 1998. Crustal structure and orogenic material budget in the west central Pyrenees: *Tectonics*, **17**, p. 395–406.

Teixell, A. i García-Sansegundo, J., 1995. Estructura del sector central de la Cuenca de Jaca (Pirineos meridionales): *Rev. Soc. Geol. España*, **8**, p. 215–228.

Thomson, K.D., Stockli, D.F., Clark, J.D., Puigdefàbregas, C. i Fildani, A., 2017. Detrital zircon (U-Th)/(He-Pb) double-dating constraints on provenance and foreland basin evolution of the Ainsa Basin, south-central Pyrenees, Spain: *Tectonics*, **36**, p. 1352–1375, doi: 10.1002/2017TC004504.

Valloni, R., Marchi, M. i Mutti, E., 1984. Studio conoscitivo della moda detritica delle torbiditi eoceniche del Gruppo di Hecho (Spagna): *Giornale di Geologia*, **46**, p. 45–56.

Vergés, J., Fernàndez, M. i Martínez, A., 2002. The Pyrenean orogen: pre-, syn-, and post-collisional evolution: *Journal of the Virtual Explorer*, **8**, p. 57–76, doi: 10.3809/jvirtex.2002.00058.

Vermeesch, P., 2004. How many grains are needed for a provenance study? *Earth and Planetary Science Letters*, **224**, p. 441–451, doi: 10.1016/j.epsl.2004.05.037.

Vincent, S.J., 2001. The Sis palaeovalley: A record of proximal fluvial sedimentation and drainage basin development in response to Pyrenean mountain building: *Sedimentology*, **48**, p. 1235–1276, doi: 10.1046/j.1365-3091.2001.00421.x.

Weltje, G.J. i von Eynatten, H., 2004. Quantitative provenance analysis of sediments: Review and outlook: *Sedimentary Geology*, **171**, p. 1–11, doi: 10.1016/j.sedgeo.2004.05.007.

Whitchurch, A.L., Carter, A., Sinclair, H.D., Duller, R.A., Whittaker, A.C. i Allen, P.A., 2011. Sediment routing system evolution within a diachronously uplifting orogen: Insights from detrital zircon thermochronological analyses from the South-Central pyrenees: *American Journal of Science*, **311**, p. 442–482, doi: 10.2475/05.2011.03.

Yuste, A., Luzón, A. i Bauluz, B., 2004. Provenance of Oligocene-Miocene alluvial and fluvial fans of the northern Ebro Basin (NE Spain): An XRD, petrographic and SEM study: *Sedimentary Geology*, **172**, p. 251–268, doi: 10.1016/j.sedgeo.2004.10.001.

Zuffa, G.G., 1980. Hybrid arenites: their composition and classification: *Journal of Sedimentary Petrology*, **50**, p. 21–29.

Zuffa, G.G., 1985. Optical analyses of arenites: influence of methodology on compositional results. In: *Provenance of Arenites* (Zuffa, G.G., ed.) Boston, p. 165–189.

Zuffa, G.G., 1987. Unravelling hinterland and offshore palaeogeography from deep-water arenites. In: *Marine Clastic Sedimentology* (Legget, J.K., and Zuffa, G.G., eds.) Concepts and Case Studies. Graham and Trotman, London, p. 39–61.

Agraïments

Ha arribat l'hora de tancar aquest capítol de la meva vida, i encara no me'n sé avenir de la sort que tinc d'haver pogut viure aquesta experiència. No solsament del fet en si, de poder dedicar part del meu temps a investigar en un indret tant magnífic com els Pirineus, sinó que també per tota la gent que d'una manera o altra, m'ha acompanyat i ha contribuït a que hagi pogut disfrutar del doctorat. Les paraules següents no són suficients per a agrair tot això, però espero que almenys puguin donar una idea de la immensa gratitud que sento.

En primer lloc vull agrair als meus directors, David Gómez i Eduard Remacha, per haver confiat en mi i donar-me la oportunitat de treballar amb ells, i per haver-me proporcionat tots els mecanismes per a realitzar la aquesta tesi.

David, vas confiar en mi des del primer moment, i durant tots aquests anys m'has fet sentir lliure fent tot allò que m'ha apassionat. Vull agrair-te especialment tot el que m'has ensenyat, tot el suport que mai m'has deixat de mostrar, i com de valorada m'has fet sentir. Em quedo amb totes les tardes al microscopi, discutint fins a no poder més, i sobretot amb el treball de camp, on hem pogut divagar sobre moltíssims temes, que m'han ensenyat a no deixar de sentir curiositat envers tots aquests "gresets" que ens envolten. Gràcies per les xerrades, pels cafès, i algun que altre caramel. En fi, mil gràcies!

Eduard, et vull agrair que ara ja fa no se quants anys m'introduïssis al Pirineu, i que m'hagis acompanyat i ensenyat tantíssimes coses durant aquests temps. Has invertit molt temps en la meva formació, i mai podré expressar-te suficientment la meva gratitud per tot això. Mai oblidaré els treballs de camp a Aínsa, intentant trobar algo que no fos "fi", i sobretot el temps que vaig passar a Jaca, concretament a Yebra de Basa. Per tot això, i moltíssimes coses més, t'agraeixo de tot cor tot el que m'has donat.

Vull agrair també a tots els membres del departament de Geologia, que m'han acompanyat i m'han fet sentir més que còmoda durant tot aquest temps. Moltes gràcies pel vostre suport i simpatia. I a tu Pini, per tots els viatges en cotxe cap a Barcelona i pels innumerables dinar, moltes gràcies!

En especial vull donar les gràcies al Toni Teixell, que ha estat per mi com un tercer codirector. Moltes gràcies per totes les discussions, per totes les sortides al camp, i per haver pensat en mi i haver-me obert les portes, sobretot durant aquesta época final de la tesi.

També vull agrair al Paco Martínez totes les converses que hem tingut, i l'ajuda que sempre has estat disposat a donar-me.

A l'Oriol Oms, per haver confiat en mi per introduir-me en el món de la paleogeografia del Cretaci, i per tota l'ajuda i suport durant tots aquests anys, moltes gràcies.

I would like to extent my gratitude to Danny Stockli, Margo Odlum and Kelly Thomson for the great time that we have spent together, either in the Pyrenees or in Austin or in Barcelona. Danny, I'm very grateful for all the support during these last years, and to allow me to get introduced to the DZ U-Pb world. I would also like to thank also all the other people from the UT that made me feel so confortable during my time in Austin (Renas, Thomas, Doug, Chelsea..).

Grazie mille to William Cavazza, Irene Albino and Francesco Mittiga to allow me to work in your lab, where I could separate all this huge amount of rocks.

A tots els "becarios" i "precarios", que han estat fonamentals durant aquesta etapa (Isi, Mireia, Marc, Lucia, Camilo, Victor, Raquel Daza, Lluis Valero, Eudald, Dídac, Laura, Xavi, Norbert, Guillem, Alessandra, Gisela..).

A tu Salva, necessito mencionar-te a part. Hem viscut tantes coses junts, tants camps, tants vins, tantes columnes...No puc expressar el meu agraïment cap a tu per haver-me acompanyat i haver-me ensenyat tantes coses. Hem quedo, que d'aquesta etapa, en surto amb un gran amic.

Al Miquel Poyatos, per haver estat sempre present, encara que lluny en km, i per haver-me ajudat tant durant aquest temps. A l'Arnau Obradors i a la Luz Gomis, per tots els ànims i els "sofriments" compartits.

També es mereixen una especial menció el Victor, el Dani, la Rocio i la Marina. A tots vosaltres, us vull agrair tota la felicitat que m'heu donat durant tots aquests anys. Victor, anem a mostrejar?

Vull agrair també ha persones amb les que he tingut el plaer de treballar o compartir impressions. Al Toni Barnolas, al Pierre Labaume, al Cai Puigdefàbregas moltes gràcies per tots els coneixements compartits (merci!).

También quiero dar las gracias a Jean Gerard i Miguel Ángel Caja por brindarme la oportunidad de trabajar con vosotros, y por ayudarme siempre que lo he necesitado.

Moltes gràcies al laborants Lluis Gordon i Marc Puigcerver, per haver-me proporcionat tantes i tantes làmines primes!

A totes les “secres”, que sempre esteu aquí, pel que faci falta, per la vostra ajuda i sobretot per la felicitat que transmeteu. Mil gràcies!

El temps al camp no hauria estat el mateix sense “las chicas de Fiscal”. Muchas gracias por acogernos como si fueramos del pueblo, y por todas las risas y experiencias vividas, en especial a ti Belén.

A la gent de Santa Cruz de la Seròs, per acollir-nos tant bé, i fer-nos sentir com a casa.

I would like to express my gratitude to Ricki and Barrie from Conwy Valley Systems, and Rob Duller, to allow me to learn more about point counting analysis.

A tots els meus amics, que m’han donat suport durant aquest temps i s’han vist involucrats en aquest doctorat. Vull agrair-te a tu especialment Paula, per estar sempre aquí, i acompanyar-me a tot arreu. A tu Agustí, per totes les xalades Àgerenques i Gracienques, mil gràcies. Al Sergi Alarcón, per animar-me i donar-me suport sempre, tant volant com treballant. També a tots vosaltres Marta, Àngel, Helena, Patri, Moll, i un llarg etc...

A la meva família, que m’heu donat tot el recolzament i amor necessari per que avui pugui ser aquí, fent allò amb el que disfruto. Sobretot vull agraïr als meus pares, el Jaumet i la Carmeta, per preocupar-se tant per mi i per assegurar-se sempre de que tot anés bé. Mai tindré les suficients paraules per donar-vos les gràcies. A tu, Imma per ser la més especial de totes les germanes que existeixen, per estar sempre amb mi (a tu també Jesu). Als meus padrins per la confiança en mi i tot el suport durant tots aquests anys, moltes gràcies.

I a tu Oreig, per ser just la brisa suau que m’has acompanyat en aquests últims mesos tempestosos. Gràcies pel teu amor i pel teu suport incondicional (a vegades irracional).